INVESTIGATION OF SILICON MOS SOLAR CELLS UNDER CONCENTRATION AND AT DIFFERENT TEMPERATURES

By
SUDIP BHATTACHARYA

INTERDISCIPLINARY PROGRAMME IN MATERIAL SCIENCE
INDIAN INSTITUTE OF TECHNOLOGY, KANPUR
NOVEMBER, 1978

INVESTIGATION OF SILICON MOS SOLAR CELLS UNDER CONCENTRATION AND AT DIFFERENT TEMPERATURES

A Thesis Submitted
in Partial Fulfilment of the Requirements
for the Degree of
MASTER OF TECHNOLOGY

By
SUDIP BHATTACHARYA

to the
INTERDISCIPLINARY PROGRAMME IN MATERIAL SCIENCE
INDIAN INSTITUTE OF TECHNOLOGY, KANPUR
NOVEMBER, 1978

MS-1978-M-BHA-INV

7.11.78
2i

CERTIFICATE

This is to certify that the thesis entitled " Investigatio of Silicon MOS Solar Cells Under Concentration and at Different Temperatures" by Sudip Bhattacharya is a record of work carried out/under my supervision and has not been submitted elsewhere for a degree.

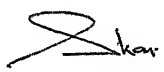

Dr. S. Kar
Department of Electrical Engineering
and
Materials Science Programme
Indian Institute of Technology
Kanpur

November 4, 1978.

15.11.78 2i

Acknowledgement

I take this opportunity to express my most sincere thanks to Dr. S. Kar, who did more than simply guiding me through the course of this work. But for his constant interest in the problem and help in some critical metal evaporations, the work presented here would not have been complete. Also discussions with him on various points were of immense help and many of the conclusions arrived at in the present work are the outcome of these discussions. My association with Dr. Kar during the course of present work has been rewarding since this has also given me a feeling of the art of semiconductor device fabrication.

Thanks are due to Messers S. Varma, D. Shanker, and R. Varghese for rendering constant help throughout the tenure of this work in device fabrication as well as in measurements. Some discussions with them on various points have also been fruitful.

Messers U. Mishra, A. Agnihotri and D. Patil have a claim to my thanks for helping me with some of the measurements.

Thanks are also due to Mr. B.N. Srivastava for making neat tracings and to Mr. L.S. Bajpai for making some excellent typing.

Lastly, the financial assistance from the Department of Science and Technology, Government of India is gratefully acknowledged.

Table of Contents

Notations

A	cell area [cm^2]
A^*	effective Richardson's constant, [$A/cm^2.{}^oK^2$]
C	total device capacitance, [F/cm^2]
C_{is}	interface state capacitance, [F/cm^2]
C_{ox}	oxide capacitance, [F/cm^2]
C_{sc}	space charge capacitance, [F/cm^2]
D_p	diffusion coefficient for holes, [cm^2/sec]
E_c	conduction band edge in silicon, [eV]
E_{FM}	Fermi level in metal, [eV]
E_{FS}	Fermi level in bulk silicon, [eV]
E_G	silicon bandgap, [eV]
E_G^{ox}	oxide bandgap, [eV]
E_v	valence bandedge in silicon, [eV]
F	fill factor
I_D	diode current, [A]
I_L	light generated current, [A]
I_{RT}	recombination tunneling current, [A]
I_{sc}	shortcircuit current of the cell, [A]
I_{TT}	thermionic tunneling current, [A]
J_D	diode current density, [A/cm^2]
J_L	light generated current density, [A/cm^2]
J_{RT}	recombination tunneling current density, [A/cm^2]
J_{sc}	shortcircuit current density of the cell, [A/cm^2]
J_{TT}	thermionic tunneling current density, [A/cm^2]
k	Boltzmann's constant, [$eV/{}^oK$]
n	diode quality factor

N_c effective density of states in the conduction band, [cm^{-3}]

N_D donor density, [cm^{-3}]

N_{is} interface state density, [$cm^{-2}\ V^{-1}$]

N_t trap density, [cm^{-3}]

q elementary charge, [C]

R_s solar cell series resistance, [Ohm]

t_m metal layer thickness, [A]

t_{ox} oxide thickness, [$\mathring{A}$]

T absolute temperature, [^oK]

t_m metal layer transmittance

T_{ox} oxide tunneling transmission factor

T_{ox}^{oc} oxide tunneling transmission factor at open circuit

$\bar{v}$ thermal velocity of the carriers, [cm/sec]

V device voltage, [V]

V_{oc} opencircuit voltage of solar cell, [V]

V_{ox} oxide voltage, [V]

V_{ox}^o oxide voltage at zero bias, [V]

V_{ox}^{oc} oxide voltage at zero bias, [V]

ϕ_{Bn} Schottky barrier height for n-type silicon, [V]

ϕ_M metal work function, [eV]

ϕ_{MS}^* $\phi_M - \chi_s$, [eV]

ϕ_n $(E_c - E_{FS})/q$ for n-type silicon, [V]

φ_i interface potential in silicon, [V]

φ_i^o interface potential in silicon at zero bias, [V]

φ_i^{oc} interface potential in silicon at opencircuit, [V]

ε_{ox} oxide permittivity, [F/cm]

ε_s silicon permittivity, [F/cm]

ν photon frequency, [sec^{-1}]

η conversion efficiency of solar cell

χ_{ox} oxide electron affinity, [eV]

χ_s silicon electron affinity, [eV]

σ_p capture cross section for holes, [cm^2]

τ_p life time of holes, [sec].

Abstract

In the present investigation, studies on MOS solar cells under concentration and at different temperatures were carried out. For this purpose, MOS solar cells were fabricated on n-type silicon with Au, Ag, and Cu as the barrier metals. High open-circuit voltages in excess of 450 mV were obtained on Ag solar cells. For Cu solar cells, V_{oc} was much less due to the lower barrier of Cu on n-type Si than Ag or Au. The shortcircuit current density for Ag and Au solar cells were found to be very high, the highest being 39.0 and 37.4 mA/cm^2 respectively without any ARC. For Cu solar cells, the shortcircuit current is lower than this and may possibly be improved with the help of suitable antireflection coating. The fill factor for Au and Ag solar cells were generally good, the highest being 0.68 for both. Cu solar cells had fill factors in the range of 0.55. Thus Au and Ag solar cells had efficiencies much higher than Cu solar cells. For gold devices, the highest efficiency was 7.8 percent while for silver devices it was 9.8 percent without ARC and under 1.0 Sun illumination. A maximum efficiency of 2.5 percent could be obtained for Cu solar cells. Moreover, dependence of the cell performance on different fabrication parameters was also established.

Au and Ag solar cells were studied under concentration and at different elevated temperatures because of their better performance at 1.0 Sun and room temperature. The cells were studied as such with no optimised grid contact or other modifications which have been found to be essential for operation under concentration. The opencircuit voltage increased rapidly in the begining and the

increase slowed down at higher concentrations. This was due to an increase in the oxide voltage following an increase in the interface state charge with concentration. Due to the absence of proper grid contact, the fill factor deteriorated with concentration. A reduction in the interface state density by careful fabrication steps would reduce the recombination current and the decrease in the fill factor. The opencircuit voltage of the devices would also then increase more rapidly at higher concentrations. The results of the present investigation are certainly encouraging in view of the simplicity of the cell structure. The overall efficiencies usually went down slightly at higher concentration but increased in one case. It was found that with optimised grid contact, it should be possible to operate these cells profitably at 50-100 Suns concentration.

The elevated temperature measurements were carried out to get an idea of the temperature range in which the cell can be effectively operated and to obtain a better understanding of the device physics. At higher temperatures, V_{oc} decreased at the rate of 1.60-1.85 mV/^{o}K and I_{sc} increased at the rate of 0.09 mA/^{o}K/cm^{2}. The rate of decrease of V_{oc} is less than what has been found earlier for p-n junction as well as MOS solar cells. This is advantageous for operation under concentration. The fill factor showed a non-linear decrease with temperature. The cell efficiency went down at a slower rate at temperatures close to the room temperature. Thus it was found that these cells can be effectively used in the temperature range of 300 to 330 ^{o}K without appreciable degradation in their performance. These changes were explained in terms of the changes in the diode current

and other device parameters.

Au, Ag, and Cu cells were also studied at the liquid nitrogen temperature primarily for better physical understanding of the devices. Despite some reduction in the light generated and hence in the shortcircuit current, the device performance improved significantly at the reduced temperature. The open-circuit voltage and the fill factor of the cells increased considerably with an enhancement of the device efficiency. For Au cells, the highest V_{oc} obtained at 77 ^{o}K was 710 mV, the highest fill factor 0.91 and the highest efficiency 16.3 percent. The principal reason for this was found to be a reduction in the diode current by many orders of magnitude at reduced temperatures.

1. INTRODUCTION

1.1 Schottky barrier solar cell

Solar cells utilizing homojunctions in Si and heterojunction in GaAs have already demonstrated their effectiveness in photovoltaic conversion of sunlight into electricity. Recent interest in photovoltaic devices originate from the possibility of using them for large scale terrestrial application. Because of the prohibitive cost of conventional p-n junction solar cells, other simpler structures are now being looked into as an alternative. Of these, the idea of a deposited metal/semiconductor junction, i.e. a Schottky barrier, seems to be attractive. Surface barrier devices have several advantages over conventional p-n homojunction devices in view of their simple structure and ease of fabrication. These have been discussed at length elsewhere [1,2]. Metal-silicon surface barrier photocells were first developed by Mayer [3] and Gartner [4] almost two decades back for use as solid state high-speed photo- and α-particle detectors. After a considerable gap, efforts were revived towards developing Schottky barrier solar cells (SBSC) for photovoltaic conversion. A 3.0 percent efficient SBSC using Au-n Si system was reported by Rupprecht and Pampanini [5]. On p-Si, Anderson et. al [6] reported a 2.0 percent cell using Cr as the barrier metal. The main drawbacks of these cells were low opencircuit voltages and poor conversion efficiencies.

1.2 Metal-insulator/oxide-semiconductor solar cell

Deliberate introduction of a thin insulating layer between the metal and the silicon was found to improve the opencircuit

voltage of the cell to a great extent without affecting the shortcircuit current [1,7-11,12]. Kar et. al [1] reported an efficiency of 8.0 percent with Au-n Si and 9.8 percent with Ag-n Si MOS solar cells. Using room air oxidation, they could obtain an opencircuit voltage of 440 mV for gold and 400 mV for silver solar cells. Lillington et. al [7] could increase the opencircuit voltage of an Au-n Si cell from 290 mV to 410 mV by using a thin interfacial layer. The overall efficiency of their Au-n Si MOS solar cell was 6.5 percent. Similar results have also been reported by others on both n- and p-type silicon using different barrier metals [8-11]. A wide variety of oxidation processes have been reported by these workers for better control over the oxide thickness and oxide properties. The interfacial layer should have a thickness less than 30 Å beyond which the tunneling of carriers through the oxide has been found to decrease rapidly [13]. Moreover, it should be devoid of pinholes and gross inhomogeneity and have a low interface state density. The highest reported value in the literature of the opencircuit voltage for Au-n Si system is 550 mV using a deposited oxide [8] and 444 mV using thermal oxide [12]. The highest value of the shortcircuit current density obtained so far with ARC is 40.0 mA/cm^2 [9] and that for the fill factor is 0.73 [8].

1.3 MOS solar cells under concentration and at different Temperatures

In the recent years, p-n junction solar cells under concentrated light have been the subject of considerable theoretical and experimental investigations. This certainty offers an attractive

alternative for reducing the cost of photovoltaic systems. By reducing the area of semiconductor devices required per watt of output power, the cost of electrical energy produced can be lowered substantially. For this, one has to concentrate sunlight on the cell and see that the efficiency of the cell at increased insolation is not very much deteriorated. Efforts in achieving this have been directed towards varying different design parameters of the cell and optimizing its performance. For p-n junction cells, these include an optimal grid contact, junction depth, and the base resistivity apart from different cell structure. Now that it is possible to obtain for MOS solar cells opencircuit voltages and efficiencies comparable to those for p-n junction solar cells, a systematic study of the former type of devices under concentration should be in order. Should this prove to be beneficial, MOS solar cells with their inherent advantage over their p-n junction counterpart may lower the cost of photovoltaic power generation further. As in p-n junction solar cells, the series resistance of these devices have to be minimized for operation under concentrated light. This requires an optimum grid contact on top of the thin metal layer, a proper choice of the back ohmic contact metal, the silicon resistivity, and the metal layer thickness.

Studies on p-n junction solar cells under concentration have amply been carried out during the last few years. Existing literature gives a detailed account of such studies [14]. These were carried out with a view to optimize the cell parameters under concentrated light for large scale terrestrial application. Information regarding the opencircuit voltage, the shortcircuit current, the fill factor and the efficiency were derived from the measured

I-V characteristics of the devices. Generally, the efficiency increased by a factor of 1.1 to 1.2 at about 10 Suns and then gradually decreased back to their one Sun efficiency at about 40-50 Suns. But a detailed study of these devices under concentrated light, which would bring out the possible variation of other physical parameters of the cells at increased illumination levels, is yet to be reported.

The effect of illumination on the shortcircuit capacitance of p-n homojunction solar cells have been studied by Berry[15] and Moore [16]. From considerations of excess minority carriers generated in the depletion region under illumination, Berry arrived at a simple formula relating the space charge layer width and the shortcircuit capacitance in dark and under illumination. The excess minority carrier density in the depletion region was found to be 10^{14} cm^{-3}. This additional charge was thought to have increased the capacitance of the cell and decreased the space charge layer width. However, his assumptions were contradicted by Moore, who showed that similar expressions could be derived assuming minority carrier concentration to be zero at the edge of the space charge layer. But neither of these workers measured the capacitance under illumination as a function of bias. Also the level of illumination was not raised above the Sun. If performed, these experiments could have provided information regarding any possible variation of the built-in-voltage and the carrier density with the level of illumination.

Till date no one has reported studies on MOS solar cells under concentrated light, though way back in 1962, Ahlstrom et.al [4] made a study of the silicon surface barrier photocells at different intensities and temperatures. The structure studied was

150 Å Au contact on n-type Si. The intensity was varied from 1 to 100 mW/cm^2 and the temperature from -200 °C to 40 °C. They reported approximately linear decrease of V_{oc} with temperature with $d V_{oc}/dT = - 2.5$ mV/°C, photocurrent density proportional to the the 0.88th power of the incident intensity and logarithmic increase of V_{oc} with light intensity. These results were able to indicate the nature of change of different cell parameters with changing light intensity and temperature. But from the point of gaining an insight into the device operation at higher insolations and temperatures, they were not of much help.

Anderson [17] has studied the current-voltage and the capacitance-voltage relationships at varying light intensities from 0 to 100 mW/cm^2 for n- In_2O_3/I/p-Si and n-SnO_2/I/n-Si heterojunction solar cells. He observed a photocurrent suppression in presence of a thin oxide layer and it increased with oxide thickness or illumination level. Thus he inferred that this would preclude the use of these or similar devices under concentrated light. It will be shown later that this certainly does not hold good for MOS solar cells studied by us. As argued by Kar [1], the interfacial oxide layer, if kept within a certain limiting thickness, does not cause any photocurrent suppression. This is because the diffusion time of the minority carriers through the bulk is much larger than their tunneling time through the oxide. Anderson also noted an increase in the device capacitance with illumination. He attributed it to a reduction in the silicon barrier due to increased trapped charges at the potential notch produced by the oxide. If the oxide layer is not too thick, such charge trapping at the interface may be absent due to reasons mentioned above.

Even then, the silicon barrier may reduce with increased intensity because of an increase in the interface state charge.

Dependence of the various cell parameters on illumination level have been studied for a Cu_2S/CdS solar cell by Bryant et. al [18]. They registered a linear increase of the light generated current with light intensity from 0 to 140 mW/cm^2. The open-circuit voltage also increased logarithmically and the fill factor showed a slight decrease with increasing light intensity. From the behaviour of some other parameters they indicated that the barrier height at the interface changed with intensity. A more definite way of reaching such a conclusions would have been to obtain the barrier height from a plot of $1/C^2$ against V at various illumination levels.

The motivation behind the present study becomes clear in light of the above discussion. In the first place, studies on MOS solar cells at concentration ratios greater than one have not been carried out so far. This is probably because of the notion that these cells will not be suitable for this purpose. However, such studies are necessary inorder to determine the possibility of using MOS solar cells under concentration. Secondly, a detailed study of these cells under concentration is necessary to determine the dependence of various physical parameters on the concentration ratio. It is important to know the performance of cells under concentration because they may show a strong deviation from the ideal behaviour. This has also not been carried out so far. It should be of considerable interest to study the effect of increasing incident energy on the various physical parameters such as the barrier height, the diode current, and the interface state charge.

All these parameters are not independent of one another and any change in one may be reflected in a change in the other. Thus, an insight into the operation of MOS solar cells under concentration can be gained from such an investigation.

Another important means of gaining an insight into the physical parameters responsible for the action of MOS solar cells is to study these devices at different temperatures. In some form or the other, such studies on p-n junction [19] and MOS solar cells have been reported in the literature. But a comprehensive study leading to a better understanding of the physics of the device is lacking.

Anderson and Vernon [20] have reported the effect of elevated temperatures on a 9.5 percent Al p Si MOS solar cell. They observed almost a linear decrease of the opencircuit voltage, the fill factor, and the efficiency of the cell with increasing temperature. These studies were made at an illumination level of 20 mW/cm^2. The shortcircuit current was found to increase at the rate of 0.005 $mA/cm^2/^oK$ over the temperature range of 25 ^oC to 125 ^oC. The reason for this was believed to be a 0.03 eV decrease in the bend gap due to 100 ^oC rise in temperature and a consequent improvement in the long wavelength response. But at an illumination of 100 mW/cm^2, the shortcircuit current may increase at a faster rate as has been observed in case of p-n junction solar cells [21]. The rate of decrease of the fill factor was 0.11 percent/^oK. This also may be different for increased illumination levels. The opencircuit voltage went down at the rate of 2.3 $mV/^oK$. The nonideality factor n of the device was found to decrease with rise in temperature so that the product nT was

independent of the temperature. From this they concluded field emission to be the dominant mechanism for current transport. But n may also change due to a change in the interface state density and have little to do with the current transport mechanism. Further evidence on tunneling currents was obtained by Anderson et. al [22] from a study on an 8.6 percent Cr-p Si MOS solar cell over a wide range of temperature. From a plot of the diode current against the reciprocal temperature at certain bias, they concluded that the temperature independent portions corresponded to a tunneling type mechanism. The temperature dependent portions were used to determine the barrier height.

Colbrie et. al [23] have performed similar temperature studies on an Al-p Si MOS solar cell using incident radiation of different frequencies. They observed about 9.5 percent change in I_{sc} for 100 ^{o}C rise in temperature. The change was independent of the generation site of the carriers. The decrease in V_{oc} with increasing temperature was explained on the basis of an increase in the diode current. This change was found to be in excess of 70 percent for 100 ^{o}C rise in temperature. They also suggested that devices with smaller barrier heights would show stronger degradation of V_{oc} with temperature increase. This has yet to be verified. Moreover, these workers did not attempt a detailed study of the device to determine the effect of temperature on various other cell parameters.

These studies were performed with a view that for terrestrial applications the cells would have to operate at elevated temperatures. This problem can be solved with efficient cooling of the device. Even then temperature studies are significant from the

point of view of setting the temperature range of operation and also getting a better physical understanding of the device operation. A knowledge of the device performance at elevated temperatures is necessary to get an idea about how effective the cooling system needs to be. Also, the effect of temperature on the various device parameters, such as, the barrier height, the diode current, and the interface state charge can be known and related to the observed changes in V_{oc}. Low temperature studies may not be relevent from the point of view of terrestrial applications. But they can be helpful for a better understanding of the current transport mechanisms at different applied bias. For example, at very low temperatures current may be dominated by recombination at low values of bias in absence of significant thermionic emission. But at higher applied bias, other mechanisms like tunneling may dominate.

1.4 Scope of present work

The objective of the present investigation has been to study SB/MOS solar cells under concentration and at different temperatures. Inorder to do so, initially SB/MOS solar cells were fabricated on n-type Si with Au, Ag, and Cu as the barrier metals. Various fabrication parameters like the metal layer thickness, the rate of deposition, and the oxide thickness were varied to improve device performance. Based on initial characterization at room temperature and under one Sun illumination, gold and silver cells were chosen for study under concentration and at different elevated temperatures. This would indicate the effectiveness of these devices for terrestrial application and lead to a better

understanding of the device physics. Low temperature studies on gold, silver, and copper solar cells were taken up with the aim of gaining an insight into the device operation.

2. THEORETICAL ANALYSIS

2.1 SB and MOS solar cells

The energy band diagram of a Schottky barrier solar cell under illumination has been shown in Fig. 2.1. The basic principle of its operation is that photons with energy higher than the bandgap of silicon excite electrons from the valence band to the conduction band. These photo-carriers are separated quickly by the built-in field produced by the metal silicon-barrier. The metal is in the form of a semitransparent film to let major portion of the incident light reach the junction. A photovoltage is thus generated which tends to forward bias the device resulting in a diode current I_D. The latter can be seen as the reflection of the photocarriers by the photovoltage. For better performance of an SBSC one should choose a metal which would give a high barrier either on n or on p-type silicon. Also the series resistance of the device, which can have contribution from the spreading resistance of the front metal contact, the bulk resistance, the grid resistance, and the back contact resistance, have to be minimized. Like all solar cells, an SBSC is also characterized by the open-circuit voltage, the shortcircuit current, the fill factor and the efficiency. A suitable choice of various design parameters would lead to an enhancement of these factors and a better performance of the device. This has amply been investigated in the recent years [1,2,6,24].

While all practical metal-silicon contacts are inevitably separated by a thin layer of silicon oxide ($\simeq 10$ Å), a slightly

thicker oxide has been shown theoretically [25-27] and experimentally [7-10,28] to improve the cell performance. The MOS solar cell thus formed has a large reduction in the diode current and a consequent increase in the opencircuit voltage for a given photogenerated current. As has been depicted in Fig. 2.2, the majority carriers overcome the silicon barrier by thermionic emission and the oxide barrier by tunneling. The mechanism of carrier transport through the oxide becomes very significant because of this. The resulting thermionic tunneling current density J_{TT} constitutes the major part of the diode current and can be written as [27]:

$$J_{TT} = T_{ox}(V) A^* T^2 \exp[-q(\varphi_i + \Phi_n)/kT], \qquad (2.1)$$

where the various symbols have the meanings as listed earlier. In absence of a significant contribution from the recombination-tunneling current via interface states, at opencircuit the light generated current can be equated to the thermionic-tunneling current. An expression for the opencircuit voltage has been obtained by Kar [27,28] from these considerations. This becomes

$$V_{oc} = \varphi_i^o + \Phi_n + (kT/q) \ln (J_L/T_{ox}^{oc} A^* T^2) + (V_{ox}^o - V_{ox}^{oc}). \qquad (2.2)$$

With the help of relations,

$$\varphi_i^o + V_{ox}^o = \varphi_i^{oc} + V_{ox}^{oc} + V_{oc} = (\Phi_{MS}^*/q) - \Phi_n,$$

equation (2.3) can be written as [28],

$$V_{oc} = (\Phi_{MS}^*/q) + (kT/q) \ln (J_L/T_{ox}^{oc} A^* T^2) - V_{ox}^{oc}. \qquad (2.3)$$

With increasing oxide thickness, T_{ox}^{oc} reduces and brings about an increase in the opencircuit voltage. Also, depending upon the fabrication parameters, φ_i^o may increase with t_{ox} due to rapid reduction of the interface state density [29]. This would contribute towards an increase in V_{oc}. But beyond a certain limiting thickness the tunneling time of the minority carriers through the oxide becomes larger than their diffusion time through the bulk and the solar cell ceases to function effectively [27].

Some of the elements mentioned in the theories proposed by Fonash [25] and Card et.al [26] are contained in the above theory but with appropriate modifications. The idea of diode current reduction by the tunneling transmission factor of the oxide barrier occurs in the theories put forward by Fonash as well as by Card and Yang. These authors made simple assumptions regarding the oxide barrier height and the oxide thickness in calculating the tunneling transmission factor T_{ox} and treated it as a constant. But as discussed by Kar [27], the barrier height and the thickness of very thin oxide layers on silicon could be influenced by a multitude of factors like the variation in O/Si ratio and the image force effect. Moreover, T_{ox} will critically depend on the oxide potential and be a strong function of the applied bias [27]. Hence, in real MOS solar cells, a straight forward calculation of T_{ox} may not be an easy task. Fonash also suggested the possibility of enhancing V_{oc} by creating a large voltage division across the oxide and the semiconductor barriers. But as pointed out by Kar [27], the zero bias silicon band-bending will also be reduced at the same time that $(V_{ox}^{o}-V_{ox}^{oc})$ is

increased. Also, the idea of increasing the silicon barrier height by introducing fixed charges in the oxide may work for p-type silicon alone because so far it has not been possible to introduce negative fixed charges into thermal silicon oxide. In his theoretical calculations Fonash considered the influence of different parameters on dark I_D-V characteristics and predicted an enhancement in V_{oc}. But it has been shown experimentally [1,28] tha the diode current under illumination differs from its value in dark owing to an increase in the interface state charge. This happens because under illumination, the minority carrier quasi Fermi level dictates the interface state occupancy and the oxide voltage is increased [27]. This is in direct contradiction to the argument of Card and Yang[26] who maintain that the oxide voltage becomes negligible under illumination. Those authors considered only the change in the tunnel transmission factor to be influenced by the interfacial oxide layer. But under suitable fabrication conditions, the zero bias silicon band bending may also be increased [29].

2.2 MOS solar cells under concentration

As the level of illumination incident on a solar cell is raised, the photon flux responsible for generating the electron-hole pairs is multiplied. Provided that the spectral distribution of the light remains unchanged and the collection efficiency of the device is independent of the photon density, this would produce a linear increase in the light generated current. At sufficiently high intensities, the effect of high level injection

may show up. Under such conditions, when the photogenerated carrier density becomes comparable to the base doping level, the base life time may increase. If the series resistance effects are small, this may cause superlinear increase of the photocurrent with light intensity [30]. Also the shortcircuit current would increase linearly with the light intensity if the series and the shunt resistance effects are small.

The opencircuit voltage of an MOS solar cell has been expressed in terms of the various device parameters in equation (2.3). This expression has been derived [27,28] assuming that the recombination tunneling current is zero so that at opencircuit, $J_D^{oc} = J_{TT} = J_L$. Also implicit is the assumption that $R_s = 0$. Thus with increase in J_L due to an enhanced incident radiation, the opencircuit voltage of the device should go up. But an exact dependence of V_{oc} on the concentration ratio is difficult to predict because T_{ox}^{oc} and V_{ox}^{oc} are also strong functions of illumination level.

With enhancement of V_{oc} one would expect an improvement in the fill factor of the cell. But in many practical devices, the series resistance causes the fill factor to go down with increased illumination. This is due to the increased drop across it under concentrated light and inorder to keep the drop same at higher concentration levels, the series resistance should be reduced by a factor of C. The recombination current, which is likely to be present at low values of forward bias under illumination, also may contribute to the reduction of the fill factor.

The overall efficiency of the cell may increase, remain the same, or decrease with increasing concentration depending

primarily on the behaviour of the fill factor. If the reduction in the fill factor is compensated by the increase in the open-circuit voltage, the efficiency of the device will more or less remain constant. At higher concentrations, when the fill factor is likely to decrease faster, reduction in the efficiency is expected.

To understand the effect of increasing illumination on the diode current and various other devide parameters, the energy band diagram in Fig. 2.2 of an MOS solar cell under illumination has to be referred to. In dark, the major contribution to the diode current comes from the thermionic-tunneling current density J_{TT}, the recombination-tunneling component J_{RT} being small. Under illumination, this can be enhanced either due to a large recombination current or a lowering of the silicon band bending or a combination of both [27]. The bulk recombination current increases following a much faster generation rate of the minority carriers in the quasi-neutral region. The communication time of the carriers with the interface states depends upon the rate at which they are supplied to the interface. Under illumination, this rate is much faster than in dark. In addition, as the minority carrier density at the interface increases with illumination, minority carrier recombination at the interface is enhanced. Consequently, the interface state occupancy under illumination is increasingly influenced by the minority carrier quasi Fermi level while the majority carrier quasi Fermi level dictates it in dark [27]. For n-type silicon, the interface state charge becomes more positive as a result and the oxide voltage increases. Since for an MOS solar cell, $\varphi_i^o + V_{ox}^o = (\Phi_{MS}^*/q) - \Phi_n$, the zero bias silicon band

bending decreases under illumination. This causes an enhanced transport of the majority carriers over the silicon barrier, resulting in an increase in the diode current I_{TT}. As more intense light is shone upon the cell, the recombination current further increases due to a larger number of photogenerated carriers available. Also, the minority carrier quasi Fermi level shifts towards the minority carrier band edge. This produces further increase in the interface state charge and hence in the oxide voltage. As a result, the silicon band bending keeps on getting reduced under concentration resulting in enhanced diode currents. These tend to neutralize the increase of V_{oc} due to multiplication of J_L. From equation(2.3), it can be seen that the increase in V_{ox}^{oc} would, to some extent, check the increase of V_{oc} with J_L. The opencircuit voltage, therefore, tends to saturate at high concentrations and if V_{ox}^{oc} increases at a fast rate, V_{oc} may decrease at higher insolations.

The diode I_D-V plots of the device in dark and under various concentrations reveal these facts. The opencircuit voltage corresponds to the forward bias at which the diode current equals the shortcircuit current. Its value obtained from the dark I_D-V characteristic is always higher than that obtained from the characteristics under illumination. At higher concentrations, the opencircuit voltage may correspond to the series resistance dominated portion of the I_D-V plot. This slightly increases the value of V_{oc} from the one that would have been obtained had the I_D-V plot been exponential upto the opencircuit voltage. Thus the detrimental effect of the increasing diode current can be somewhat

compensated by the series resistance, however the fill factor deteriorates.

The effect of illumination on the device capacitance is to increase its value from that in dark. This is expected owing to a decreasing silicon band bending and a reduced space charge layer width. The device capacitance would increase monotonically as the concentration ratio is increased due to reasons discussed above. The density of photo-excited minority carriers, though mainly generated in the quasi-neutral region, does not in fact reduce to zero at the depletion layer edge. Under illumination there is always an excess minority carrier concentration in the depletion layer. This can add up to the ionized dopants to account for all the charge in the space charge layer. Hence the slope of $1/C^2$-V plot would give the total density of the charge carriers and not the bulk doping density. Since with concentration the minority carriers generated keeps multiplying, the slope of $1/C^2$-V plot would decrease continuously and indicate enhanced depletion layer charge density.

2.3 MOS solar cells at different temperatures

The diffusion length L_p and the absorption coefficient α are two important physical parameters which can influence the behaviour of silicon MOS solar cells at elevated or reduced temperatures. The diffusion length has its temperature dependance through the diffusion coefficient and the life time according to the relation $L_p = \sqrt{D_p \tau_p}$. The diffusion coefficient, in turn, is related to the carrier mobility through the Einstein relationship $D_p = \mu_p . kT/q$. The minority carrier mobility is determined by a

parallel combination of lattice scattering, which varies as $T^{-3/2}$ and ionized impurity scattering which varies as $T^{3/2}$. For Si cells with doping level below 10^{17} cm^{-3}, the mobility decreases somewhat with increasing temperature [31]. Consequently, D_p decreases slightly with temperature [31]. A simple expression for life time of the minority carriers can be written as $\tau_p = 1/\bar{v}\ \sigma_p\ N_t$. In Si, the life time has been found to increase several fold with increasing temperature in the -150 to 150 ^{o}C range for both n- and p-type samples [32]. The combined effect of the life time and the diffusion coefficient with increasing temperature is reflected in an improvement of the minority carrier diffusion length. This proves to be beneficial so long as $L_p < W$, W being width of the sample. At lower temperatures, the diffusion length is likely to reduce. Silicon being an indirect bandgap material, phonons are required during band to band transitions. As the temperature goes up, the phonon density increases and the absorption coefficient of silicon in the wavelength of interest shows an increase [31]. All these factors contribute towards improving the light generated current in a silicon solar cell as the temperature is increased. Conversely, a decrease in the temperature should cause the light generated current to go down.

The opencircuit voltage of an MOS solar cell is expected to go down rapidly with increasing temperature as predicted by $T^2 \exp - [q(\varphi_i^{oc} + \Phi_n)/kT]$ term in the diode current. Reverse is true for a decrease in the temperature. A simple expression giving the rate at which V_{oc} changes with temperature can be obtained by differentiating equation (2.3) with respect to T. Neglecting the possible temperature dependence of T_{ox}^{oc} and V_{ox}^{oc} for simplicity,

we obtain,

$$dV_{oc}/dT = (k/q) \ln (J_L/T_{ox}^{oc} A^* T^2) + (kT/q)(1/J_L)(dJ_L/dT) - (2k/q). \quad (2.4)$$

The contribution from the second term is very small and for an SBSC, it one takes $T_{ox}^{oc} = 1$ and $J_L = 40$ mA cm^{-2}, then the contribution from the first term becomes -1.66 mV/^{o}K for T = 300 ^{o}K and -1.71 mV/^{o}K for T = 400 ^{o}K. The slight variation is due to the variation of lnT with T. The last term equals to 0.17 mV/^{o}K. Hence dV_{oc}/dT is expected to be within -1.8 to -1.9 mV/^{o}K without contributions from the second term, which can only be determined experimentally.

The fill factor of the device is expected to follow the same trend as the opencircuit voltage, i.e. it decreases with increase in temperature and increases when the temperature is lowered. The change in the diode current has been found to have pronounced effect on the fill factor of an MOS solar cell [28]. As it degrades with rise in temperature, the shortcircuit current tends to deviate from the light generated current. In this situation, the shortcircuit current may not vary linearly with temperature.

The overall efficiency of the device would depend upon all the aforesaid factors and a straight forward relationship of its change with temperature may be difficult to predict. However , it can be said in general that the efficiency would go down with increase in temperature. This is because the increase in the shortcircuit current is not likely to out-weigh the decrease in V_{oc} and the fill factor.

The diode current in an MOS solar cell can also increase due to a reduction in the silicon band bending with increasing temperature. This may occur due to an increase in the interface state charge as the majority carrier Fermi level moves towards the mid-gap at elevated temperatures. The oxide voltage increases and the silicon band bending is reduced as a result. At low temperatures, the opposite is likely to happen producing an increase in the silicon band bending. The device capacitance may be influenced by this change in the silicon barrier and hence in the depletion layer width. One can expect a higher capacitance at higher temperatures and the density of ionized impurities is not likely to change except at very low temperatures when the ionization may be incomplete.

3. EXPERIMENTAL PROCEDURE

3.1. Fabrication of SB/MOS solar cells

The essential steps involved in the fabrication process and their sequence are outlined in Fig. 3.1. For Schottky barrier solar cells, these are surface cleaning, back ohmic contact evaporation and evaporation of thin barrier metal at the front followed by evaporation of thick contact pad. Fabrication of MOS solar cells consists of an additional step, namely growing an interfacial oxide layer. All the fabrication steps were carried out in clean room environment using clean benches and vacuum systems equipped with liquid nitrogen traps to ensure better reproducibility and device performance.

3.1.1. Surface cleaning

Since it is the starting process in the fabrication process, surface cleaning is perhaps the most critical among all the fabrication steps. The processing was carried out on monocrystal silicon wafers with <111> crystal orientation. These had one side polished and the other lapped, thickness of about 250 microns and resistivity ranging from 0.2 to 13.0 Ohm.cm. with boron doping Surface cleaning consisted of degreasing with organic solvents and etching with acids in a clean chemical bench. The steps followed in sequence are listed below.

i) The wafer was treated in warm trichloroethylene for about 2 minutes to remove greasy materials, if any, from the wafer surface and then in warm acetone for 2 minutes to remove traces of trichloroethylene. This was followed by warming in methanol

for 2 minutes to remove traces of acetone.

ii) The degreased wafer was then rinsed in deionized water and etched in HF to remove ahy oxide layer present on the wafer surface.

iii) This was followed by rinsing the wafer several times in deionized water to remove traces of HF.

iv) An oxide layer 50-60 Å thick was then grown on the clean silicon surface by treating it in warm HNO_3. This step was necessary to reduce any possible mechanical damage on the silicon surface.

v) The wafer was then rinsed in deionized water several times to remove traces of HNO_3.

vi) The grown oxide layer was finally etched off in HF, thus reducing the mechanical damage on the wafer surface.

vii) Finally the wafer was rinsed several times in deionized water to remove traces of HF.

The steps (iii) and (v) were necessary to prevent any chances of the silicon surface getting etched for this would damage the flatness of the surface. The cleaning, if properly carried out, should render the polished surface hydrophobic, i.e. there should not be any beads of water sticking anywhere on the polished surface. After this had been achieved, the wafer was ready for further processing.

3.1.2. Metallization

The metallization step consisted of evaporation of the back ohmic contact, the front barrier metal and the thick metal pad from tungsten filament sources in a vacuum system equipped with

rotary oil pump and oil diffusion pump. While majority of the devices were fabricated in a vacuum system (Grainville phillips Co. USA, series 252) having a digital quartz crystal thickness monitor (Perkin Elmer, USA, Model 605-1210), some of the initial fabrication was carried out in a Hind High Vacuum Company, Model 12A4 vacuum system. The latter had a greater leak rate than the former and no in-process thickness monitoring arrangement. Liquid nitrogen traps were always used with rotary and diffusion pumps to reduce contamination from oil vapours.

The metals evaporated on n-type silicon were Au, Ag, and Cu for the front barrier and Al and Cr for the back ohmic contact. Earlier work [1,2] had established the superiority of these metals over others as better barrier and back ohmic contact metals respectively, on n-type silicon. Whenever Cr was used, it was covered with a protective layer of Au to avoid oxidation. The metals had 5N purity and were obtained in form of wires, 1.0 to 1.5 mm in diameter. Cr could be obtained only in form of small pellets and while most of these metals melted before evaporation, Cr slowly sublimed. Evaporation data of different metals have been listed elsewhere [1]. Au and Al on melting wets tungsten filament easily and hence could be evaporated from tungsten helix. In fact, Al alloys with tungsten after melting and chances of contamination from the filament increases. Cu could be evaporated from a conical basket. But for Ag, which does not wet tungsten, a tiny piece of molybdenum was used to plug the bottom of the basket to hold the charge. Since different metals evaporated in the same system, precautions to avoid cross contamination were taken.

The tungsten filaments were thoroughly degreased in trichloroethylene, acetone and methanol prior to outgassing in vacuum by passing currents higher than that needed for evaporation. The metals with the exception of Cr, were taken in the form of wires of about one inch in length and thoroughly degreased in warm trichloroethylene, acetone and methanol before loading into the chamber. These were first melted by slowly increasing the current through the filament while a shutter was placed in between the filament and the substrate. The source to substrate distance was always kept more than 10 cm so as to reduce substrate heating and to have a more uniform film. Evaporation on the polished silicon surface through aluminum masks with holes of different diameters was then accomplished by removing the shutter and increasing the current to the required value. The rate of deposition could be controlled by controlling the current and reading it off from a digital display. Its value during formation of the thin barrier metal layer was usually held around 1.0 Å/sec for Au and Cu. The barrier metal contact was 1.0 or 2.0 mm in diameter and had thickness in the range of 40-100 Å. The slow evaporation rate was to ensure better structural properties of the evaporated film [33]. But for Ag thin films the rate of deposition was kept around 2.0-6.0 Å/sec since these films have been reported to have better electrical properties when the deposition rate was high [34]. It will be shown later that this has also been borne out by our investigation.

The thick contact pad with diameter of 0.5 ot 1.0 mm depending on the diameter of the thin dot, was deposited in the

middle of the latter through aluminum masks. It was observed that the thick dot, if evaporated partly on the thin dot and partly on the bare silicon, causes a reduction in the opencircuit voltage of the cell. This could be due to a reduced metal silicon barrier height for the thick metal pad on the polished face of the wafer. V_{oc} was found to increase to the expected value after removal of the shorting caused by the thick dot. The rate of deposition for the back contact and the thick dot was kept at around 10.0 Å/sec. During all evaporations, the chamber pressure was kept well below 1.0×10^{-5} torr.

3.1.3. Oxidation

Oxidation of the silicon surface was mostly carried out in clean room air and at room temperature. This was done immediately after deposition of the back ohmic contact. Room temperature oxidation of silicon surface has been reported in the literature [35] and successfully employed in the fabrication of silicon MOS solar cells [1,36]. Oxidation time was varied in between 40-90 hrs since it has been reported [1,2] that an interfacial layer of thickness in the vicinity of 20-24 Å is best suited for improving the solar cell performance. During oxidation, the wafers with back contact were kept in a clean weighing bottle.

3.2. Measurements

3.2.1. Oxide layer thickness, metal layer thickness and transmittance

Bare silicon surface grows an oxide layer, about 10 Å thick upon exposure to room air at room temperature. Subsequent increase in oxide thickness bears a parabolic relationship to the time as

has been measured with an ellipsometer and reported in the literature [35]. These empirical data were used to obtain an idea about the oxide thickness, though these values may not be very accurate.

Th metal layer thickn ss were obtain d from the digital display of the quartz crystal thickness monitor. To find the transmittance of the deposited films, deposition was made on clean glass slides at various rates. The shortcircuit currents of a standard OCLI solar cell were then measured under AMI illumination with and without glass slides in between the tungsten lamp and the cell. The transmittance on glass slides of the metal films could be obtained from this assuming the shortcircuit current to be proportional to the transmitted light intensity. Correction for the transmittance of a bare glass slide was made for more accurate data. However, these transmittance values may be different for the metal films on silicon.

3.2.2. Characterization of the solar cells

The solar cells fabricated were characterized by measuring the photogenerated current-voltage characteristics, the diode current at different values of the applied bias and the capacitance-voltage characteristics both in dark and under illumination. These measurements were carried out at room temperature for initial characterization. Subsequently, some of the devices were measured under concentration and at different temperatures.

3.2.2.1. Room temperature measurements

The device was placed on a copper block with a finely machined top surface, which formed one contact terminal. The

other contact was made from the top on the thick metal pad at the front with the help of a telescopic spring probe. To prevent temperature of the cell from going up during measurements under illumination, the copper block was kept partially submerged in a constantly circulating pool of water at room temperature. Care was taken to prevent any lateral movements of the block after the top contact was made. A tungsten filament lamp was used to simulate AMI illumination in the laboratory, the illumination level being checked with the help of a standard OCLI solar cell. For measurements in dark, the whole set up was enclosed in a shielded light tight box.

3.2.2.2.Measurements under concentrated light

The level of illumination could be increased from 1.0 Sun to about 11.0 Suns with the help of a special tungsten filament lamp whose intensity could be changed by varying the voltage through a variac. At higher concentrations, water had to be circulated at a faster rate around the copper block to prevent any temperature rise. The temperature of the front surface of the cell was assumed to be the same as that of the copper block, though this may not really hold good as has been observed by Goradia et. al [37]. The temperature of the water was monitored with a thermometer. Care was taken not to let the water come in contact with the cell in which case the back contact had the chance of getting damaged.

3.2.2.3. Measurements at different temperatures

A simple heating arrangement consisting of two polished brass discs with a heating element wound on a mica sheet in between was employed. This was placed in a hollowed out teflon block in which it fitted closely. The cell was placed on top of the upper brass disc, the temperature of which could be accurately measured with the help of a chromed-alumel thermocouple and a Leeds and Northrup type 8691 millivolt potentiometer. Measurements were made only after the temperature had stabilized. Deviations from this temperature when the set up was used under illumination were checked. The illumination level was held constant during a particular set of measurements. Low temperature measurements could not be made due to the problem of undesired increase in the diode current because of condensation of moisture on top of the cell at near zero temperatures or reduction of the shortcircuit current because of ice formation at subzero temperatures. However, measurements at liquid nitrogen temperature could be made by placing the copper block mounting the cell in a styrofoam encasing and pouring liquid nitrogen into it till the temperature had stabilized. Free evaporation of nitrogen gas mostly prevented formation of ice on top of the cell. For each of the set ups described above, the following measurements were made on the solar cells.

3.2.2.4. Current-voltage measurements

The photogenerated current-voltage characteristics of the device were measured using a set up, the circuit diagram of which is shown in Fig. 3.2(a). The load across the outer terminals

to be varied to get the current and the corresponding voltage. From the plot of current against voltage on a linear graph, various parameters like V_{oc}, I_{sc}, η and F characterizing the cell could be obtained as has been the usual practice.

The circuit diagram of the set up used for measuring the diode currents at various values of the applied bias is depicted in Fig. 3.2(b). Measurements were made both under illumination and in dark. The diode currents under illumination were found by subtracting the terminal currents from the shortcircuit current. These along with the device current in dark were plotted against the voltage on a semilogarithmic graph. The diode nonideality factor n was found at different values of the bias according to the relation, $n = (q/kT)(dV/d \ln I)$.

The opencircuit voltage was obtained from the I_D-V characteristics by reading the forward voltage at which the diode current under illumination was equal to the shortcircuit current. The series resistance was obtained from the linear range of the dark I-V characteristics. For SB solar cells, the reverse saturation current was obtained by extrapolating the exponential region in the I_D-V plot to zero bias. This was used to determine the barrier height and hence the opencircuit voltage from $V_{oc} = n\,(\Phi_B - 0.5\ V)$.

3.2.2.5. Capacitance-voltage measurements

The capacitance-voltage characteristics were measured using a Boonton 94C-S18 model capacitance bridge and Yamuna 1010 digital voltmeter as schematically depicted in Fig. 3.2(c). The

measurement frequency was fixed at 100 kHz and the ac voltage of the bridge was adjusted to 14-15 mV peak-to-peak so as not to cause much inaccuracy due to the non-linear charge-voltage characteristics of the device. The device capacitance was measured starting at high reverse bias, going towards zero-bias at regular bias intervals, and then at small values of forward bias. The plot of squared reciprocal of the capacitance against the bias was a straight line, the slope and the intercept on the bias axis of which could be related to the doping density and the zero bias silicon band bending respectively by the relations [1]:

$$N_D = 2/(q.\varepsilon_s.d(1/C^2)/dV) \text{ and } \Phi_n = (kT/q)\ln(N_C/N_D)$$

and $\varphi_i^o = V_{intercept} - (kT/q)$ for n-type silicon.

Subsequently, the silicon barrier was obtained from,

$$\Phi_B^n = \varphi_i^o + \Phi_n \quad \text{for n-type silicon.}$$

4. RESULTS AND DISCUSSIONS

4.1 Room temperature measurements on Au, Ag, and Cu SB/MOS solar cells

4.1.1. Gold solar cells

Solar cells with gold as the barrier metal were fabricated on n-type single crystal silicon wafers with bulk resistivity of 3-7 Ohm.cm. All these cells had Al back ohmic contact. Table 4.1 presents a summary of the experimental values of important parameters of these cells. The metal layer thickness was varied from 40 to 60 Å since Au films in this thickness range have been found to be continuous [1]. This, in general, resulted in high shortcircuit current densities. The highest shortcircuit current density obtained without ARC has been 37.4 mA/cm^2. The effective areas of the devices were measured under a microscope. The rate of evaporation was in between 1-2 Å/sec. The values of transmittance were obtained from the measured data of films deposited on glass slides. Figure 4.1 presents a plot of the transmittance against the metal layer thickness for different deposition rates of Au films on glass slides. The transmittance for metal films on silicon may be different from these values, and therefore the values of T in Table 4.1 may not always correspond to the measured shortcircuit current density. The opencircuit voltages for these devices were around 300 mV at room temperature which is expected for devices with t_{ox} in the vicinity of 10-13 Å. The highest value of V_{oc} obtained was 347 mV for a device with t_{ox} approximately equal to 16 Å. The devices, in general, show a reasonably good fill factor in the vicinity of 0.60, the highest being 0.67.

Inspite of the low opencircuit voltages, the overall efficiencies for these devices ranged from 5.0 to 7.8 percent. The value of the series resistance obtained from the linear portion of the diode current-voltage plot is generally low, the lowest value obtained so far being 0.09 Ohm for an area of 1 cm^2.

The measured I-V characteristics for some of these devices have been presented in Fig. 4.2. Figures 4.3 and 4.4 depict the diode current-voltage plots for devices Au 21 and Au 29 respectively. While the former device shows near ideal exponential relationship with n = 1.33 in dark, the latter shows significant deviations from it. For this, the factor n is a function of the bias and an exponential current-voltage relationship is absent. In case of device Au 21, both the dark and the illuminated characteristics are essentially exponential upto the opencircuit voltage. The diode current under illumination does not differ much from its value in dark. The values of the zero bias silicon band bending in dark and under illumination have been obtained from the reverse saturation currents. These values agree well with those obtained from the $1/C^2$-V plots, cf. Tables 4.2 and 4.3. These data indicate that the oxide is largely transparent to the majority carriers and that the metal Fermi level is pinned to the interface states. Also the value of V_{oc} obtained from the values of n and Φ_B^n under illumination matches quite well with that obtained from the I-V characteristic. On the other hand, in case of device Au 29, the barrier heights could not be obtained from the ln I_D-V plots due to a non-exponential behaviour. Also under illumination, the diode current is much larger than that

in dark which may result from a large density of recombination current and a lowering of the silicon barrier under illumination, cf. Table 4.3. Table 4.2 contains the data obtained from the I_D-V plots. It can be seen that n at $I_D = I_{sc}$ under illumination is usually greater than or equal to its value in dark. In some cases, n increases with the opencircuit voltage but this is not valid always. The values of opencircuit voltage obtained from the forward voltage, for which $I_D = I_{sc}$, generally match with the observed values only under illumination.

Table 4.3 gives the values of the doping density and the silicon band bending at zero bias obtained from the measured capacitance data. Two typical $1/C^2$-V plots for devices Au 15 and Au 29 are presented in Fig. 4.5. From this as well as from Table 4.3, it is evident that a higher band bending under illumination corresponds to a higher opencircuit voltage which is expected from equation 2.2. Also, the silicon band bending goes down under illumination due to an increase in the interface state charge [27], and the doping density values agree well with those obtained from the resistivity data.

4.1.2 Silver solar cells

The results of measurements on typical Ag solar cells have been summarized in Tables 4.4-4.6. The cells had aluminium as the back ohmic contact, and the effective areas as indicated below Table 4.4. The silicon resistivity was 3-7 Ohm.cm. It can be seen from Table 4.4 that high opencircuit voltages in excess of 450 mV can be achieved for these cells. Figure 4.6 presents the measured I-V characteristics for solar cells Ag 18, Ag 10, Ag 35,

and Ag 15. The rate of evaporation during the deposition of the barrier metal layer was in between 2-7 Å/sec. This gave better fill factors along with high opencircuit voltages. High short-circuit current densities were obtained even with relatively thick metal layers. In case of device Ag 7 which had a film thickness of 42 Å, the shortcircuit current density without ARC reached 39.1 mA/cm^2. This compares very well with the highest reported value of 40 mA/cm^2 for J_{sc} in the literature [9]. This indicates that Ag thin film have a high transmittance. On the other hand, when the metal deposition rate was below or around 1.0 Å/sec, the fill factor was poor. This shows that higher deposition rates for silver give better electrical properties of the devices. The reason may be that recrystallization of silver films is favoured under such conditions[34]. Silver solar cells exhibited high efficiencies and the highest obtained so far is 9.8 percent under AM1 insolation and without ARC. This compares fairly well with the results obtained earlier on Ag [1] and Au [8] MOS solar cells. The series resistance in most of the cases could not be found out from the diode current-voltage plot in dark due to the absence of a linear region. But its value for the devices, where it was possible to calculate it, has been found to be low, cf. Table 4.4. The opencircuit voltage for device Ag 27 showed an increase with time after the contact had been made with the spring probe. It increased from an initial value of 460 mV and saturated at 498 mV. All the measurements on this cell were made after this. Though the reason for such a phenomenon is not clear at this stage, a large density of interface state might be,

in some way or the other, related to it. However, an opencircuit voltage of 498 mV is the highest value so far reported for MOS solar cells on n-type Si using non-deposited oxides. The low shortcircuit current density for this device is due to a 95 Å thick metal layer and the poor fill factor may be due to a high series resistance. At this point, it may be mentioned that had the highest value of V_{oc}, F, and J_{sc} been obtained on a single device, an effieiency of 12.9 percent would have been possible without ARC under AM1 illumination.

Table 4.5 lists the data obtained from the diode current-voltage characteristics for some of the silver solar cells. A typical such plot for device Ag 16 has been presented in Fig. 4.7. This shows a double exponential type relationship for the dark diode current-voltage characteristics. The factor n for lower values of forward bias is more than that at higher bias values. The reason may be a predominant recombination current component at lower values of the bias. Using the linear range at higher bias region, the series resistance of the cell was calculated. This came out to be 0.18 Ohm.cm^2 which is the lowest value of the series resistance obtained on silver solar cells and its effect is reflected in the high value of the fill factor for the device. The diode current under illumination is not much different from that in dark. The values of n and the opencircuit voltages obtained from the I_D-V plots for Ag solar cells follow the same trend as in case of Au devices. The discrepancy in the value of V_{oc} obtained from I-V and I_D-V plots for someof the silver cells could have been due to a change in the device characteristics with time.

The doping density and the silicon band bending as obtained from the measured capacitance have been listed in Table 4.6. Two typical $1/C^2$-V plots for devices Ag 21 and Ag 16 have been presented in Fig. 4.8. The doping density, in general, is well within the range obtained from the resistivity data. The silicon band bending φ_i^o at zero bias as well as $\varphi_i^o + \Phi_n$ under illumination increase with the oxide thickness. This partly explains the increase in the opencircuit voltage with the oxide thickness. Also reduction in T_{ox}^{oc} with increasing oxide thickness is likely to contribute towards enhanching V_{oc}. But as suggested elsewhere [28], the barrier metal also may influence the oxide potential barrier profile, change T_{ox}^{oc}, and modulate its influence on V_{oc}. Even for the same barrier metal, contribution of T_{ox}^{oc} will vary from one MOS solar cell to the other depending on the fabrication steps.

4.1.3 Copper solar cells

The experimental results obtained on Cu SB/MOS solar cells have been listed in Tables 4.7-4.9. Like Au and Ag solar cells, these devices were also fabricated on n-type single crystal silicon wafers. The resistivity of silicon for devices Cu 3 and Cu 27 was 3-7 Ohm.cm, for devices Cu 10, Cu 13 and Cu 16 it was 7-13 Ohm.cm, while for device Cu 17 it was 0.2-1.0 Ohm.cm. Device Cu 10 had Cr-Cu and device Cu 13 had Cr for back ohmic contact. Devices Cu 3 and Cu 27 had Al and devices Cu 16 and Cu 17 Cr-Au back contact.

The opencircuit voltage is low for these cells and this is expected because of a lower barrier for Cu on n-type Si than that

for Au or Ag. However, data in Table 4.7 shows that with increasing oxide thickness V_{oc} increases. The shortcircuit current density for these cells is lower than that for Au or Ag cells. This is not unexpected since Cu thin films have lower transmittance compared to Au and Ag thin films. The current can be enhanced by a suitable choice of antireflection coating. These cells have low series resistance. But even then the fill factor is not very good due to low opencircuit voltage of the devices. Measured I-V characteristics of devices Cu 13 and Cu 3 are presented in Fig. 4.9.

Figure 4.10 depicts the diode current-voltage characteristics of device Cu 27 which had a 10 Å thick oxide. The other diode current-voltage characteristics on the same figure correspond to the measurements at the liquid nitrogen temperature. This will be discussed later. At room temperature, the behaviour is essentially that of a Schottky barrier with n equal to 1.04 in dark as well as under illumination. The diode current under illumination is not very different from that in dark indicating low interface state density. The barrier height obtained from saturation current data agrees well with that obtained of $1/C^2$-V plot under illumination, cf. Table 4.8 and 4.9. Almost similar results have been obtained for device Cu 3 which also had a 10 Å thick oxide [1]. But the diode current-voltage characteristics for device Cu 13 with 20 Å thick oxide were found to be somewhat different from those for Cu 3 or Cu 27. In this case, n is higher and the characteristics far from ideal. The barrier height could not be calculated from the saturation current data because of this. The difference between the diode currents in dark and

under illumination is also large. Table 4.8 which presents data similar to those in Tables 4.5 and 4.2 shows that n at $I_D = I_{sc}$ increases with oxide thickness. Also the values of V_{oc} obtained from the forward voltage for which the $I_D = I_{sc}$ under illumination and those using the values of n and the barrier height under illumination match closely with the observed values.

A typical $1/C^2$-V plot for device Cu 27 has been presented in Fig. 4.12. The upper most plot results from the measurements at 77 ^{o}K and will be dealt with later. Table 4.9 shows that the doping densities obtained are well within the expected range and that the band bending decreases with illumination and increases with the oxide thickness. The trend in similar to that for Au and Ag solar cells and the increase in V_{oc} with the oxide thickness can be partially accounted for by this.

Table 4.1 : Important experimental results from SB/MOS solar cells with Au as the barrier metal on n-type silicon.

Device	t_{ox} (Å)	t_m (Å)	Rate of deposition (Å/sec)	T* (%)	V_{oc} (mV)	J_{sc} (mA/cm^2)	F	η (%)	R_s (Ohm.cm^2)
Au 1	10	50	-	-	256	34.0	0.65	5.6	0.09
Au 20	10	51	1.0-1.1	58	278	26.9	0.63	4.7	0.56
Au 21	10	64	1.0-1.1	51	323	22.6	0.67	4.9	0.41
Au 22	10	40	1.1	69	304	30.9	0.57	5.3	1.19
Au 23	10	50	1.1	58	317	31.8	0.62	6.2	-
Au 32	10	44	1.8-2.3	64	312	33.8	0.64	6.7	1.10
Au 40	10	61	1.0-1.3	53	285	29.1	0.62	5.1	0.55
Au 24	13	40	1.1	69	305	31.8	0.62	6.0	-
Au 25	13	50	1.1	58	320	26.7	0.63	5.4	-
Au 28	13	53	1.1-1.4	51	316	37.4	0.66	7.8	0.47
Au 29	13	53	1.1-1.4	51	326	36.9	0.51	6.1	-
Au 7	16	-	-	-	347	28.0	0.54	5.3	2.53

The effective area of most of the devices was 2.3×10^{-2} cm^2. For devices Au 25 and Au 32, the effective area was 2.1×10^{-2} cm^2 and for devices Au 20 and Au 24, it was 2.0×10^{-2} cm^2.

*Transmittance obtained from the plot in Fig. 4.1.

Table 4.2 : Experimental values of n, ϕ_n^B, and V_{oc} of SB/MOS solar cells with Au as the barrier metal on n-type silicon.

Device	t_{ox}	$n(I_D = I_{sc})$		ϕ_n^B		V_{oc}				
						I-V	I_D-V		$n(\phi_n^B - 0.50\ V)$	
		Dark	Illum	Dark	Illum		Dark	Illum	Dark	Illum
	(Å)			(V)	(V)	(mV)	(mV)	(mV)	(mV)	(mV)
Au 20	10	1.60	1.60	0.79	-	278	310	280	345	-
Au 40	10	2.50	2.60	0.80	0.73	287	310	275	336	287
Au 21	10	1.33	1.33	0.78	0.74	323	325	317	372	319
Au 32	10	2.20	2.40	0.72	0.69	312	350	310	360	315
Au 28	13	1.50	1.50	0.81	0.76	316	335	315	337	320
Au 29	13	3.25	4.00	-	-	326	405	328	-	-
Au 7	16	5.00	5.00	-	-	347	410	335	-	-

Table 4.3. Doping density N_D and zero bias band bending φ_i^o obtained from measured capacitance of Au solar cells in dark and under illumination.

Device	t_{ox}	N_D		ρ_{bulk}	φ_i^o		ϕ_n		$\varphi_i^o + \phi_n$		V_{oc}
		Dark	Illum		Dark	Illum	Dark	Illum	Dark	Illum	
	($\AA$)	(cm^{-3})	(cm^{-3})	(Ohm.cm)	(V)	(V)	(V)	(V)	(V)	(V)	(mV)
Au 15	10	7.8×10^{14}	8.5×10^{14}	3.0-7.0	0.46	0.36	0.27	0.27	0.73	0.63	283
Au 18	10	7.2×10^{14}	7.7×10^{14}	3.0-7.0	0.50	0.38	0.27	0.27	0.77	0.65	285
Au 40	10	8.2×10^{14}	8.4×10^{14}	3.0-7.0	0.52	0.40	0.27	0.27	0.79	0.67	285
Au 22	10	9.4×10^{14}	1.0×10^{15}	3.0-7.0	0.50	0.43	0.27	0.27	0.77	0.70	304
Au 41	10	1.2×10^{15}	1.3×10^{15}	3.0-7.0	0.50	0.47	0.26	0.26	0.76	0.73	298
Au 21	10	9.8×10^{14}	1.0×10^{15}	3.0-7.0	0.51	0.47	0.27	0.27	0.78	0.74	323
Au 28	13	1.0×10^{15}	1.1×10^{15}	3.0-7.0	0.52	0.47	0.27	0.26	0.79	0.73	316
Au 29	13	9.1×10^{14}	9.7×10^{14}	3.0-7.0	0.52	0.48	0.27	0.27	0.79	0.75	326

Table 4.4 : Important experimental results from SB/MOS solar cells with Ag as the barrier metal on n-type silicon.

Device	t_{ox} (Å)	t_m (Å)	Rate of deposition (Å/sec)	V_{oc} (mV)	J_{sc} (mA/cm^2)	F	η (%)	R_s ($Ohm.cm^2$)
Ag 7	13	42	1.6	162	39.1	0.45	2.8	1.20
Ag 21	22	107	3.4-5.1	400	25.6	0.53	6.4	-
Ag 18	22	85	3.4-5.1	415	29.5	0.56	6.9	-
Ag 10	22	85	1.6	421	33.1	0.55	7.7	-
Ag 47	22	91	2.6-3.4	453	23.0	0.66	6.9	0.88
Ag 35	22	91	1.7-3.4	457	26.1	0.64	7.6	0.66
Ag 19	24	85	3.4-5.1	466	28.6	0.63	8.4	-
Ag 15	24	81	2.1	490	30.2	0.61	9.0	-
Ag 16	24	81	2.1	492	29.3	0.68	9.8	0.18
Ag 27	24	95	6.7	498	22.6	0.52	5.9	-

The effective area of devices Ag 21, Ag 18, Ag 19, Ag 16, and Ag 27 was 2.1×10^{-2} cm^2, for devices Ag 7 and Ag 10 it was 2.2×10^{-2} cm^2, and for devices Ag 47, Ag 35, and Ag 15 it was 2.3×10^{-2} cm^2.

Table 4.5 : Experimental values of n, ϕ_n^B, and V_{oc} of SB/MOS solar cells with Ag as the barrier metal on n-type silicon.

Device	t_{ox}	$n(I_{sc})$		ϕ_n^B		V_{oc}				
						I-V	I_D-V		$n(\phi_n^B - 0.50V)$	
		Dark	Illum	Dark	Illum		Dark	Illum	Dark	Illum
	(Å)			(V)	(V)	(mV)	(mV)	(mV)	(mV)	(mV)
Ag 7	13	2.30	2.50	0.69	0.63	195	235	195	209	203
Ag 18	22	2.96	3.16	0.67	0.65	415	435	415	403	474
Ag 21	22	4.30	4.60	-	-	400	405	380	-	-
Ag 47	22	2.06	2.55	0.83	-	453	475	450	514	-
Ag 35	22	2.50	2.60	0.76	-	457	440	420	431	-
Ag 15	24	2.80	2.90	-	-	490	555	505	-	-
Ag 16	24	1.50	1.50	-	-	492	485	475	-	-
Ag 27	24	4.00	16.00	-	-	498	690	500	-	-

Table 4.6 : Doping density N_D and zero bias band bending φ_i^o obtained from measured capacitance of Ag solar cells in dark and under illumination.

Device	t_{ox}	N_D		ρ_{bulk}	φ_i^o		ϕ_n		$\varphi_i^o + \phi_n$		V_{oc}
		Dark	Illum		Dark	Illum	Dark	Illum	Dark	Illum	
	(Å)	(cm^{-3})	(cm^{-3})	(Ohm.cm)	(V)	(V)	(V)	(V)	(V)	(V)	(mV)
Ag 21	22	$1.1x10^{15}$	$1.2x10^{15}$	3.0-7.0	0.56	0.46	0.26	0.26	0.82	0.72	400
Ag 18	22	$1.0x10^{15}$	$1.1x10^{15}$	3.0-7.0	0.60	0.50	0.26	0.26	0.87	0.76	415
Ag 47	22	$1.8x10^{15}$	$1.8x10^{15}$	3.0-7.0	0.60	0.50	0.25	0.25	0.85	0.75	453
Ag 35	22	$1.1x10^{15}$	$1.1x10^{15}$	3.0-7.0	0.60	0.50	0.26	0.26	0.86	0.76	457
Ag 19	24	$1.0x10^{15}$	$1.1x10^{15}$	3.0-7.0	0.55	0.52	0.27	0.26	0.82	0.78	466
Ag 15	24	$1.1x10^{15}$	$1.1x10^{15}$	3.0-7.0	0.60	0.52	0.26	0.26	0.86	0.78	490
Ag 16	24	$1.1x10^{15}$	$1.2x10^{15}$	3.0-7.0	0.56	0.52	0.26	0.26	0.82	0.78	492

Table 4.7 : Important experimental results from SB/MOS solar cells with Cu as the barrier metal on n-type silicon.

Device	t_{ox} (Å)	t_m (Å)	Rate of deposition (Å/sec)	V_{oc} (mV)	J_{sc} (mA/cm^2)	F	η (%)	R_s ($Ohm.cm^2$)
Cu 3	10	77	-	165	23.5	0.58	2.3	0.22
Cu 27	10	87	0.6-1.4	185	24.3	0.55	2.5	0.63
Cu 17	18	-	-	262	14.3	0.56	2.1	0.29
Cu 13	20	-	-	284	23.0	0.38	2.4	3.70

The effective area of all these devices was 2.3×10^{-2} cm^2.

Table 4,8 : Experimental values of n, ϕ_n^B, and V_{oc} of SB/MOS solarccells with Cu as as the barrier metal of n-type silicon.

Device	t_{ox}	$n(I_{sc})$		ϕ_n^B		V_{oc}				
		Dark	Illum	Dark	Illum	I-V	I_D-V		$n(\phi_n^B - 0.50V)$	
							Dark	Illum	Dark	Illum
	(Å)			(V)	(V)	(mV)	(mV)	(mV)	(mV)	(mV)
Cu 3	10	1.10	1.10	0.67	0.66	165	170	165	187	176
Cu 27	10	1.58	1.58	0.71	0.68	185	200	185	218	187
Cu 17	18	3.30	3.70	-	-	262	330	255	-	-
Cu 13	20	4.90	7.10	-	-	284	460	284	-	-

Table 4.9 : Doping density N_D and zero bias band bending φ_i^o obtained from measured capacitance of Cu solar cells in dark and under illumination.

Device	t_{ox}	N_D		ρ_{bulk}	φ_i^o		ϕ_n		$\varphi_i^o + \phi_n'$		V_{oc}
		Dark	Illum		Dark	Illum	Dark	Illum	Dark	Illum	
	(Å)	(cm^{-3})	(cm^{-3})	(Ohm.cm)	(V)	(V)	(V)	(V)	(V)	(V)	(mV)
Cu 10	10	$1.6x10^{14}$	$1.7x10^{14}$	7.0-13.0	0.37	0.35	0.31	0.31	0.68	0.66	150
Cu 16	10	$1.0x10^{14}$	-	7.0-13.0	0.36	-	0.32	-	0.68	-	144
Cu 27	10	$1.5x10^{15}$	$1.5x10^{15}$	3.0-7.0	0.54	0.42	0.26	0.26	0.80	0.68	185
Cu 17	18	$7.9x10^{15}$	$7.7x10^{15}$	0.2-1.0	0.58	0.48	0.22	0.22	0.80	0.70	262
Cu 13	20	$1.2x10^{14}$	$1.5x10^{14}$	7.0-13.0	0.56	0.51	0.31	0.31	0.87	0.82	284

4.2. SB/MOS solar cells under concentrated light

Table 4.10 presents a summary of the important results obtained under concentration on SB/MOS solar cells with Au and Ag as the barrier metals. These data have been obtained from the measured I-V and I_D-V characteristics of the devices, cf. Figs. 4.13, 4.15, 4.18, 4.19, 4.20, and 4.22. It has been assumed that the shortcircuit current density is directly proportional to the level of illumination. The variation of V_{oc}, F, and η with concentration for devices Au 21 and Ag 16 have been presented in Figs. 4.14 and 4.23. These plots and the values in Table 4.10 reveal that the opencircuit voltage of all the cells increase with concentration. The increase is rapid in the begining and then V_{oc} tends to saturate at concentration ratios greater than 10. As indicated in section 2.3, V_{oc} increases because of enhanced light generated current. But the improvement is diminished because of an increase in V_{ox}^{oc}, cf. equation (2.3). The highest measured opencircuit voltage has been 539 mV for device Ag 16 at a concentration of 10.5 Suns.

Table 4.10 shows the variation of the fill factor with concentration. In general, it decreases at higher illumination levels with the exception of device Ag 19, for which it increases from 0.63 at 1.0 Sun to 0.65 at 2.7 Suns. Even for the devices where it goes down with concentration, the rate of decrease varies from one device to the other. This certainly is related to the series resistance of the device. As mentioned in section 2.3, this parameter is mainly instrumental in affecting the fill factor at higher levels of illumination. But in the present investigation, no attempt has been made to reduce R_s for

pplication under concentration. For devices Ag 16 and Au 21, the eries resistance is low and the fill factor initially good. The ate of decrease of the fill factor is slower for device Ag 16 an that for Au 21. This is compatible with the fact that the rmer device has a lower series resistance than the latter. evice Au 28 has a higher series resistance and this is reflected n its lower fill factor at 1.0 Sun and also on the faster deterio- ation with increased insolation. For device Ag 19, the series sistance could not be obtained from the dark I-V characteristics the forward direction since a linear range was absent. However, s value cannot be large because the fill factor does not teriorate at an illumination level of 2.0 Suns and increases ightly at 2.7 Suns, cf. Fig. 4.19.

The overall efficiency, listed in Table 4.10, varies with tration in a manner determined by the variation of V_{oc} and r device Au 21, it goes through a peak since for this the ion in the fill factor upto a concentration of 4.0 Suns to be more than compensated by the increase in the open- t voltage. With further increase in the illumination level, encircuit voltage tends to saturate, the fill factor es faster and so does the efficiency. For device Au 28, ficiency follows the same trend as the fill factor and goes apidly with concentration. The efficiency of device Ag 19 an increase with concentration since the opencircuit e and the fill factor improve with concentration upto 2.7 But its behaviour at higher concentrations could not be d because of the lack of experimental data. Device Ag 16

has an efficiency of 9.8 percent at 1.0 Sun level and due to deterioration of the fill factor, goes down slightly at higher concentrations. However, its value remains close to 9 percent at 10.5 Suns. Thus it appears that with the exception of device Au 28, all these cells have reasonably good performance under concentrated light. At this point, it may be mentioned that none of the above solar cells has a specially designed grid contact which is essential for reduction of the series resistance while operating under concentration. Hence better performance can be expected out of these or similar solar cells under concentration if proper grid contacts are used on top of the barrier metal layer.

Figures 4.15 and 4.20 present the measured I_D-V characteristics for devices Au 21 and Ag 19. The effect of the oxide thickness on these characteristics can be seen by comparing them. Device Au 21 has a 10 Å thick oxide and the I_D-V plots in dark as well as under illumination at 1.0 Sun are exponential upto V_{oc}. This indicates that the metal fermi level is pinned to the interface states and that the oxide barrier is largely transparent to the majority carriers. The low opencircuit voltage is typical of Au-n Si SB solar cells. But the I_D-V plot for device Ag 19, which has an oxide thickness of about 22 Å, is much different from this. There is no single n and its value at opencircuit under normal insolation is larger than that for device Au 21. Both the plots vividly demonstrate the effect of increased illumination on the diode current of an SB/MOS solar cell. It always increases with illumination level and brings about a reduction in the

opencircuit voltage. This can be obtained by reading off the forward voltage at which the shortcircuit currents for various concentrations equal the respective diode currents. Table 4.10 shows that these values obtained from the dark characteristics are generally higher than those obtained from the I-V measurements. But those obtained from the characteristics under illumination closel match with the observed values in case of device Au 21. The discrepancy in case of device Ag 19 could be due to a rapid degradation of the cell on exposure to the atmosphere. The opencircuit voltage might have actually gone down at the time of I_D-V measurements, as the values obtained therefrom show. The decrease in V_{oc} due to an increase in the diode current is slightly made up by the fact that the opencircuit voltages at higher concentrations correspond to the series resistance dominated regions in the I_D-V plots. For device Au 21, the I_D-V plots even at higher concentrations have an exponential region which donot extend upto the opencircuit voltage. Had these been so, the opencircuit voltage obtained would have been smaller. For example, at a concentration of 6.2 suns, the forward voltage of which the $I_D = I_{sc}$ line intersects the extrapolated I_D-V characteristic is 322 mV. But from the actual I_D-V plot, the corresponding voltage is obtained to be 350 mV which is close to the observed V_{oc} of 355 mV. However, the fill factor undergoes a faster deterioration at higher concentration and had there been no series resistance, its value would have been higher at the expense of a lower V_{oc}. Thus the series resistance plays a significant role at higher concentration and its effect becomes less as the 1.0 Sun illumination level is approached.

The diode current increases with increasing illumination because of enhanced recombination and a reduction in the silicon band bending. At low values of forward bias, the increase is primarily due to recombination currents. The bulk recombination current increases following an enhanced carrier generation rate all over the semiconductor. Also the interface recombination current increases due to a reduced communication time of the minority carriers with the interface states [1]. The diode non-ideality factor n, for low values of forward bias increases with the concentration ratio from a value of 1.42 at 1.0 Sun to 1.62 at 6.2 Suns. This indicates large contribution from the recombination current at higher concentration. Figure 4.16 presents a plot of increase in the diode current normalized to its value in dark against the concentration ratio C for device Au 21. The applied forward bias has been taken as the parameter. It can be seen that the diode current at a certain applied bias increases linearly with the intensity of light and the increase is more for lower values of the forward bias. A reduction in the silicon band bending also contributes to the increase in the diode current. The reduction of the zero bias silicon band bending with illumination has been experimentally verified by means of capacitance-voltage measurements. The $1/C^2$-V plot for devices Au 21 and Ag 16 have been presented in Figs. 4.17 and 4.21 respectively and the data obtained therefrom in Table 4.11. Also included in it are the data obtained from a similar plot for device Au 20. The capacitance of the device increases monotonically with the level of illumination as the silicon band bending decreases. This is

evident from the intercept on the voltage axis of these plots, which gives the value of φ_i^o. For device Au 21, φ_i^o drops from an initial value of 0.49 V at 1.0 Sun to 0.40 V at 7.3 Suns. A higher silicon band bending of 0.52 V at 1.0 Sun for device Ag 16 is probably due to a thicker oxide [28] and is partly responsible for the larger opencircuit voltage for this device. However, with increased illumination level, the band bending at zero bias reduces rapidly and drops to 0.38 V at 2.7 Suns. As already discussed in section 2.3, such a reduction in φ_i^o can only arise from an increase in the oxide voltage due to increased interface state charge at higher intensities. The interface state charge increases with concentration due to a shift of the occupancy level towards the minority carrier band edge. This results in an increase in the diode current for moderate and high values of forward bias.

Figures 4.17 and 4.21 also show a change in slope of the $1/C^2$-V plot as the intensity of light is changed. Since the density of charge carriers in the depletion layer is inversely proportional to the slope of the straight line, it appears that with increasing illumination level its value also increases. This can be explained by saying that the minority carrier density under illumination goes up very much and modulate the carrier concentration in the depletion layer. Berry [15] found that in an abrupt p-n junction the density of injected carriers under illumination may be as high as 10^{14} cm^{-3}. If similar effect takes place in case of Au or Ag solar cells, then with increasing concentration ratio, an increase in the carrier density is expected. Table 4.11

contains the values of the density of charge carriers from $1/C^2$-V plots. For device Au 21, this increase from 8.4×10^{14} cm^{-3} in dark to 1.2×10^{15} cm^{-3} at a concentration of 7.3 Suns. Similar results have been obtained from the devices Au 20 and Ag 19. However, the value of Φ_n is not much changed so that the quantity $\varphi_i^o + \Phi_n$ varies essentially in the same manner as φ_i^o.

Table 4.10 : Important experimental parameters of Au and Ag SB/MOS solar cells under concentrated light.

Sample	t_{ox} (Å)	C (Suns)	$n(I_D=I_{sc})$	V_{oc} I-V (mV)	V_{oc} I_D-V Dark (mV)	V_{oc} I_D-V Illum (mV)	J_{sc} (mA/cm^{+2})	F	η (%)
Au 21	10	1.0	1.41	323	335	323	22.6	0.68	4.9
		2.0	1.50	342	362	340	45.3	0.68	5.1
		3.0	2.10	348	380	345	67.5	0.66	5.1
		4.1	2.60	352	400	350	91.3	0.65	5.1
		5.1	2.90	354	415	350	113.0	0.62	4.8
		6.2	3.10	355	430	350	137.0	0.59	4.7
		7.3	3.40	355	445	350	161.0	0.59	4.6
Ag 19	22	1.0	2.90	466	455	432	28.6	0.63	8.4
		2.1	3.00	490	510	480	58.8	0.63	8.8
		2.7	3.20	507	527	492	76.5	0.65	9.4
Ag 16	24	1.0		492			27.2	0.68	9.8
		3.1		511			90.5	0.64	9.6
		5.0		523			144.0	0.63	9.6
		7.1		532			204.0	0.62	9.6
		9.2		537			266.0	0.60	9.4
		10.5		539			305.0	0.56	8.8
Au 28	13	1.0		307			33.5	0.60	6.2
		1.9		322			63.0	0.54	5.9
		2.9		332			99.1	0.49	5.5
		3.9		337			130.4	0.43	4.9
		5.0		341			165.2	0.40	4.6
		6.5		347			217.4	0.35	4.0

Table 4.11 : Carrier concentration and silicon band bending at zero bias for Au and Ag SB/MOS solar cells under concentrated light.

Sample	t_{ox} (Å)	C (Suns)	φ_i^o (V)	Carrier Concentration (cm^{-3})	Φ_n (V)	$\varphi_i^o + \Phi_n$ (V)	V_{oc} (mV)
Au 20	10	0.0	0.50	7.9×10^{14}	0.27	0.77	
		1.0	0.46	8.2×10^{14}	0.27	0.73	
		3.0	0.42	9.2×10^{14}	0.27	0.69	
		5.0	0.38	9.9×10^{14}	0.27	0.65	
Au 21	10	0.0	0.51	8.4×10^{14}	0.27	0.78	
		1.0	0.49	9.1×10^{14}	0.27	0.76	323
		2.0	0.49	9.4×10^{14}	0.27	0.76	342
		3.0	0.48	1.0×10^{15}	0.27	0.75	348
		4.1	0.47	1.0×10^{15}	0.26	0.73	352
		5.1	0.45	1.1×10^{15}	0.26	0.71	354
		6.2	0.42	1.1×10^{15}	0.26	0.68	355
		7.3	0.40	1.2×10^{15}	0.26	0.66	355
Ag 19	24	0.0	0.55	1.0×10^{15}	0.27	0.82	
		1.0	0.52	1.1×10^{15}	0.26	0.78	466
		2.1	0.48	1.1×10^{15}	0.26	0.74	490
		2.7	0.38	1.2×10^{15}	0.26	0.64	507

4.3. MOS solar cells at different temperatures

4.3.1 Elevated temperature studies

The results of studies made on Au and Ag SB/MOS solar cells at different temperatures above 300 °K are summarized in Table 4.12. These data have been obtained from the measured I-V characteristics. The I-V characteristics for devices Au 25 and Ag 47 have been presented in Figs. 4.24 and 4.25 respectively. In accordance with the theory, opencircuit voltage for all the cells goes down as the temperature increases. This has been presented in Fig. 4.26(a) which also contains the variation of the fill factor with temperature for devices Ag 47, Au 21 and Au 25. Fig. 4.26(b) contains the variation of the shortcircuit current density and the efficiency with temperature for these devices. The temperature range of study was 301 °K to 398 °K for device Au 25, from 305 °K to 364 °K for device Au 21, and from 305 °K to 408 °K for device Ag 47. The maximum error in the measurement of the temperature was ± 1 °K. The opencircuit voltage for all the devices went down linearly with temperature, the rate being -1.83 mV/°K for device Au 25 and -1.85 mV/°K for device Ag 47. The theoretically calculated value of -1.8 to -1.9 mV/°K for dV_{oc}/dT slightly reduces when one considers contributions from the term $(kT/q.J_L)(dJ_L/dT)$ in the expression for dV_{oc}/dT. Experimentally this has been found to be about 0.07-0.08 mV/°K. Even then the agreement between the theory and experiment is not bad. Comparison of these data can be made with dV_{oc}/dT = -2.3 mV/°K as reported by Anderson et.al [20] for Al-p Si SBSC and

dV_{oc}/dT=-2 to -3 mV/^{o}K for p-n junction solar cells [19]. It can be seen that V_{oc} changes by 51 percent for device Au 25 and by 42 percent for device Ag 47 for about 100 ^{o}K rise in the cell temperature. Earlier Colbrie et. al [23] had reported about 73 percent change in V_{oc} of an Al-p Si SBSC for an identical temperature range. For device Au 21, dV_{oc}/dT is about -1.6 mV/^{o}K and the change in V_{oc} is about 32 percent. The slight disagreement of dV_{oc}/dT for this device with the calculated value could have partly been due to a larger contribution from the term containing J_L. However, the fact that dV_{oc}/dT of the cells studied by us is smaller than that reported by others on SB as well as p-n junction solar cells, is certainly of advantage for high temperature operation.

The shortcircuit current density for all the cells increases linearly at the rate of 0.09 mA/cm^2 ^{o}K. But this may not be a true indication of the rate at which the light generated current of the cells increases with temperature. This is because at elevated temperatures, the shortcircuit current differs from the light-generated current as can be seen from the degradation of the fill factor with temperature rise. However, there can be little doubt about the increase in the light-generated current as the temperature is increased. This has also been observed by others [19,20] and the reason, as indicated in section 2.4, could be an improvement in the minority carrier diffusion length and the phonon density with temperature. The second factor causes an improvement in the absorption coefficient for silicon. Anderson et. al [20] reported an increase of 0.005 mA/cm^2 ^{o}K for the shortcircuit

current on an Al-p Si cell of 1.1 cm^2 area. This resulted in a change of 11-12 percent for 100 ^{o}K rise in temperature. These values cannot really be compared with the data obtained by us since their measurements were taken under an illumination of 20 mW/cm^2. Increasing the level of illumination may have significant influence on the rate of increase of J_{sc} as has been observed in case of p-n junction solar cells [21].

For all these devices, the fill factor decreases with increase in temperature, cf. Fig. 4.26. The decrease is not linear but slower for temperatures closer to the room temperature. At higher temperatures, the decrease is faster. An exact behaviour of the fill factor with temperature is difficult to predict since this would depend on many factors including the series resistance. However, our results differ from those of Anderson et. al [20] who found a linear decrease of the fill factor with temperature. The fill factor decreases partly because of the decrease in V_{oc} following a rapid increase in the diode current and a simultaneous increase in I_{sc}. The slope of the ln I_D-V plot decreases with temperature. This also causes the fill factor to go down. Increased recombination currents also may contribute towards degradation of the fill factor with temperature by rounding off the knee of the I_D-V plot.

From Table 4.12, it can be seen that device Ag 47, which had a good fill factor initially, showed a better performance at elevated temperatures. Thus for high temperature operation, one should see that the fill factor of the device is initially good.

in general, the factor n decreases with temperature. For devices Au 21 and Au 25 this holds good even for the lower values of forward bias where the current voltage relationship is exponential. But for device Ag 47, n more or less remains constant, cf. Fig. 4.27. Such a behaviour of n with temperature can arise from a change in the interface state density. The band gap decreases at higher temperatures and may produce a change in the interface state density.

In this connection, it may be added that Anderson et. al [20] have concluded from a similar observation that field emission is the dominant mechanism of current transport. But since the temperature is not very low and the doping density not very high, field emission is not very likely to take place.

It can be seen from Table 4.13 that the values of V_{oc} obtained from the I_D-V characteristics under illumination closely match with the observed values. These values corresponding to the dark I_D-V characteristics are much higher than the true V_{oc} because the diode current under illumination is higher at all temperatures than its value in dark. The reason, as explained earlier, is an increase in the interface state charge under illumination. The diode current increases with temperature mainly because of the factor $T^2 \exp-[q(\varphi_i+\Phi_n)/kT]$ in its expression. But an added contribution to this can occur if the quantity $\varphi_i^o + \Phi_n$ decreases with increase in temperature. This can be ascertained from $1/C^2$-V plots at different temperatures. Two typical such plots for devices Au 24 and Ag 47 have been presented in Figs.4.28

and 4.29. The data obtained from these have been presented in Table 4.14. In all cases, the silicon band bending at zero bias decreases at elevated temperatures. This can be due to a slight reduction in the silicon band gap, an increase in Φ_n and an increase in the interface state charge. As a result, the device capacitance increases at higher temperatures. The band bending under illumination is always less than its value in dark, the reasons for which have already been explained. The density of charge carriers in the depletion layer seems to vary slightly with temperature in some cases while for others it essentially remains the same.

Table 4.12 : Important experimentally measured parameters of Au and Ag SB/MOS solar cells at different temperatures.

Device	t_{ox} (Å)	t_m (Å)	T (^oK)	V_{oc} (mV)	J_{sc} (mA/cm^{+2})	F	η (%)
Au 21	10	64	305	285	27.1	0.49	3.7
			325	254	29.1	0.49	3.6
			344	223	31.2	0.46	3.2
			364	192	32.9	0.44	2.8
Au 25*	13	50	301	328	30.5	0.51	5.1
			340	264	34.0	0.48	4.3
			367	205	36.0	0.44	3.2
			398	159	39.0	0.37	2.3
Ag 47	22	72	305	453	23.0	0.65	6.8
			330	416	26.0	0.62	6.7
			359	358	28.6	0.60	6.2
			385	313	30.4	0.55	5.2
			408	262	32.0	0.50	4.2

*P_{in} = 110 mW/cm^2.

Table 4.13 : n and V_{oc} from measured I_D-V characteristics of Au and Ag SB/HOS solar cells at different temperatures above 300 °K.

Sample	t_{ox} (Å)	T (°K)	$n(I_D = I_{sc})$ Dark	$n(I_D = I_{sc})$ Illum	V_{oc} I-V (mV)	V_{oc} I_D-V Dark (mV)	V_{oc} I_D-V Illum (mV)
Au 21	10	305	2.47	2.88	285	337	285
		325	2.20	2.47	254	295	250
		344	2.04	2.23	223	265	227
		364	1.93	2.21	192	247	197
Au 25	13	301	2.42	3.00	328	385	330
		340	2.36	2.73	264	318	265
		367	2.32	2.66	205	275	215
		398	2.27	2.33	159	215	150
Ag 47	22	305	2.06	2.55	453	475	450
		330	2.05	2.43	416	440	415
		385	1.56	1.89	313	335	308

Table 4.14 : Doping density, band bending, and barrier height of Au and Ag SB/MOS solar cell from measured capacitance at different temperatures above 300 ^{o}K.

Sample	t_{ox}	T	N_D		ϕ_n		φ_i^o		$\varphi_i^o + \phi_n$	
			Dark	Illum	Dark	Illum	Dark	Illum	Dark	Illum
	($\AA$)	(^{o}K)	(cm^{-3})	(cm^{-3})	(V)	(V)	(V)	(V)	(V)	(V)
Au 25	13	301	1.0×10^{15}	-	0.27	-	0.57	-	0.84	-
		398	1.2×10^{15}	-	0.36	-	0.42	-	0.78	-
Au 24	13	317	9.6×10^{14}	9.7×10^{14}	0.28	0.28	0.57	0.45	0.85	0.73
		370	9.8×10^{14}	1.0×10^{15}	0.34	0.34	0.46	0.35	0.80	0.69
Ag 47	22	305	1.8×10^{15}	1.8×10^{15}	0.25	0.25	0.60	0.50	0.85	0.75
		385	1.8×10^{15}	1.8×10^{15}	0.33	0.33	0.45	0.40	0.78	0.73

4.3.2 SB/MOS solar cells at 77 ^{o}K

Table 4.15 contains a summary of the results of measurements at 77 ^{o}K on Au, Ag, and Cu SB and MOS solar cells. For comparison, the corre ponding values at 300 ^{o}K has also been included. We shall first discuss the results on Au and Cu cells and then those on Ag cells. The I-V, I_D-V and $1/C^2$-V characteristics at 77 and 300 ^{o}K for device Au 32 have been presented in Figs. 4.30, 4.31 and 4.32 respectively. From Fig. 4.30 and Table 4.15 it can be seen that opencircuit voltage for device Au 32 increased from 312 mV at 300 ^{o}K to 710 mV at 77 ^{o}K together with an improvement in the fill factor from 0.64 to 0.86. For device Au 40, which had a V_{oc} of 285 mV at room temperature, the increase was similar, the opencircuit voltage at 77 ^{o}K being 677 mV. It is worth noting that the change in V_{oc} for all the Au SB solar cells is in between 390-400 mV. This more or less equals the change in the term $(kT/q)\ \ln(J_L/A^*T^2)$ in the expression of V_{oc}, cf. equation 2.3. For an SBSC, this is expected from equation (2.3) since $T_{ox}^{oc} \simeq 1$ and the change in V_{ox}^{oc} may be small. The values of J_L were taken from the experimental observations. The value of the fill factor for Au 40 increased from 0.62 at room temperature to 0.91 at 77 ^{o}K. At this point, it may be mentioned that an opencircuit voltage of 710 mV and a fill factor of 0.91 are the highest values of these parameters reported on Si SB/MOS solar cells. This is an indication that such high values are possible to obtain on Au-n Si cells and should this be possible at room temperature, it can be of great advantage.

The shortcircuit current density for all these cells decreases at the lower temperatures. Also it is seen that, generally, the change is more for the device with a lower shortcircuit current at room temperature. There can be various reasons for the observed change in the light generated and hence in the shortcircuit current. At such low temperatures as 77 ^{o}K, the values of the absorption coefficient for Si will decrease due to a decrease in the phonon density [28]. Further, as discussed in section 2.3, the diffusion length of the minority carriers will decrease at low temperatures. Also the silicon band gap increases as the temperature is reduced. thus affecting the long wave length response of the cell. The nonuniform changes in the shortcircuit current may be due to different factors like formation of ice on top of the device. This will depend on the moisture content in the atmosphere. A better way of measurement at low temperatures would require the device to be put in an enclosure, evacuate it, and pass dry nitrogen or argon gas through it.

The fill factor also improves very much at reduced temperatures along with V_{oc}. This is in agreement with the measurements at room temperature indicating that higher fill factors are obtained with MOS solar cells with higher opencircuit voltages than SB solar cells [1,8]. It has been indicated in Table 4.16 that the series resistance of the devices as measured from the I-V characteristics in dark decreases at 77 ^{o}K. This also contributes towards an improvement of the fill factor. The overall efficiencies of the devices undergo significant increase at the lower temperature, as has been shown in Table 4.15. The

possibility of reducing the diode current by several orders of magnitude at room temperature with a suitable interfacial layer has been indicated by Kar [28]. Under these conditions, such device characteristics as at 77 ^{o}K may be expected.

The diode current-voltage characteristics for device Au 32 at 77 and 300 ^{o}K have been presented in Fig. 4.31. Similar characteristics have also been measured for device Au 40. The important features to be noticed in these plots are a significant reduction in the diode currents in dark as well as under illumination and an increase in the value of n at 77 ^{o}K. The forward I_D-V plot for device Au 32 is exponential both in dark and under illumination with n equal to 1.50, cf. Fig. 4.31. Similarly, device Au 40 also has an exponential I_D-V relationship with n equal to 1.12. At 77 ^{o}K, as there is many orders of magnitude reduction in the diode current, the opencircuit voltage of the cell increases considerably. Table 4.16 contains the values of V_{oc} obtained from Fig. 4.31 by reading the forward voltage at which the broken lines representing the shortcircuit currents intersect the diode current under illumination. The measured opencircuit voltages at 300 ^{o}K and 77 ^{o}K agree fairly well with these values as has been indicated in Table 4.16.

The reduction in the diode current is mainly due to a reduced thermionic component of the current. Hence contributions from the recombination current is expected to show up at 77 ^{o}K. This is exactly what happens in this case. The values of n for both the devices increase at the reduced temperature, cf. Table 4.16. But the increase is larger for device Au 32 which is

expected in view of its larger n at 300 ^{o}K. Thus the increase in the value of n at reduced temperatures can be due to an increased recombination although there may be other factors responsible for it.

It was pointed out in Section 2.3 that an increase in the silicon band bending at reduced temperatures is due to a reduction in the value of ϕ_n and an increase in the silicon band gap. This reduces the diode current further in addition to the reduction due to the temperature dependence. Figure 4.32 presents the measured $1/C^2$-V plots for device Au 32 and the increase in the silicon barrier under illumination at 77 ^{o}K can be seen. Similar plots have been obtained for device Au 40. The data obtained have been tabulated in Table 4.17. The value of φ_i^o under illumination for device Au 32 increases from 0.38 V at 300 ^{o}K to 0.77 V at 77 ^{o}K. This is accompanied by a reduction in ϕ_n from 0.27 V at 300 ^{o}K to 0.06 V at 77 ^{o}K. The increase in φ_i^o is hence partly because of the reduction in ϕ_n and partly due to an increase in the silicon band gap. For devices Au 40 and Au 32, the density of charge carriers under illumination is slightly less at 77 ^{o}K than at 300 ^{o}K. This can be expected because of reduced degree of ionization of the impurity atoms at 77 ^{o}K.

The results of measurements on device Cu 27 have been shown in Table 4.15. Measured I-V characteristics of device Cu 27 at 77 and 300 ^{o}K have been presented in Fig. 4.33. The low open-circuit voltage of 185 mV is expected because of the low barrier for Cu on n-Si than for Au or Ag. However, improvement of V_{oc} to 550 mV at 77 ^{o}K indicates that high opencircuit voltage can

be obtained from Cu SB solar cells under suitable conditions. The change in V_{oc} of 365 mV slightly falls short of the change of 396 mV in the term $(kT/q)\ \ln(J_L/A^*T^2)$. If $T_{ox} < 1$, the mismatch can stem from the term containing T_{ox}^{oc} even if it remains unchanged in magnitude as the temperature is reduced. The fill factor also improves from 0.55 at 300 ^oK to 0.81 at 77 ^oK. The shortcircuit current density of 24.3 mA/cm^2 at 300 ^oK is rather low. This could be due to a barrier metal layer thickness of 87 $\AA$ and poor transmittance through this. The large reduction in its value at 77 ^oK is compatible with the earlier observation in case of Au SB solar cells that a low shortcircuit current corresponds to a larger change in it at reduced temperatures. This can also be due to the formation of ice on top of the device at 77 ^oK. The diode current-voltage characteristics as depicted in Fig. 4.10 are influenced is a manner similar to those for Au solar cells. The ideality factor of 1.04 at room temperature increases to 3.0 at 77 ^oK. The data obtained from Fig. 4.10 has been presented in Table 4.16. The increase in n can be attributed partly to an enhanced recombination current at reduced temperatures. Figure 4.12 shows a plot of $1/C^2$-V under illumination and at 77 ^oK for this device. The results tabulated in Table 4.17 shows basically the same trend as in Au SB solar cells. Ag MOS solar cells behave in a slightly different manner as the temperature is reduced. The reason may be the presence of a thicker oxide layer than the devices discussed ealier. These devices have higher opencircuit voltages at room temperature than Au or Cu SB solar cells. But at 77 ^oK, the increase in V_{oc} is not as high as that for the latter devices. In fact, it can be seen from Table 4.15 that the

change in V_{oc} for devices Ag 35 and Ag 27 is around 170 mV and that for device Ag 19 is 208 mV whereas the change in $(kT/q)\ln(J_L/A^*T^2)$ is about 398 mV. The discrepancy may partly be attributed to the changes in V_{ox}^{oc} and the term containing T_{ox}^{oc} in the expression for V_{oc}, cf. equation (2.3). The changes in these terms are negative and they neutralize, to some extent, the change in the term containing J_L. The I-V characteristics for device Ag 27 have been presented in Fig. 4.34. It can be seen that the improvement in the fill factor is also much less due to a small increase in V_{oc}. A large increase in V_{oc} for device Ag 19 corresponds to a larger increase in its fill factor. The diode current voltage characteristics for device Ag 19 have been presented in Fig. 4.35. The large difference between the diode currents in dark and under illumination may be due to contribution from the recombination current. A value of 2.1 for the factor n in the dark I_D-V characteristic at 77 ^oK also indicates dominant recombination current. The reduction in the diode currents in dark as well as under illumination at 77 ^oK is not as large as that in case of Au or Cu cells. This explains the smaller increase in V_{oc} for Ag solar cells. Figure 4.36 presents $1/C^2$-V plots for the device under illumination and the values of the band bending and the carrier density obtained therefrom are contained in Table 4.17. The carrier density at 77 ^oK is less than that at 300 ^oK due to reasons mentioned earlier. Also the silicon band bending undergoes a large increase at 77 ^oK accompanied by a decrease in the value of ϕ_n. The value of $(\varphi_i^o + \phi_n)$ increases by 0.2 V and a corresponding decrease in the oxide voltage is expected.

Table 4.15: Experimentally measured parameters from SB/MOS solar cells with different barrier metals at 300 and 77 ^{o}K.

Device	t_{ox} ($\mathring{A}$)	t_m ($\mathring{A}$)	V_{oc} 300 ^{o}K (mV)	V_{oc} 77 ^{o}K (mV)	J_{sc} 300 ^{o}K (mA/cm^2)	J_{sc} 77 ^{o}K (mA/cm^2)	F 300 ^{o}K	F 77 ^{o}K	η 300 ^{o}K (%)	η 77 ^{o}K (%)
Au 32	13	44	312	710	33.8	26.7	0.64	0.86	6.7	16.3
Au 40	10	61	285	677	29.1	21.3	0.62	0.91	5.1	13.1
Au 41	10	51	298	698	22.1	11.7	0.62	0.88	4.1	7.2
Cu 27	10	85	135	550	24.3	14.8	0.55	0.81	2.5	6.6
Ag 19	22	85	325	533	24.5	20.7	0.43	0.72	3.4	8.0
Ag 35	22	91	457	625	26.1	15.4	0.64	0.74	7.7	7.5
Ag 27	24	95	498	663	22.6	14.1	0.52	0.75	5.9	7.1

Table 4.16 : Ideality factor, R_s, and V_{oc} for SB/MOS solar cells with different barrier metals at 77 °K and 300 °K.

Device	t_{ox}	n				R_s		V_{oc}			
		Dark		Illum.				I-V		I_D-V Illum.	
		300 °K	77 °K	300 °K	77 °K	300 °K (Ohm.cm^2)	77 °K (Ohm.cm^2)	300 °K (mV)	77 °K (mV)	300 °K (mV)	77 °K (mV)
Au 40	10	1.12	1.95	1.25	-	0.69	0.22	285	677	280	680
Au 32	13	1.50	4.00	1.66	4.00	0.83	0.49	312	710	310	690
Cu 27	10	1.04	3.00	1.04	-	0.63	0.36	185	550	185	545
Ag 19	22	1.90	2.10	-	-	-	-	325	533	335	535

Table 4.17: Doping density N_D and band bending φ_i^o obtained from the measured capacitance of SB/MOS solar cells with different barrier metals at 300 and 77 °K.

Device	t_{ox}	N_D			φ_i^o			ϕ_n			V_{oc}	
		Dark	Illum.		Dark	Illum.		Dark	Illum.			
		300 °K	300 °K	77 °K	300 °K	300 °K	77 °K	300 °K	300 °K	77 °K	300 °K	77
	(Å)	(cm^{-3})	(cm^{-3})	(cm^{-3})	(V)	(V)	(V)	(V)	(V)	(V)	(mV)	(m
Au 40	10	8.2×10^{14}	8.4×10^{14}	7.6×10^{14}	0.53	0.40	0.77	0.27	0.27	0.06	285	6
Au 32	13	7.8×10^{14}	8.4×10^{14}	7.8×10^{14}	0.51	0.38	0.74	0.27	0.27	0.06	312	7
Cu 27	10	1.6×10^{15}	1.6×10^{15}	1.4×10^{15}	0.55	0.40	0.75	0.26	0.26	0.05	185	5
Ag 27	24	-	1.1×10^{15}	8.7×10^{14}	-	0.45	0.85	-	0.26	0.06	498	6

5. CONCLUSIONS

Schottky barrier and MOS solar cells were fabricated on single crystal n-type silicon with Au, Ag, and Cu as the barrier metals for study under concentration and at different temperatures. The gold SB cells, which generally showed opencircuit voltages in the vicinity of 300 mV, had low series resistances and fill factors greater than 0.60. The increase in the opencircuit voltage was accompanied by an increase in the zero bias silicon band bending. In case of devices showing near ideal diode current-voltage relationship, the values of φ_i^o found from the reverse saturation currents were close to those obtained from $1/C^2$-V plots. For these devices alone, the value of n and φ_i^o under illumination could be used to calculate the value of V_{oc}. The agreement in many cases with the observed values was not bad. The diode current under illumination was always found to be greater than that in dark. This is due to increased recombination currents and a reduction in the zero bias silicon band bending under illumination following an increase in the interface state charge. The value of n at opencircuit was always found to be greater than or equal to its value in dark. All these are in accordance with the earlier findings of Kar et al.[1].

High opencircuit voltages in the range of 450-500 mV were obtained for Ag MOS solar cells. In many cases, the fill factor was also good along with high V_{oc}. The silver films had high transmittance as revealed by the shortcircuit current densities. Better electrical properties of the devices were obtained with high deposition rates of the barrier metal layer. The silver devices

in general had high efficiencies, the highest being 9.8 percent without any ARC under 1.0 Sun. This compares well with the values earlier reported in the literature [1,8]. The diode current-voltage characteristics for most of these devices deviated very much from the ideal behaviour with no exponential regions present. The zero bias silicon band bending showed an increase with the oxide thickness. The copper SB solar cells had low opencircuit voltages but could be somewhat improved by introducing an interfacial oxide layer grown at room temperature. The shortcircuit current density was also low for these cells. The fill factor was generally around 0.55 because of low V_{oc}. As a result, the efficiency was low, the maximum obtained at 1.0 Sun and without ARC being 2.5 percent. The zero bias band bending in silicon increased with the oxide thickness and the behaviour of the diode current-voltage characteristics in dark and under illumination was essentially the same as that for the gold devices. Higher shortcircuit current densities could be obtained with a suitable ARC and higher opencircuit voltages with better quality oxides. With these improvements, Cu solar cells may prove to be attractive.

Based on the cell performance under 1.0 Sun illumination and at room temperature, Au and Ag solar cells were chosen for study under concentrated light and at elevated temperatures. On MOS solar cells, concentration studies have not been carried out so far. These studies were useful in understanding the operation of MOS solar cells under concentration and in getting an indication of their performance under concentrated light. The cells were exposed to increased levels of illumination, however, they did not

have the benefit of any special design which help in effective collection of the photocarriers, reduce the series resistance of the device, and have been found to be essential in case of p-n junction solar cells for use under concentrated light. In absence of these, the experimental data obtained give only an indication of the feasibility of operating these cells under concentrated light and do not indicate their maximum effectiveness under such conditions. The experimental data indicated the following. The opencircuit voltage of all the devices increased with concentration because of multiplication of J_L. The increase was rapid in the begining and slowed down at higher concentrations. This was found to be due to an increase in the diode current of the device as revealed by the measured diode current-voltage characteristics. The measured plots of $1/C^2$ vs V indicated that the increase in diode current was due to a reduction in the silicon band bending with concentration following an increase in the interface state charge. Thus if the interface state density can be reduced by careful fabrication steps, one can expect V_{oc} to increase more rapidly even at high concentrations. The fill factor in most of the cases decreased slowly with concentration and in one device increased slightly at higher concentrations. The decrease in the fill factor is due to the series resistance and increased recombination under concentrated light. Smaller interface state density would reduce recombination current and an optimal grid contact, the series resistance. Thus the reduction in the fill factor can be brought down by having careful fabrication and a proper contact. This automatically would cause the efficiency to improve with concentration, as has been found in

case of p-n junction solar cells. In the present investigation, the efficiency of the devices went down slightly at higher concentrations and for some of the devices, it went through a peak. These preliminary studies of MOS solar cells under concentration make it clear that with modifications, as mentioned in the foregoing, these cells will be able to perform as satisfactorily as p-n junction solar cells under concentration. From $1/C^2$-V plots it appears that the carrier concentration in the depletion region increases with concentration. This may be due to added contribution from the excess minority carriers in the depletion region to the ionized donors. The capacitance at higher concentration increases due to reduction in the depletion layer width following a reduction in the silicon band bending.

The effect of elevated temperatures on the solar cell characteristics was found to degrade them, bringing about a reduction in the overall efficiency of the cell. This was because the open-circuit voltage of the device went down rapidly with temperature because of an increase in the diode current. The rate of decrease was found to be -1.60 to -1.85 mV/^{o}K. This is much less compared to the data earlier reported in the literature on both p-n junction and MOS solar cells and certainly is of advantage. The fill factor showed a reduction at elevated temperatures. This was partly compensated for by an increase in the shortcircuit current with temperature. The rate of increase was found to be 0.09 mA/cm^2/^{o}K for all the devices and indicated that it was the bulk silicon properties that were effected by the temperature. The reasons are an increase in the phonon density leading to an

improvement of the absorption coefficient, an increase in the diffusion length and a slight reduction in the silicon bandgap. However, the increase in the shortcircuit current was outweighed by the reduction in V_{oc} and F. The efficiency of the cell was thus reduced at elevated temperatures, the exact nature of variation being dictated by all these factors. The temperature range of useful operation was found to be 300-330 ^{o}K, and with further modifications, it should not be difficult to have cells which can operate without much deterioration in the temperature range of 300-350 ^{o}K. The value of n in some of the devices has been found to go down with temperature. The diode current under illumination has been found to be greater than that in dark at all temperatures. The zero bias band bending in silicon decreased at higher temperatures due to a reduction in the silicon band gap and an increase in ϕ_n. As a result, higher capacitance was obtained at higher temperatures.

The measurements at the liquid nitrogen temperature on Au, Ag, and Cu solar cells revealed that the device characteristics improve at low temperatures. The opencircuit voltage for gold and copper SB solar cells increased by a large amount while for silver solar cells, the increase was smaller. The increase in V_{oc} for gold and copper solar cells was found to be more or less equal to the change in the term $(kT/q)\ \ln(J_L/A^{*}T^2)$ in the expression for V_{oc}, cf. equation (2.3). But for silver MOS solar cells, the increase in V_{oc} was less, being partly neutralized due to changes in V_{ox}^{oc} and T_{ox}^{oc}. The fill factors for gold and copper solar cells also showed vast improvement at 77 ^{o}K whereas the corresponding change for silver solar cells was less. As expected, the

the short-circuit current density went down for all the devices. The diode current went down by several orders of magnitude for Au and Cu solar cells. But the decrease was smaller for Ag solar cells. The value of n, in general, increased at 77 ^{o}K relative to its value at 300 ^{o}K, probably due to increased contribution from the recombination current at lower temperatures. The zero bias silicon band bending increased at the reduced temperature due to a decrease in ϕ_n, an increase in the silicon bandgap, and a decrease in the interface state charge. The device capacitance decreased as a consequence. The overall efficiency of the devices generally increased significantly at 77 ^{o}K, the chief reason being a reduction in the diode current due to a reduction in the temperature.

The measurements at 77 ^{o}K indicate that if the diode current can be reduced at room temperature by many orders of magnitude by an optimal design of the interfacial layer, very high opencircuit voltages, fill factors, and efficiencies can be achieved for MOS solar cells.

BIBLIOGRAPHY

1. S. Kar et al, 'Fabrication of Silicon MOS solar cells', Annual Report, Project No. EDL/SK/SK/76-77/35, I.I.T. Kanpur (1977).
2. J. Shankar, M. Tech. Thesis, I.I.T. Kanpur (1977).
3. J.W. Mayer, 'Performance of Germanium and Silicon surface barrier diodes as α-particle spectrometers', J. Appl. Phys. 30, 1937 (1959).
4. E. Ahlstrom and H. J. Gartner, 'Silicon surface barrier photocells', J. Appl. Phys. 33, 2502 (1962).
5. G. Rupprecht and A. Pampanini, Proc. 4th IEEE Photo. Spec. Conf., B-3-1 (1964).
6. W.A. Anderson and A. L. Delahoy, 'Schottky barrier diodes for solar energy conversion', Proc. IEEE, 60, 1457 (1972).
7. D.d. Lillington and W.C. Townsend, 'Effects of interfacial layers on the performance of silicon Schottky barrier solar cells', Appl. Phys. Lett. 28, 97 (1976).
8 J.P. Ponpon and P. Siffert, 'Open-circuit voltage of MIS silicon solar cells', J. Appl. Phys. 47, 3248 (1976).
9. A.H.M. Kipperman and M.A. Omar, 'Improved efficiency of MIS silicon solar cells by HF treatment of the oxide layer', Appl. Phys. Lett. 28, 621 (1976)
10. W.A. Anderson and R.A. Milano, 'I-V characteristics for silicon Schottky solar cells', Proc. IEEE, 63, 206 (1975).
11. E. Fabre, J. Michel and Y. Baudet, 'Photocurrent analysis in MIS silicon solar cells', Proc. 12th IEEE Photo. Spec. Conf., 904, IEEE, New York (1976).

12. R. Childs, J. Fortuna, J. Geneczko and S.J. Fonash, 'MIS solar cells: theory and experimental results', Proc. 12th IEEE Photo. Spec. Conf, 862 (1976).

13. S. Kar, 'Characterization of silicon MOS tunnel diodes', IEDM Technical Digest, 79, IEEE (NY) (1976).

14. 12th IEEE Photovoltaic Specialists Conference Record, Washington, D.C. (1975).

15. W.B. Berry, 'Photovoltaic shortcircuit minority carrier injection', Appl. Phys. Lett. 25, 195 (1974).

16. A.R. Moore, 'Short-circuit capacitance of illuminated solar cells', Appl. Phys. Lett. 27, 1 (1975).

17. R.L. Anderson, 'Photocurrent suppression in heterojunction solar cells', Appl. Phys. Lett. 27, 691 (1975).

18. F.J. Bryant and R.W. Glew, 'Analysis of the current voltage characteristics of Cadmium Sulphide solar cells under varying light intensities', Energy Conversion, 14, 129 (1975).

19. T.T. Rule, S.Y. Harmon, C.E. Backus and D.L. Jacobson, 'The testing of specially designed silicon solar cells under high sunlight illumination', Proc. 12th IEEE Photo. Spec. Conf., 744, IEEE, New York (1976).

20. S.M. Vernon and W.A. Anderson, 'Temperature effects in Schottky barrier silicon solar cells', Appl. Phys. Lett. 26, 707 (1975).

21. J.D. Sandstrom, Proc. 6th IEEE Photo. Spec. Conf., 199 (1967).

22. W.A. Anderson, S.M. Vernon, A.E. Delahoy, J.K. Kim and P. Mathe, 'Factors which maximize the efficiency of Cr-p Si Schottky (MIS) solar cells', J. Vac. Sci. Technol., 13, 1158 (1976).

23. D.F. Colbric, R. Wichner and E.J. Charlson, 'Temperature dependence of the photovoltaic performance of Si cells under blue, white and near band gap irradiation', Proc. 12th IEEE Photo. Spec. Conf., 40 (1976).

24. D.L. Pulfrey, 'Photovoltaic Power Generation,' Van Nostrand Reinhold : New York (1978).

25. S.J. Fonash, 'Outline and comparison of the possible effects present in a metal-thin film insulator-semiconductor solar cells', J. Appl. Phys. 47, 3597 (1976).

26. H.C. Card and E.S. Yang, 'MIS-Schottky theory under conditions of optical generation in solar cells', Appl. Phys. Lett. 29, 51)(1976).

27. S. Kar,' Effects of interface states, tunneling and metal in silicon MOS solar cells', IEDM Technical Digiest, 56A, Washington D.C. (1977).

28. S. Kar, D. Shanker, S.P. Joshi and S. Bhattacharya, 'Experimental and theoretical study of silicon MOS solar cells with different barrier metals', Proc. 13th IEEE Photo. Spec. Conf., (1978)

29. S. Kar,' Experimental study of interface properties of MOS tunnel devices', Proc. 12th IEEE Photo. Spec. Conf., 922 (1976).

30. A.J. Novel,'Solar cells, Semiconductor and Semimetal series, Vol. 11, Ch. 8, Academic Press : New York (1975).

31. H.F. Wolf, 'Silicon Semiconductor data', P.25, 87 and 111, Pergamon Press (1969).

32. B. Ross and J.R. Madigan, 'Thermal generation of recombination centres in silicon', Phys. Rev. 108, 1428 (1957).

33. P.G. Wilkinson, 'Lattice distortion spectrum of evaporated Au', J. Appl. Phys. 22, 419 (1975).

34. H. Jaeger et al, 'Nucleation and growth of silver films deposited on mica substrates in ultrahigh vacuum', Surf. Science, 11, 265 (1968).

35. F. Lukes, 'Oxidation of Si and GaAs in air at room temperature', Surf. Science, 30, 91 (1972).

36. D.J. Charlson and J.C. Lien, 'An Al-p Silicon MOS photovoltaic cell', J. Appl. Phys. 46, 3982 (1975).

37. Chandra Goradia, Ronald Ziegman and Bernard L. Sater, 'Characteristics of high intensity edge-illuminated multijunction solar cells - Experimental results and theory', Proc. 12th IECL Photo. Spec. Conf., IEEE (1976).

38. S. Kar, 'Interface charge characteristics of MOS structures with different metals on steam grown oxides', Sol. St. Elec. 18, 723 (1975).

List of Figures

Fig.4.7 Measured diode current-voltage characteristics of device Ag 16 with Ag front contact and 24 Å thick oxide. The broken line represents the shortcircuit current.

Fig.4.8 Measured $1/C^2$ vs V characteristics of devices Ag 16 and Ag 21.

Fig.4.9 Measured current-voltage characteristics of two typical Cu solar cells.

Fig.4.10 Measured diode current-voltage characteristics of device Cu 27 with 10 Å thick oxide at 300 and 77 °K. The broken lines represent the shortcircuit currents at the two temperatures.

Fig.4.11 Measured diode current-voltage characteristics of device Cu 13 with 20 Å thick oxide. The broken line represents the shortcircuit current.

Fig.4.12 Measured $1/C^2$ vs V characteristics for device Cu 27 at 300 and 77 °K.

Fig.4.13 Measured current-voltage characteristics under concentration of device Au 21 with 10 Å thick oxide and Au front contact.

Fig.4.14 Variation of the opencircuit voltage, the fill factor, and the efficiency for device Au 21 with the concentration ratio.

Fig.4.15 Measured diode current-voltage characteristics of device Au 21 at various light intensities.

Fig.4.16 A plot of $\Delta I_D/I_D^\circ$ vs the concentration ratio for device Au 21 at different values of the applied bias. ΔI_D is the increase in the diode current relative to its value I_D in dark.

Fig.4.17 Measured $1/C^2$ vs V characteristics for device Au 21 at different illumination levels.

Fig.4.18 Measured current-voltage characteristics at various illumination levels for device Au 28 with 13 Å thick oxide and Au front contact.

Fig.4.19 Measured current-voltage characteristics at different illumination levels for device Ag 19 with 22 Å thick oxide and Ag front contact.

Fig.4.20 Measured diode current-voltage characteristics of device Ag 19 under concentrated light.

Fig.4.21 Measured $1/C^2$ vs V characteristics of device Ag 19 under concentrated light.

Fig.4.22 Measured current-voltage characteristics under concentration of device Ag 16 with 24 Å thick oxide and Ag front contact.

Fig.4.23 Variation of the opencircuit voltage, the fill factor, and the overall efficiency of device Ag 16 with the concentration ratio.

Fig.4.24 Measured current-voltage characteristics at 301, 340, 36[illegible] and 398 °K of device Au 25 with 13 Å thick oxide and Au front contact.

Fig.4.25 Measured current-voltage characteristics at 305, 330, 35[illegible] 385, and 408 °K of device Ag 47 with 22 Å thick oxide and Ag front contact.

Fig. 4.25 Variation of the opencircuit voltage, the shortcircuit current density, the fill factor, and the efficiency with temperature for devices Au 25, Au 21, and Ag 47.

Fig. 4.27 Measured diode current-voltage characteristics at 305, 330, and 385 °K of device Ag 47. The dotted lines represent the shortcircuit currents at these temperatures.

Fig. 4.28 Measured $1/C^2$ vs V characteristics at 317 and 370 °K of device Au 24 in dark and under illumination.

Fig. 4.29 Measured $1/C^2$ vs V characteristics at 305 and 385 °K of device Ag 47 in dark and under illumination.

Fig. 4.30 Measured current-voltage characteristics at 300 and 77 °K of device Au 32 with Au front contact and 10 Å thick oxide.

Fig. 4.31 Measured diode current-voltage characteristics at 300 and 77 °K of device Au 32. The dashed lines represent the shortcircuit currents at the two temperatures.

Fig. 4.32 Measured $1/C^2$ vs V characteristics of device Au 32 in dark and under illumination at 300 °K and under illumination at 77 °K.

Fig. 4.33 Measured current-voltage characteristics at 77 and 300 °K of device Cu 27 with 10 Å thick oxide and Cu front contact.

Fig. 4.34 Measured current-voltage characteristics at 77 and 300 °K of device Ag 27 with 24 Å thick oxide and Ag front contact.

Fig. 4.35 Measured diode current-voltage characteristics of device Ag 19 at 300 and 77 °K in dark and under illumination.

Fig. 4.36 Measured $1/C^2$ vs V characteristics under illumination at 77 °K of device Ag 27.

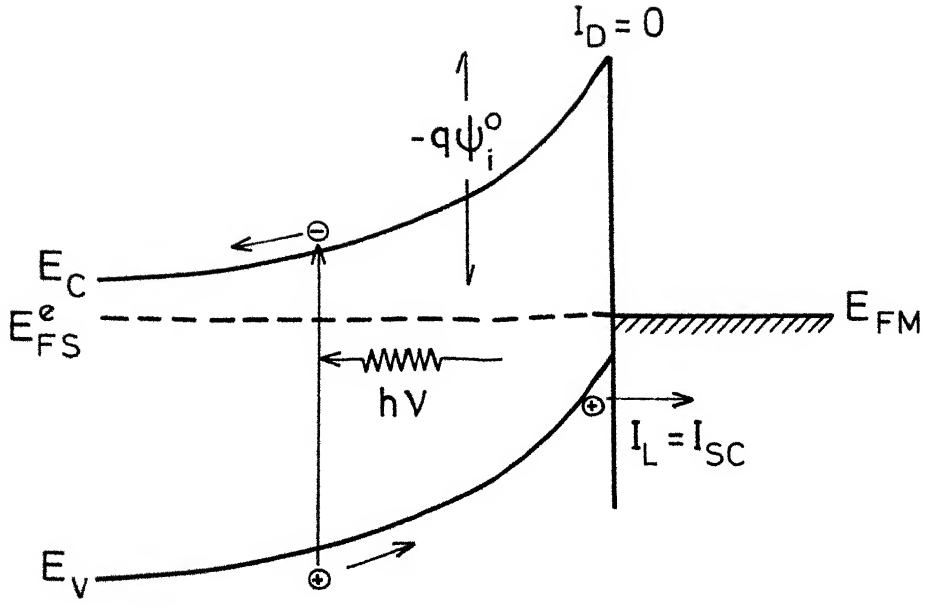
$I_D = 0$
$-q\psi_i^o$
E_C
E_{FS}^e
E_{FM}
$h\nu$
$I_L = I_{SC}$
E_V

FIG. 2.1

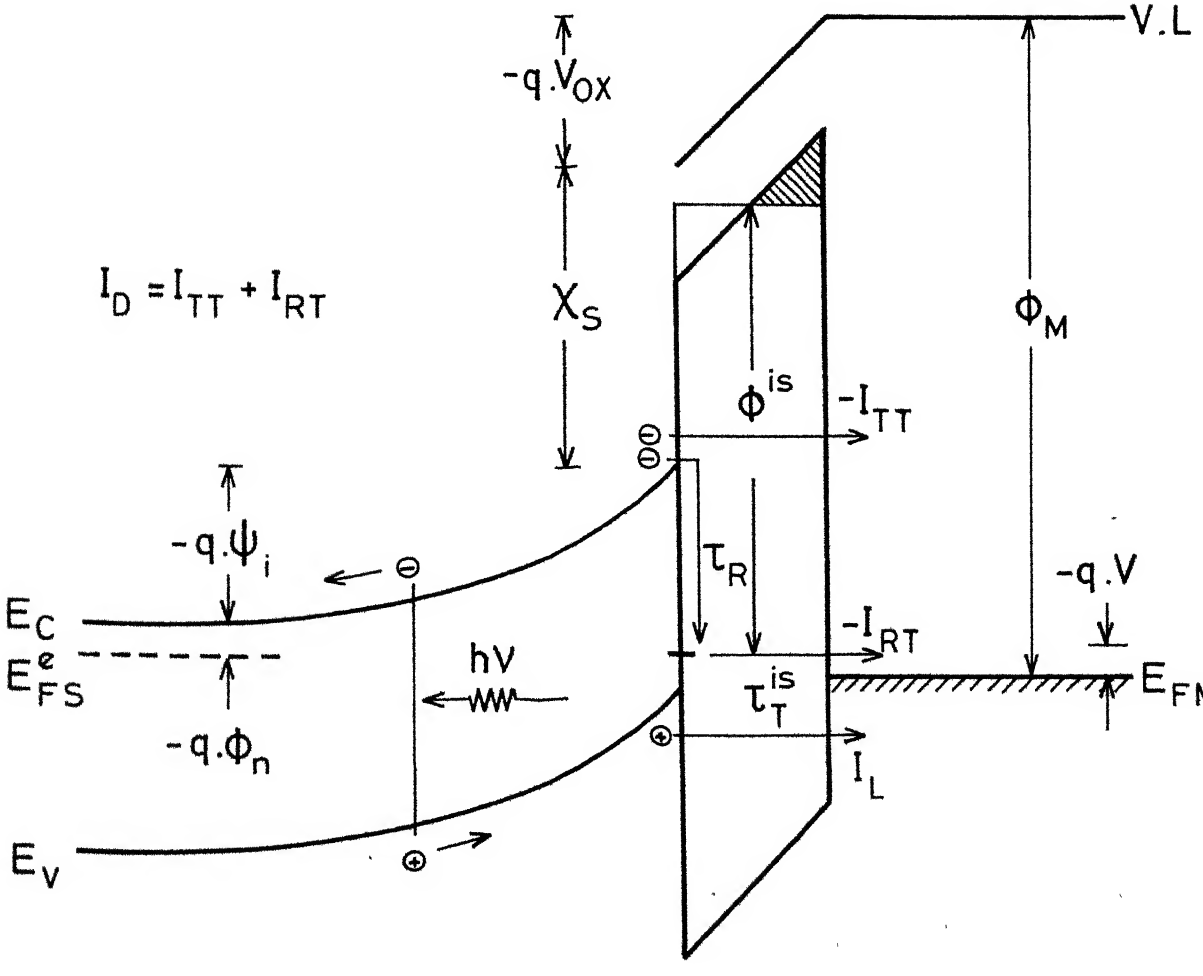
V.L
$-q.V_{OX}$
$I_D = I_{TT} + I_{RT}$
χ_S
Φ_M
ϕ^{is}
$-I_{TT}$
$-q.\psi_i$
τ_R
$-q.V$
E_C
$-I_{RT}$
$h\nu$
E_{FS}^e
τ_T^{is}
E_{FM}
$-q.\Phi_n$
I_L
E_V

FIG. 2.2

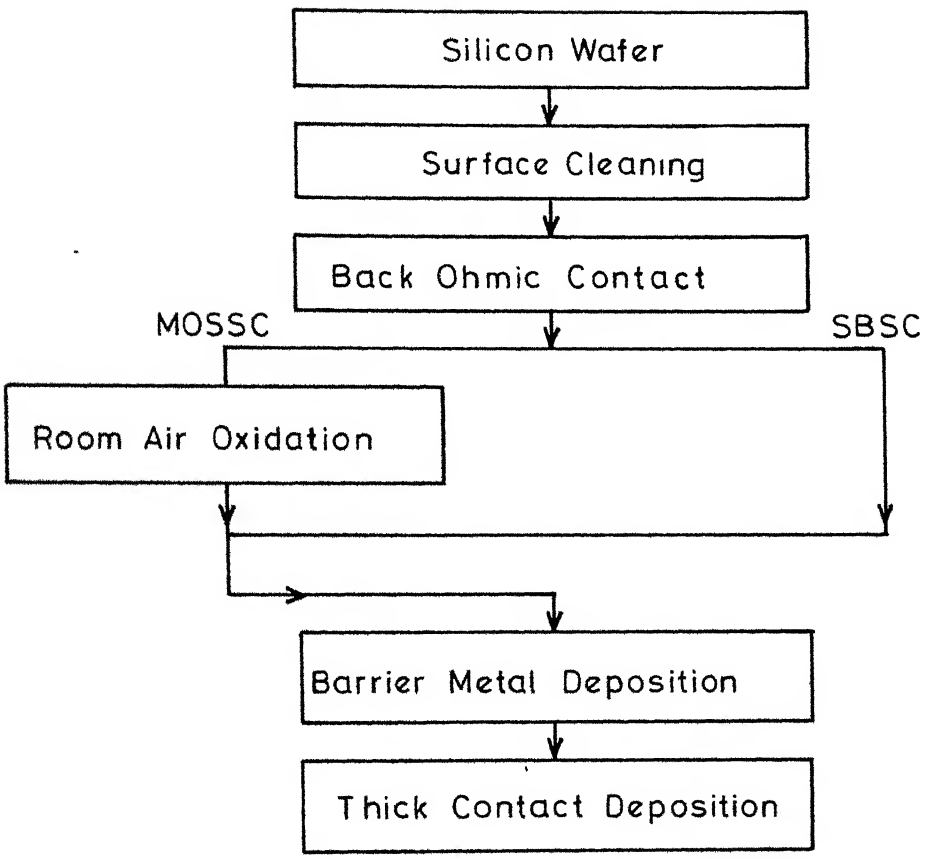
Silicon Wafer
Surface Cleaning
Back Ohmic Contact
MOSSC
SBSC
Room Air Oxidation
Barrier Metal Deposition
Thick Contact Deposition

FIG. 3.1

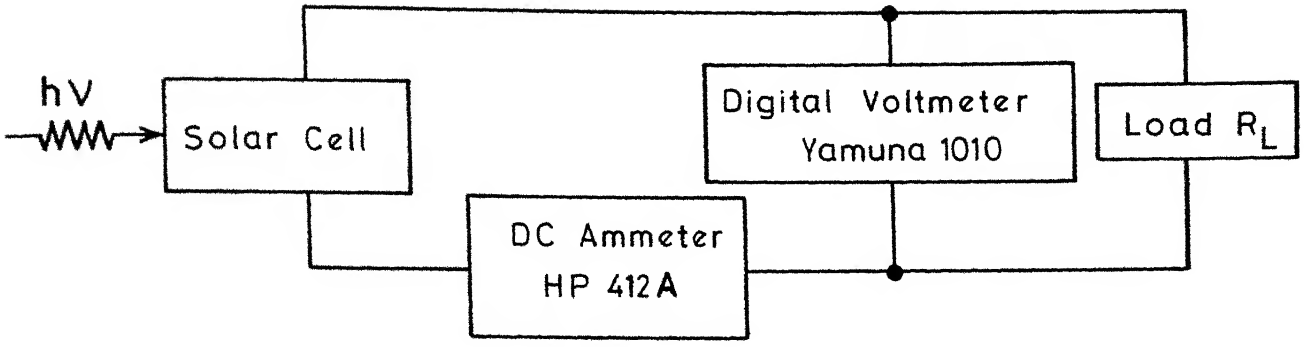

FIG.3.2a

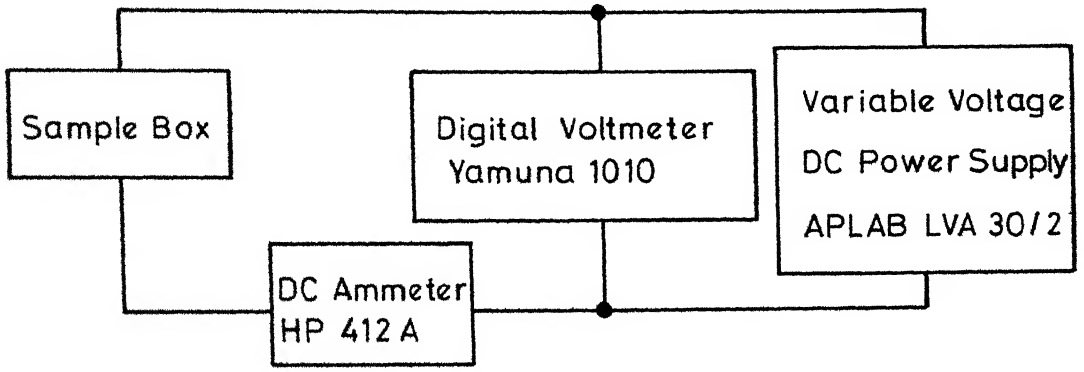

FIG.3.2b

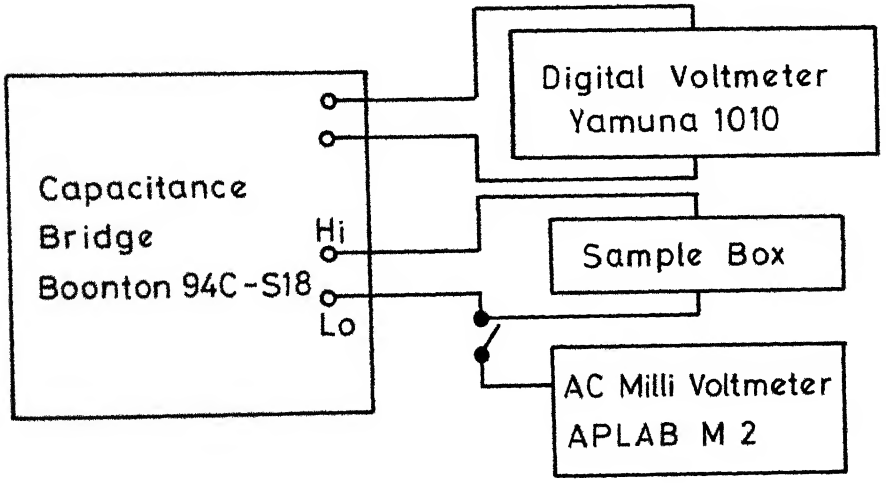

FIG.3.2c

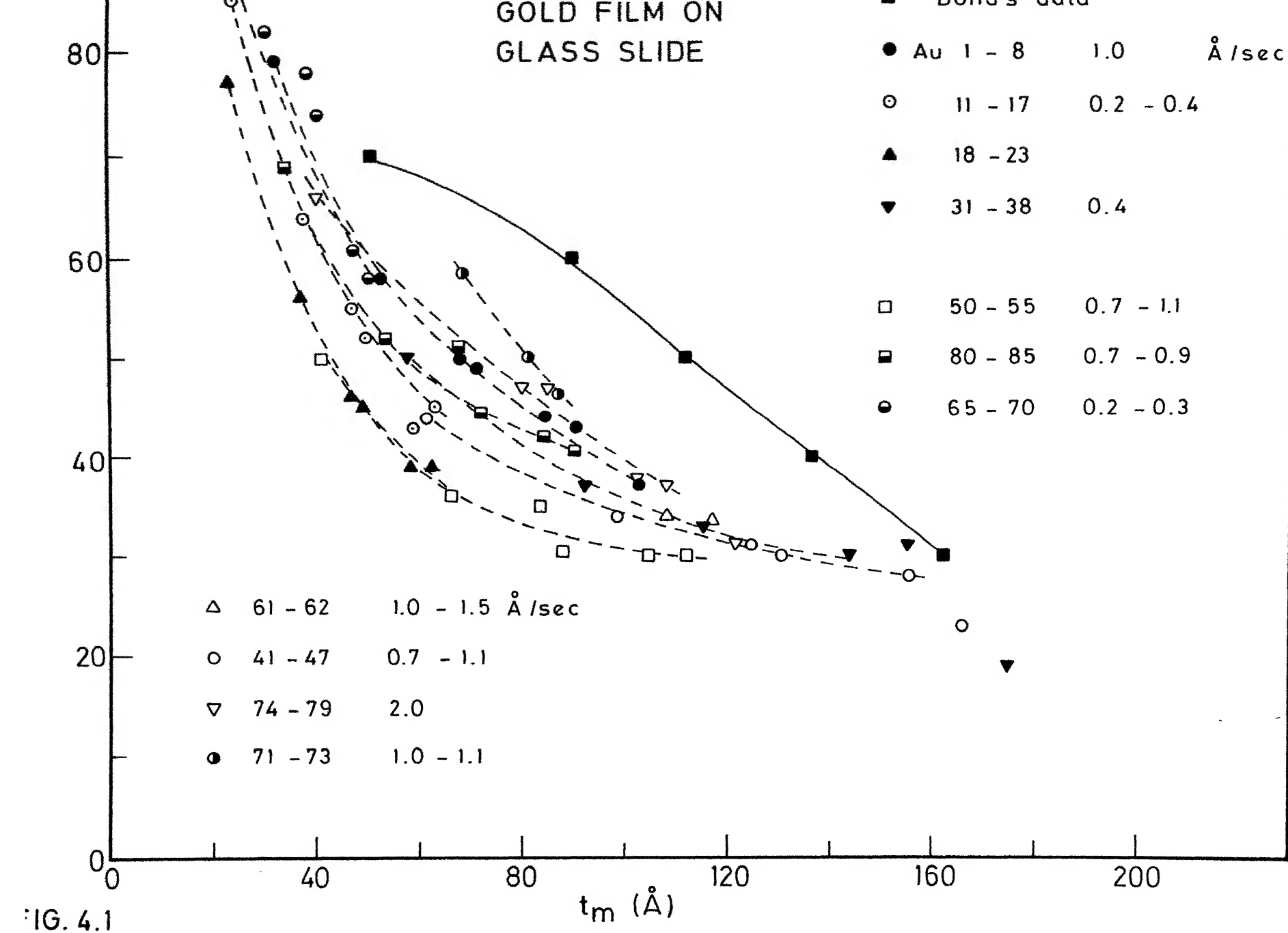
GOLD FILM ON
GLASS SLIDE
Bond's gold
Au 1 - 8 1.0 Å/sec
11 - 17 0.2 - 0.4
18 - 23
31 - 38 0.4
50 - 55 0.7 - 1.1
80 - 85 0.7 - 0.9
65 - 70 0.2 - 0.3
61 - 62 1.0 - 1.5 Å/sec
41 - 47 0.7 - 1.1
74 - 79 2.0
71 - 73 1.0 - 1.1
0
20
40
60
80
0
40
80
120
160
200
t_m (Å)

FIG. 4.1

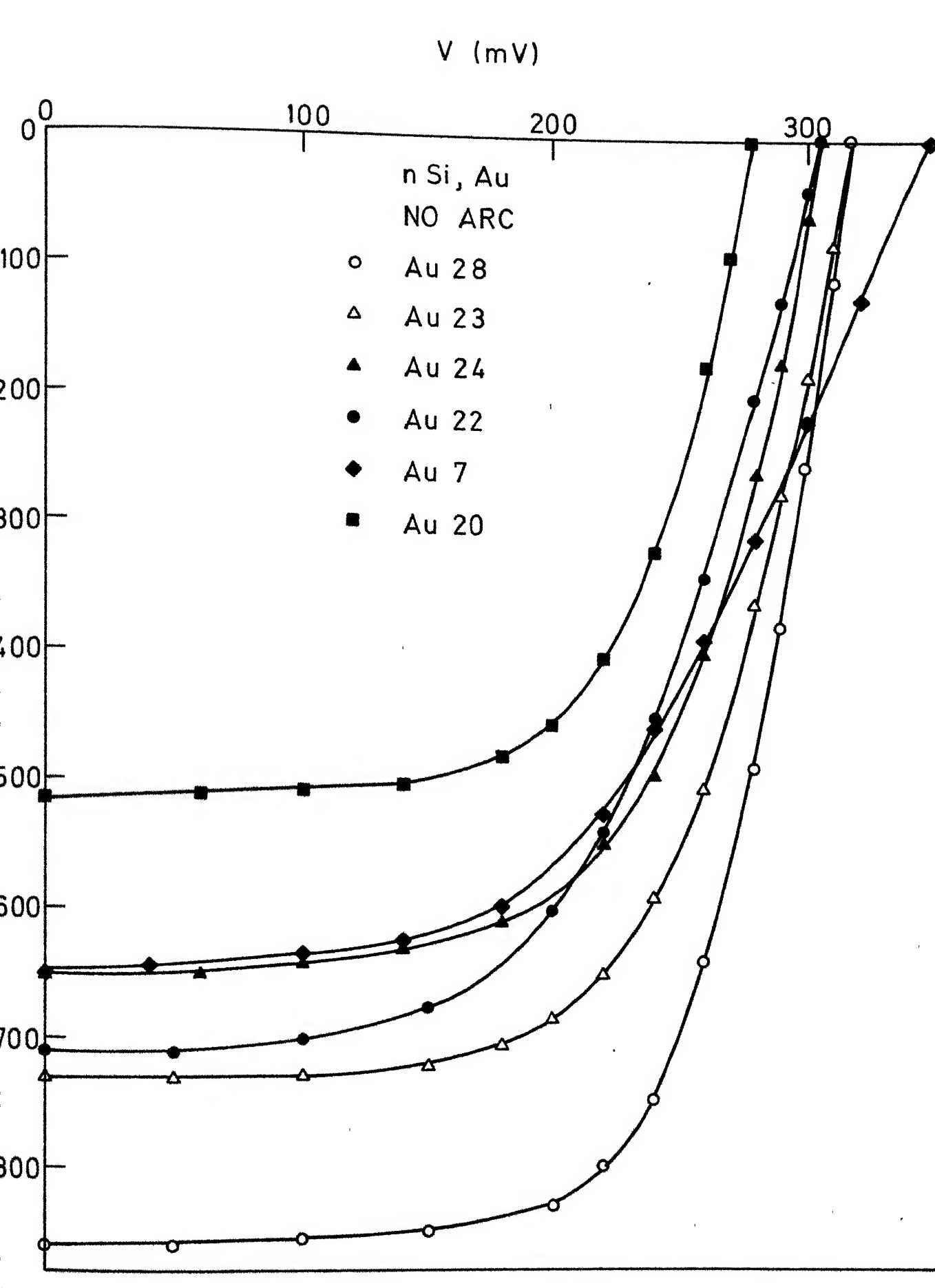

FIG.4.2

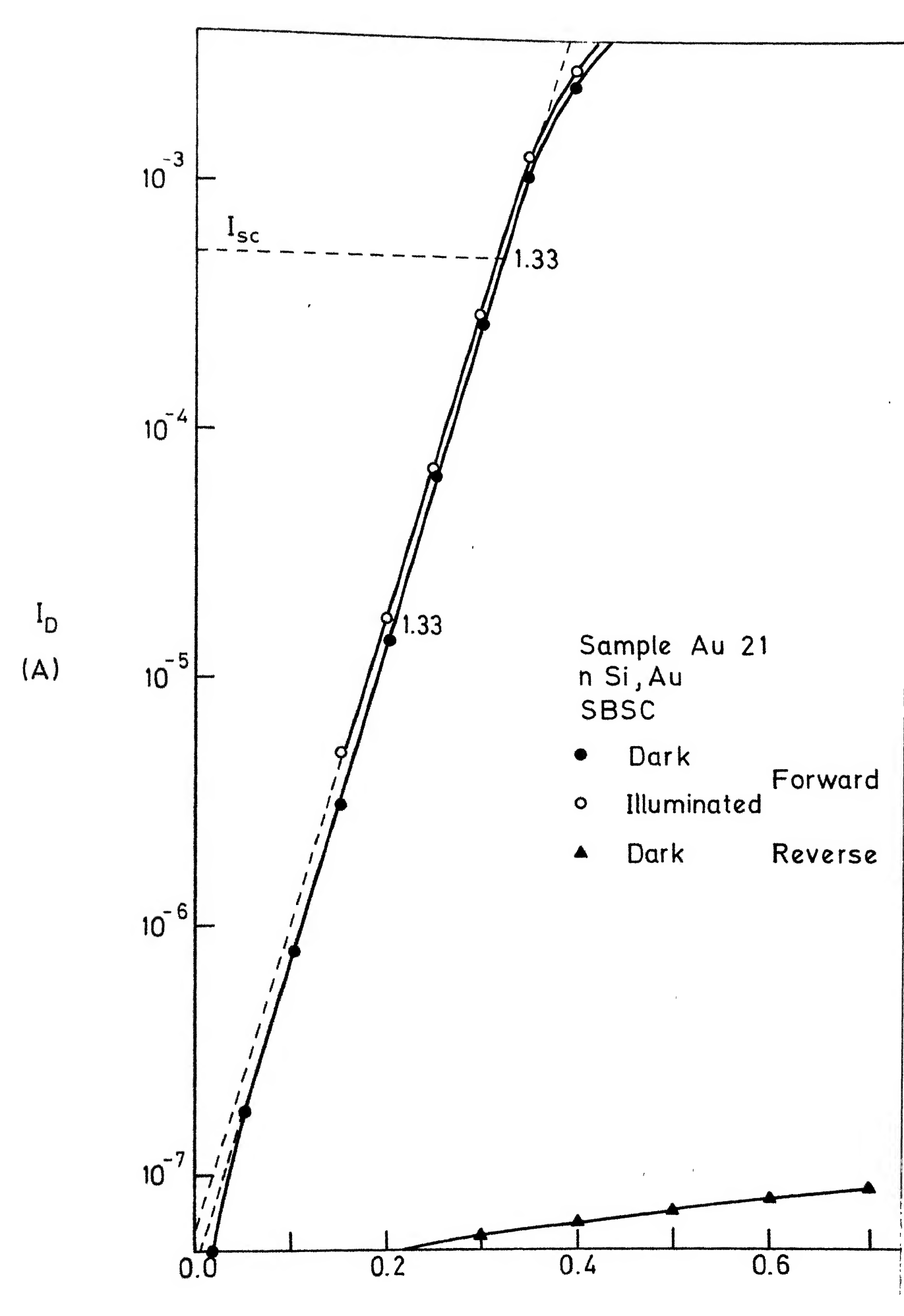
10^{-3}
I_{sc}
1.33
10^{-4}
I_D
(A)
1.33
10^{-5}
Sample Au 21
n Si, Au
SBSC
Dark
Forward
Illuminated
Dark
Reverse
10^{-6}
10^{-7}
0.0
0.2
0.4
0.6

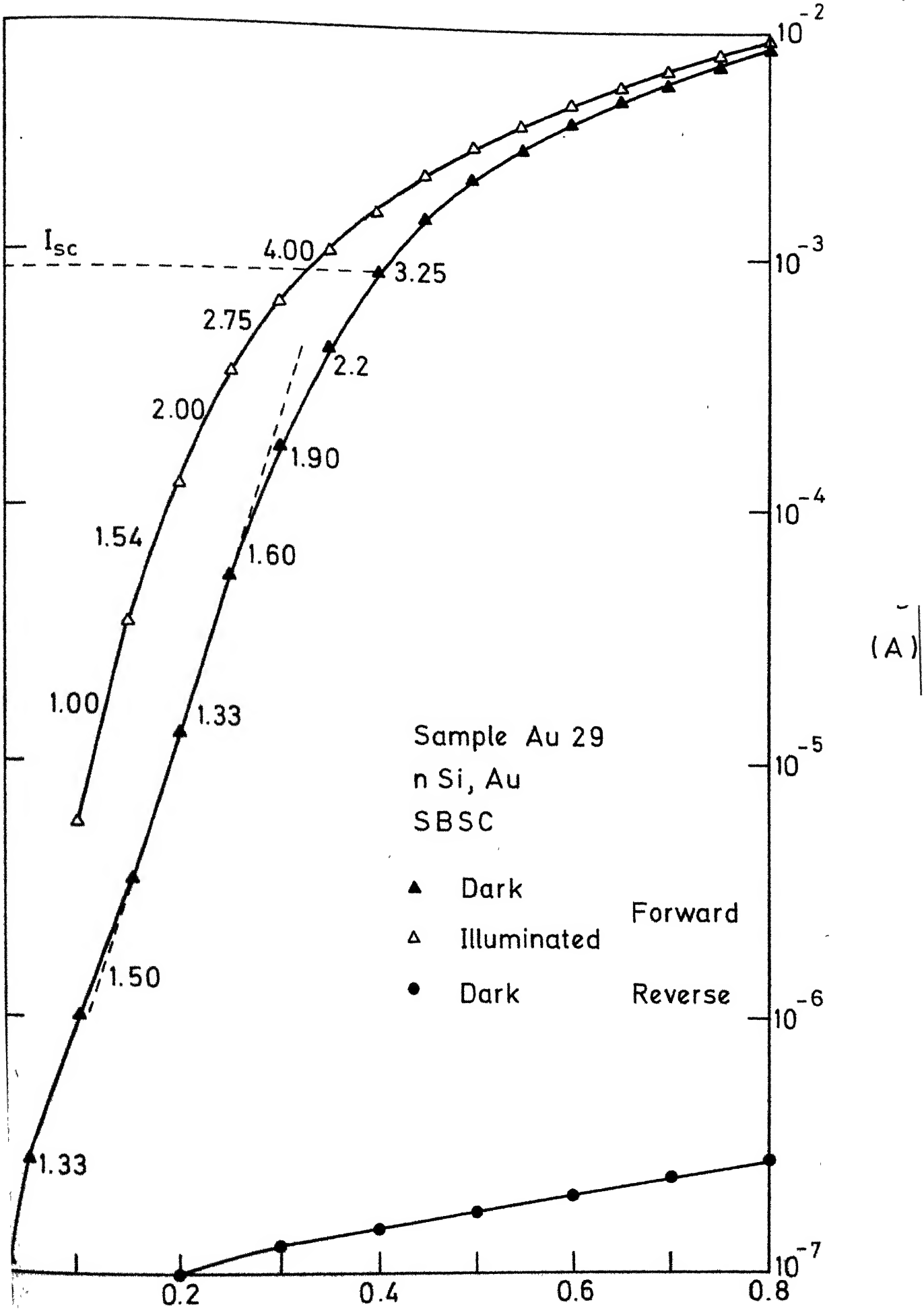
I_{sc}
4.00
3.25
2.75
2.2
2.00
1.90
1.54
1.60
1.00
1.33
1.50
1.33
Sample Au 29
n Si, Au
SBSC
Dark
Illuminated
Forward
Dark
Reverse
10^{-2}
10^{-3}
10^{-4}
10^{-5}
10^{-6}
10^{-7}
(A)
0.2
0.4
0.6
0.8

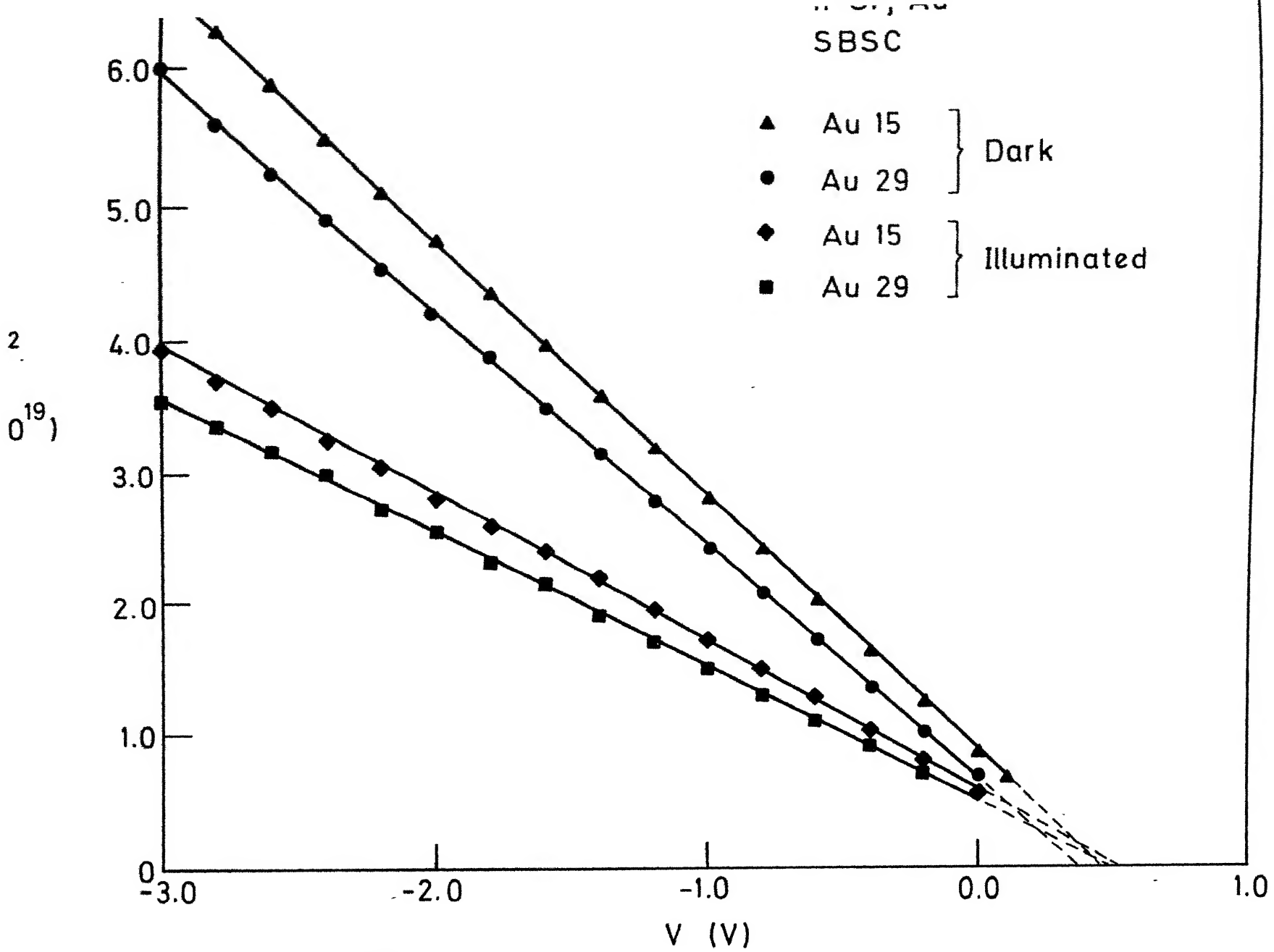
SBSC
Au 15
Au 29
Dark
Au 15
Au 29
Illuminated
6.0
5.0
4.0
3.0
2.0
1.0
0
-3.0
-2.0
-1.0
0.0
1.0
V (V)

FIG 4.5

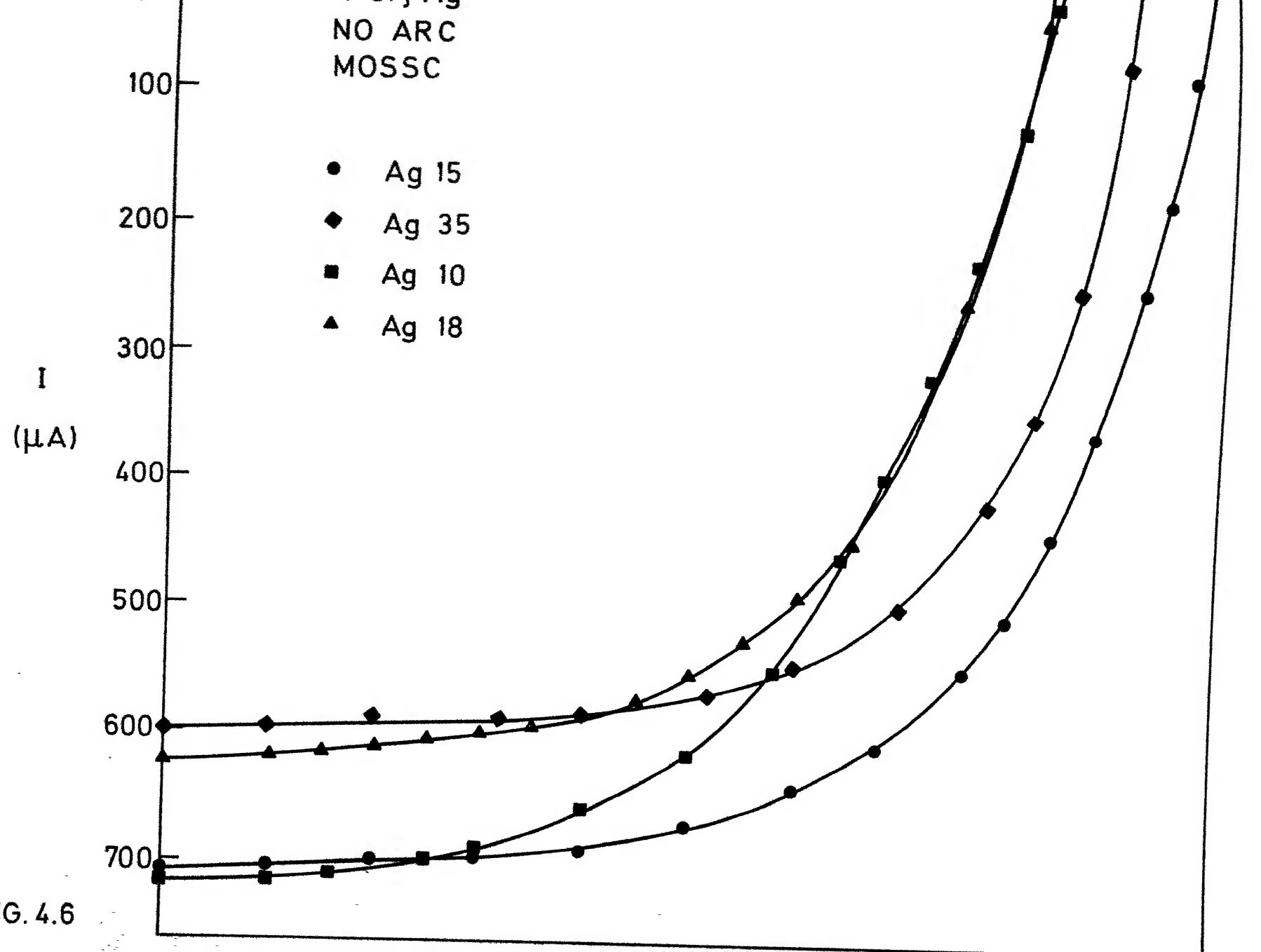
NO ARC
MOSSC
Ag 15
Ag 35
Ag 10
Ag 18
I
(μA)
100
200
300
400
500
600
700

FIG. 4.6

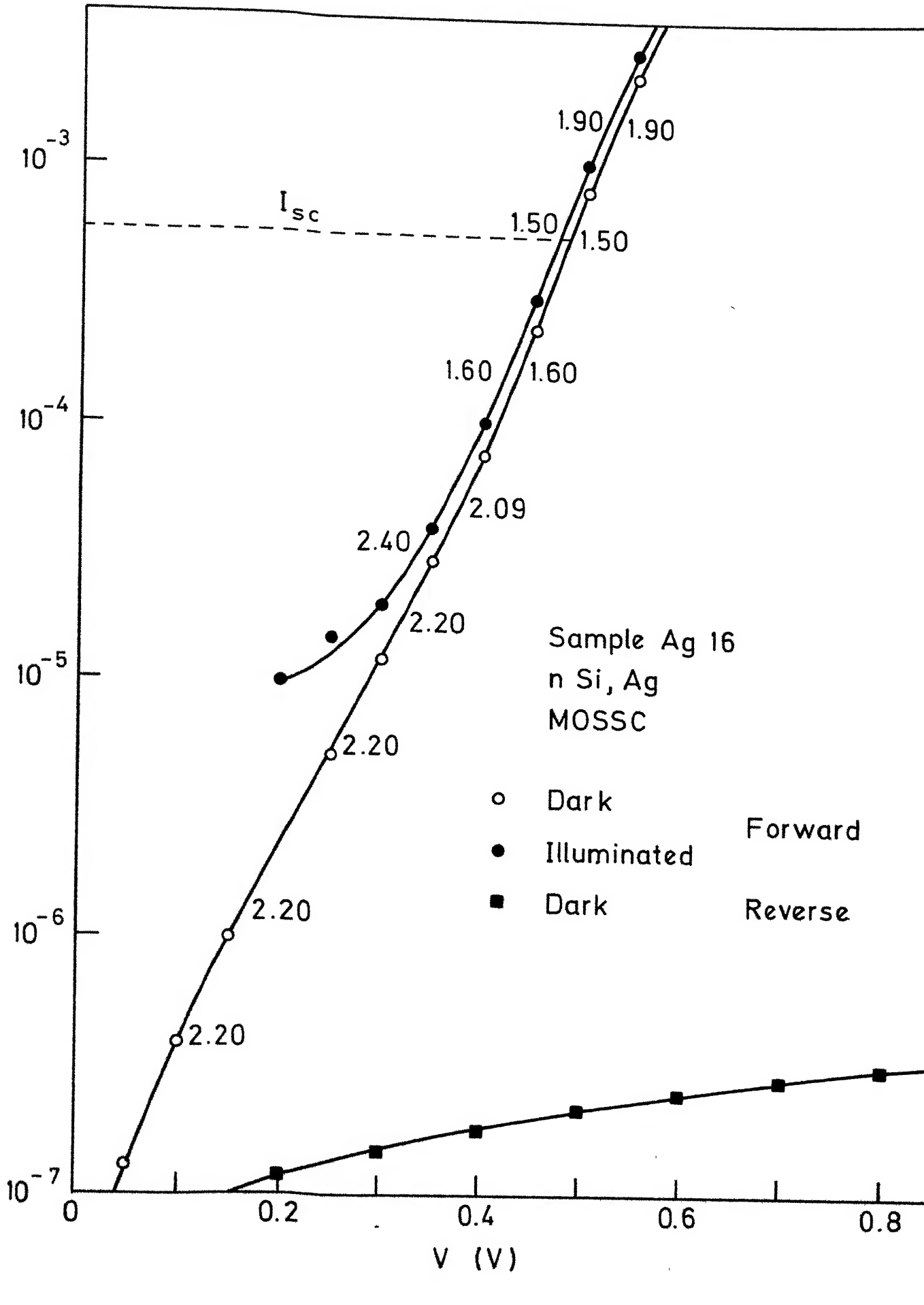
10^{-3}
10^{-4}
10^{-5}
10^{-6}
10^{-7}
I_{sc}
1.90
1.90
1.50
1.50
1.60
1.60
2.09
2.40
2.20
2.20
2.20
2.20
Sample Ag 16
n Si, Ag
MOSSC
Dark
Illuminated
Dark
Forward
Reverse
0
0.2
0.4
0.6
0.8
V (V)

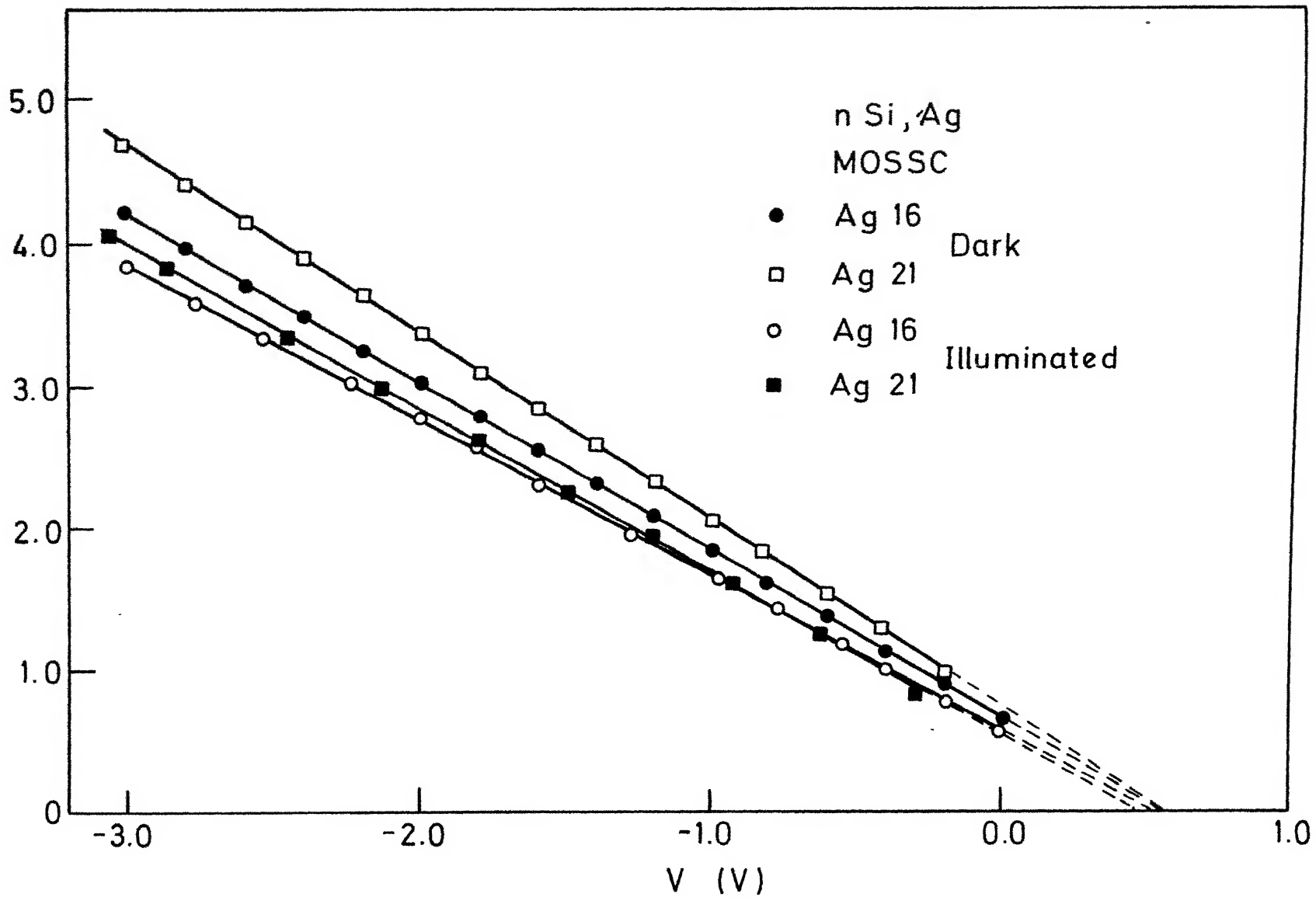
n Si, Ag
MOSSC
Ag 16
Ag 21
Dark
Ag 16
Ag 21
Illuminated
5.0
4.0
3.0
2.0
1.0
0
-3.0
-2.0
-1.0
0.0
1.0
V (V)

FIG. 4.8

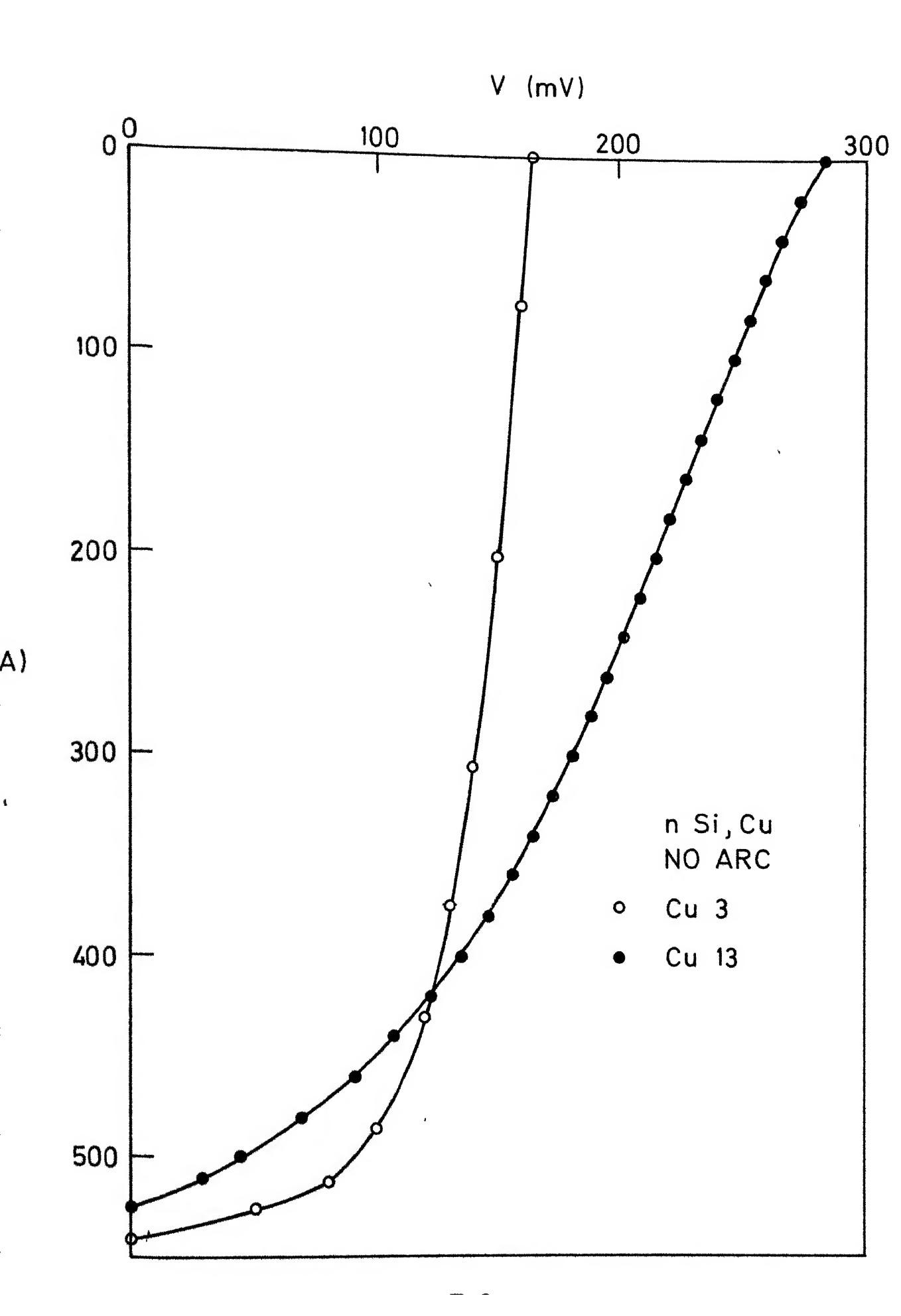
V (mV)
0
100
200
300
100
200
300
400
500
n Si, Cu
NO ARC
Cu 3
Cu 13

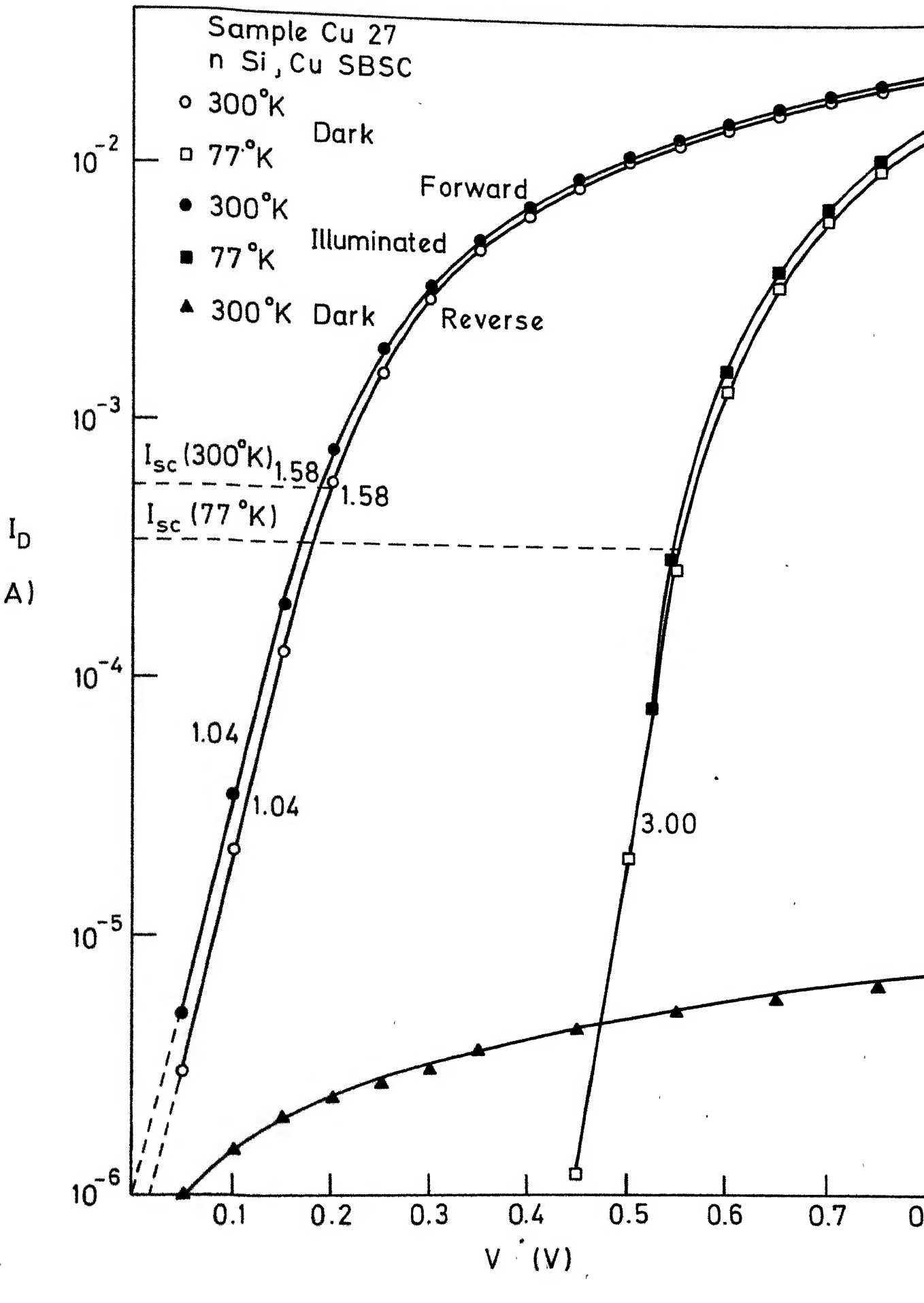
Sample Cu 27
n Si, Cu SBSC
300°K
77°K
300°K
77°K
300°K Dark
Dark
Illuminated
Forward
Reverse
10^{-2}
10^{-3}
10^{-4}
10^{-5}
10^{-6}
I_{sc} (300°K)
I_{sc} (77°K)
1.58
1.58
1.04
1.04
3.00
I_D
A)
0.1
0.2
0.3
0.4
0.5
0.6
0.7
V (V)

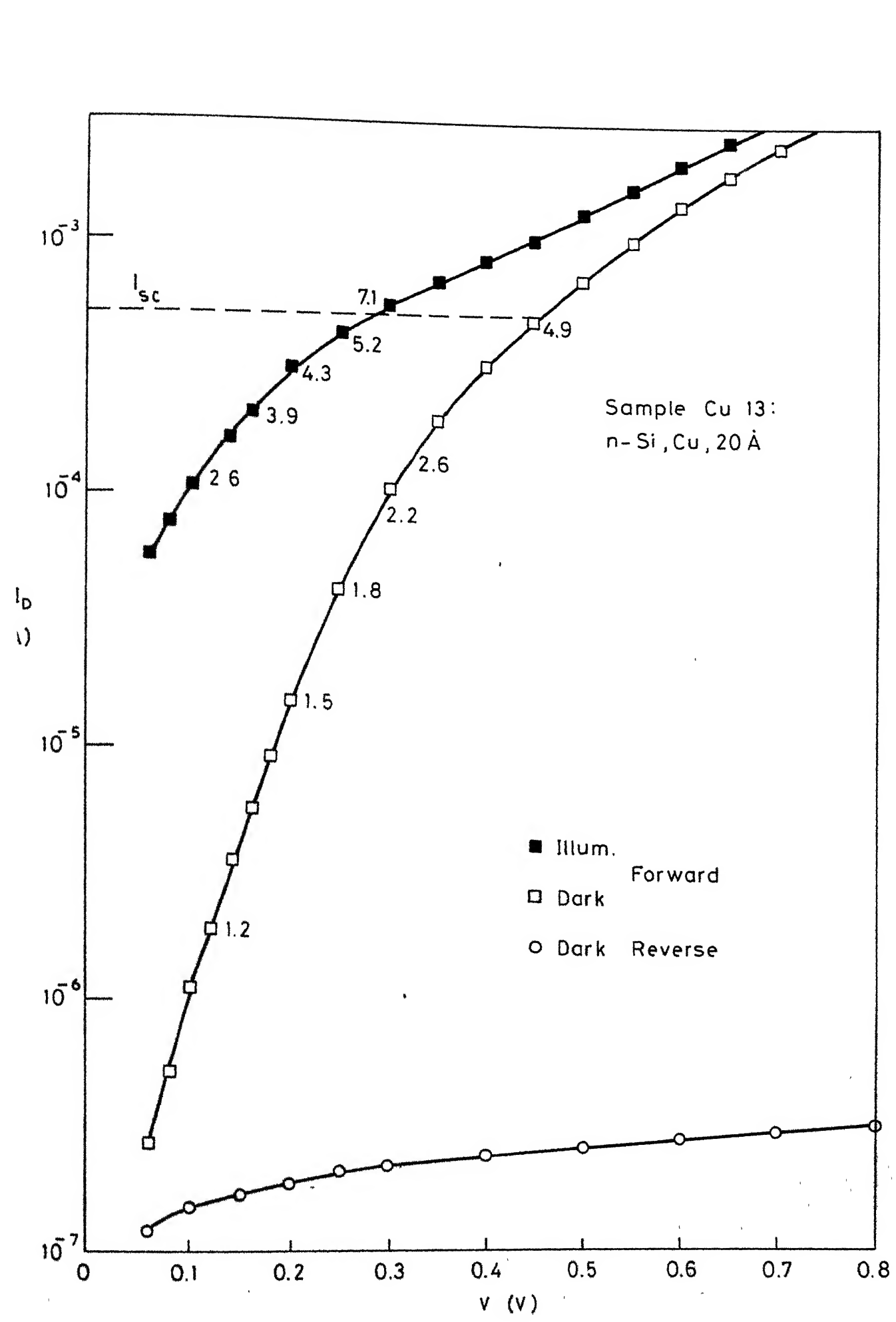
10^{-3}
10^{-4}
10^{-5}
10^{-6}
10^{-7}
I_{sc}
7.1
5.2
4.3
3.9
2 6
4.9
2.6
2.2
1.8
1.5
1.2
Sample Cu 13:
n-Si, Cu, 20 Å
Illum. Forward
Dark
Dark Reverse
0
0.1
0.2
0.3
0.4
0.5
0.6
0.7
0.8
V (V)

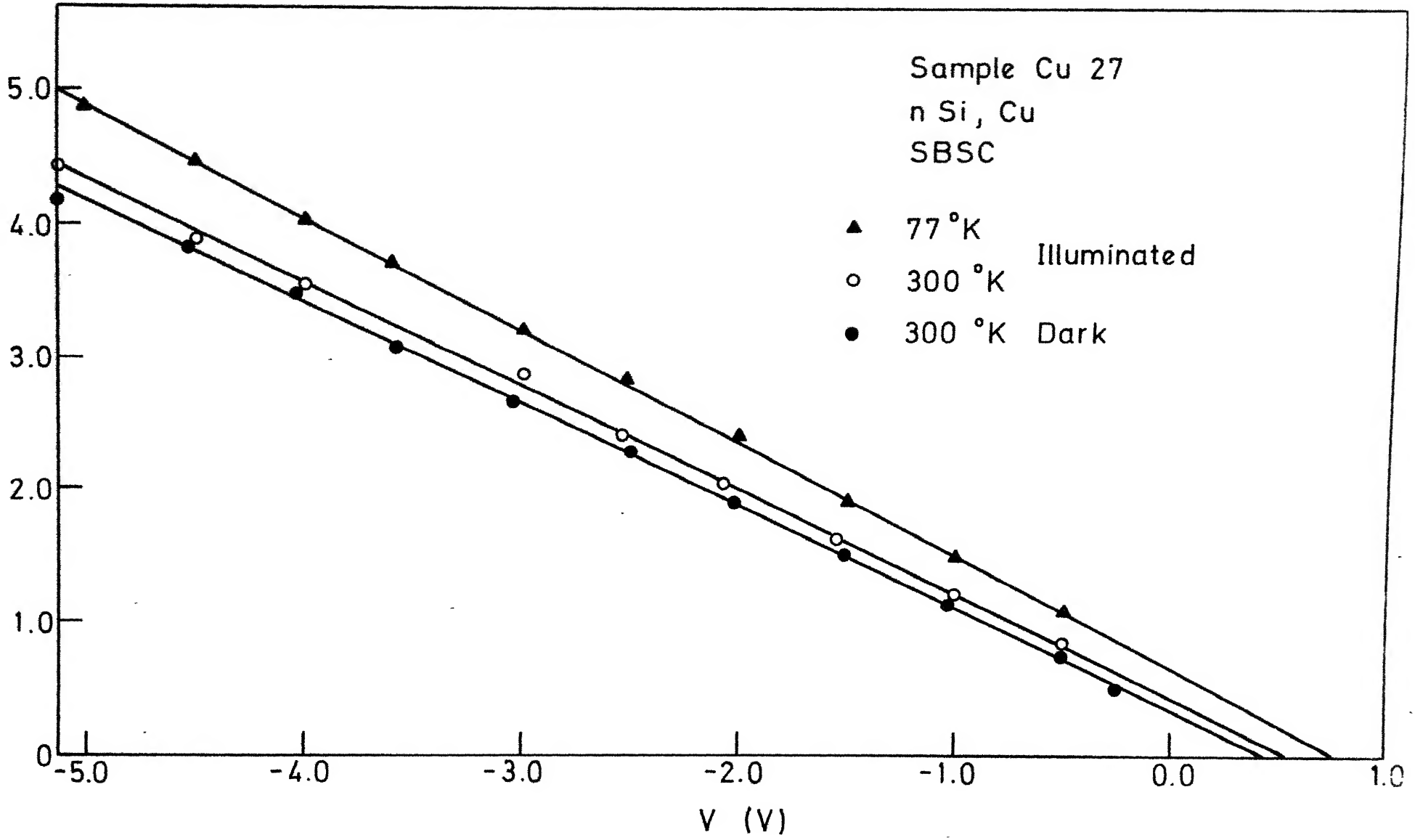
Sample Cu 27
n Si , Cu
SBSC
77 °K
300 °K
Illuminated
300 °K Dark
5.0
4.0
3.0
2.0
1.0
0
-5.0
-4.0
-3.0
-2.0
-1.0
0.0
1.0
V (V)

FIG. 4.12

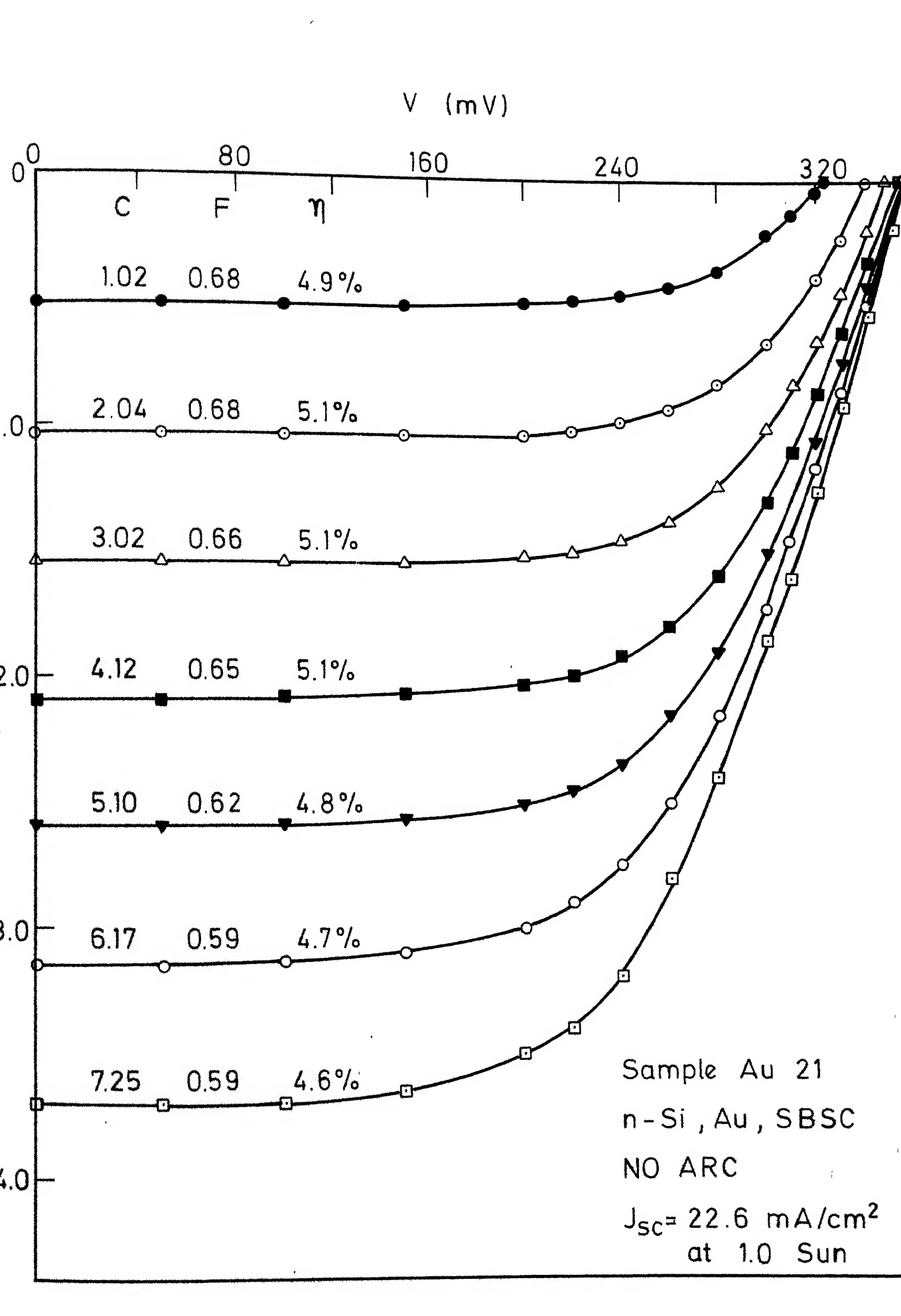
V (mV)
0
80
160
240
320
C
F
η
1.02 0.68 4.9%
2.04 0.68 5.1%
3.02 0.66 5.1%
4.12 0.65 5.1%
5.10 0.62 4.8%
6.17 0.59 4.7%
7.25 0.59 4.6%
Sample Au 21
n-Si, Au, SBSC
NO ARC
J_{sc}= 22.6 mA/cm²
at 1.0 Sun

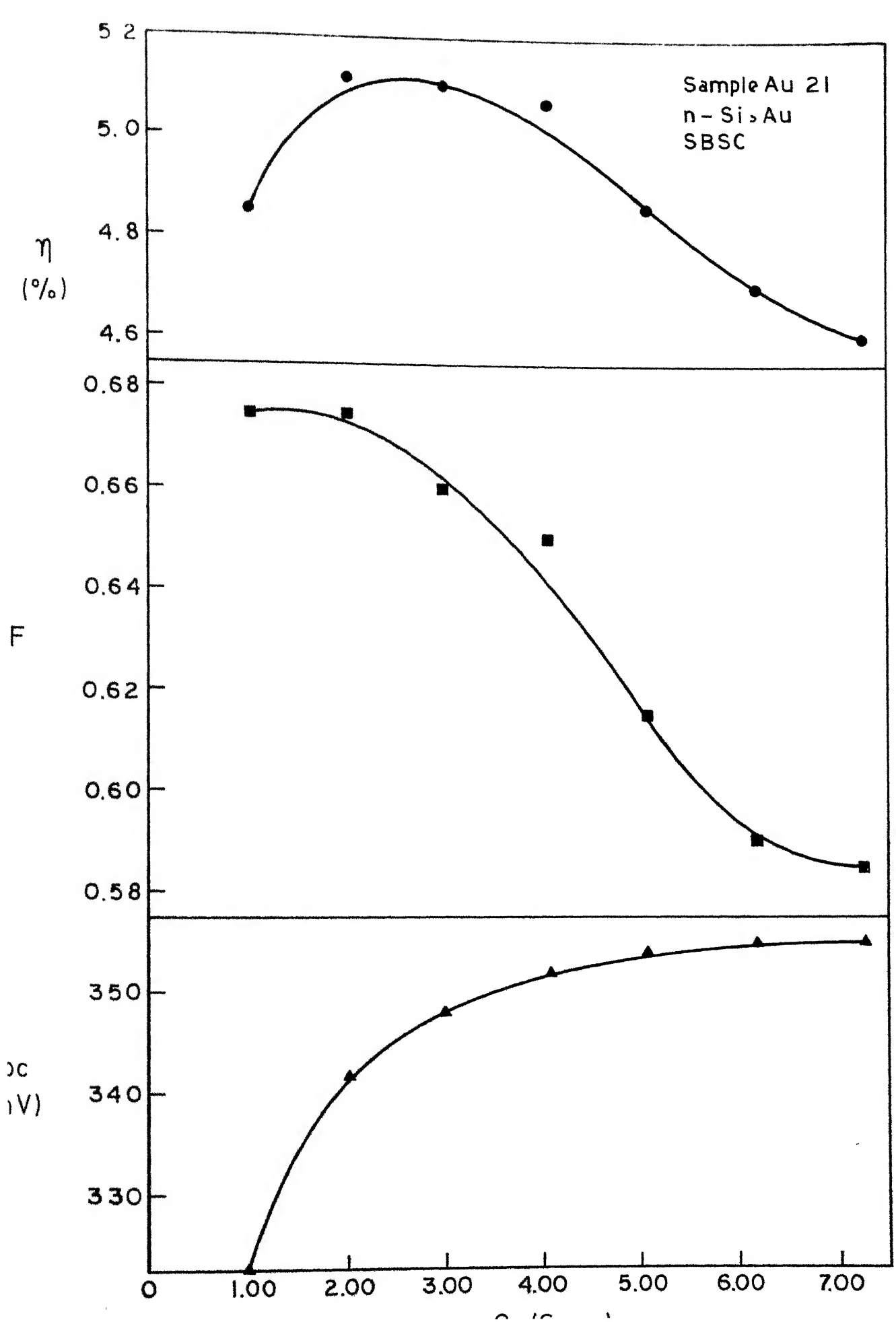
Sample Au 21
n – Si › Au
SBSC
η
(%)
5 2
5.0
4.8
4.6
F
0.68
0.66
0.64
0.62
0.60
0.58
)c
)V)
350
340
330
0
1.00
2.00
3.00
4.00
5.00
6.00
7.00

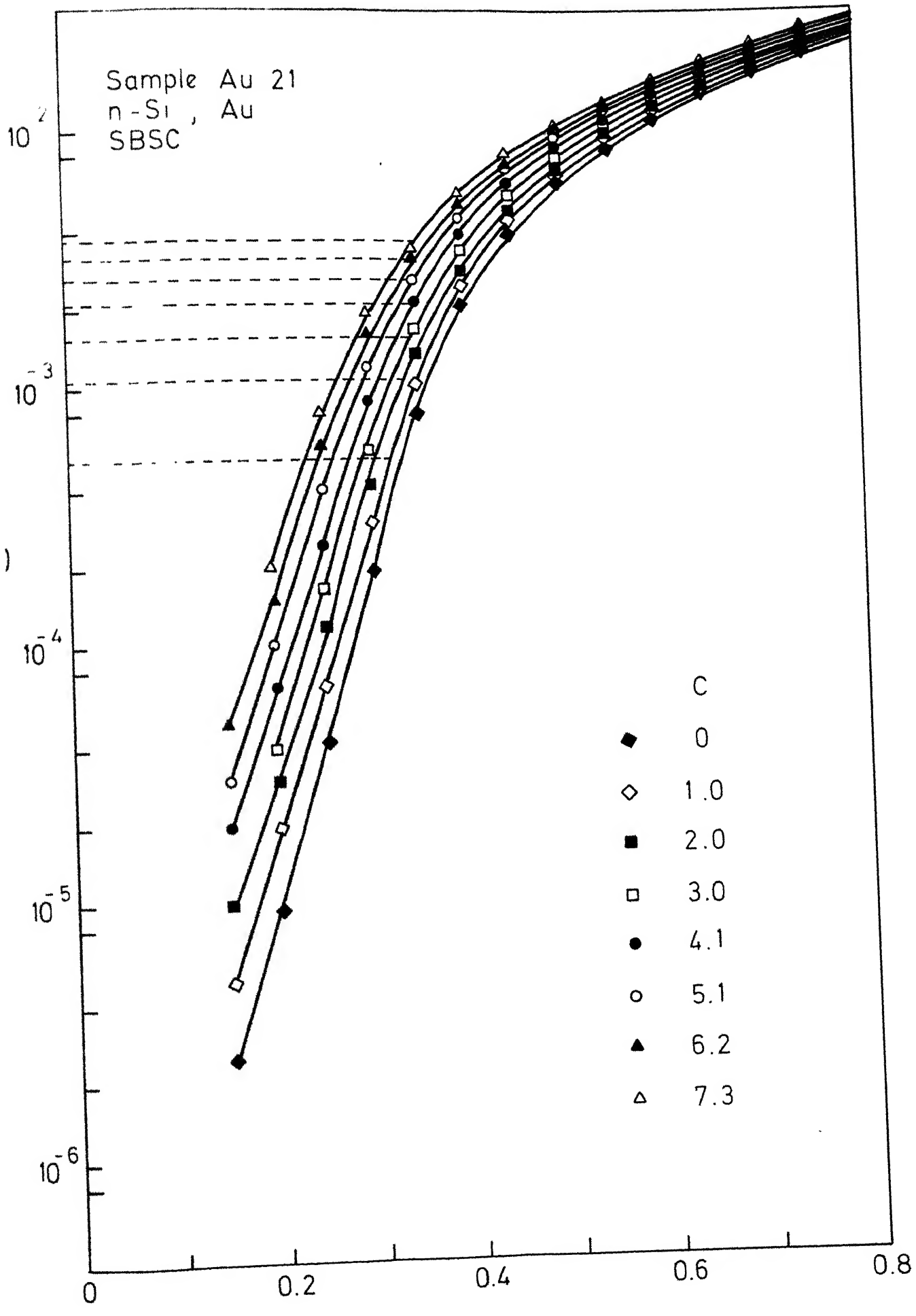
Sample Au 21
n-Si , Au
SBSC
10^{-2}
10^{-3}
10^{-4}
10^{-5}
10^{-6}
C
0
1.0
2.0
3.0
4.1
5.1
6.2
7.3
0
0.2
0.4
0.6
0.8

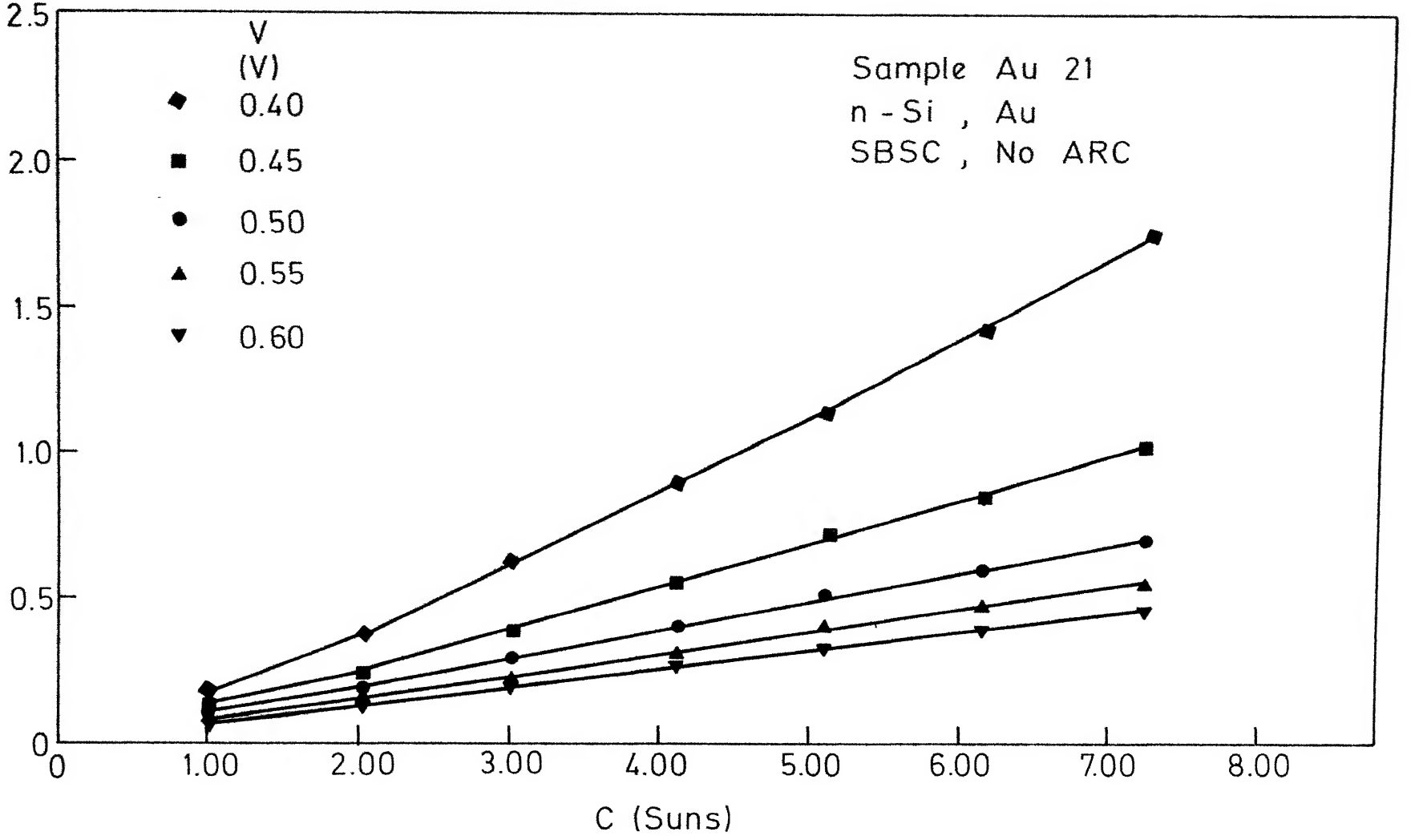
V
(V)
0.40
0.45
0.50
0.55
0.60
Sample Au 21
n - Si , Au
SBSC , No ARC
2.5
2.0
1.5
1.0
0.5
0
0
1.00
2.00
3.00
4.00
5.00
6.00
7.00
8.00
C (Suns)

FIG. 4.16

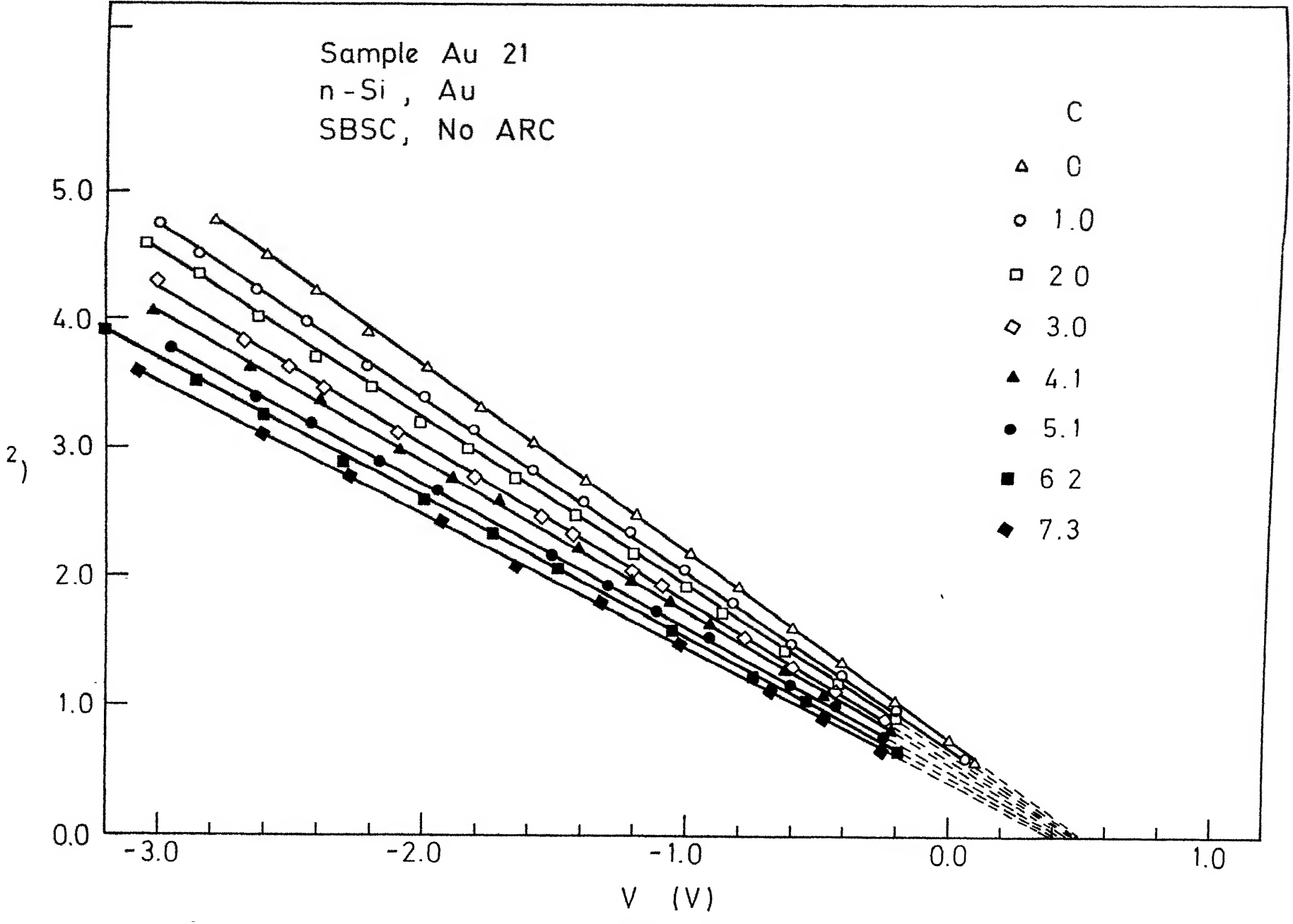
Sample Au 21
n-Si , Au
SBSC, No ARC
C
0
1.0
2 0
3.0
4.1
5.1
6 2
7.3
5.0
4.0
3.0
2.0
1.0
0.0
-3.0
-2.0
-1.0
0.0
1.0
V (V)

FIG. 4.17

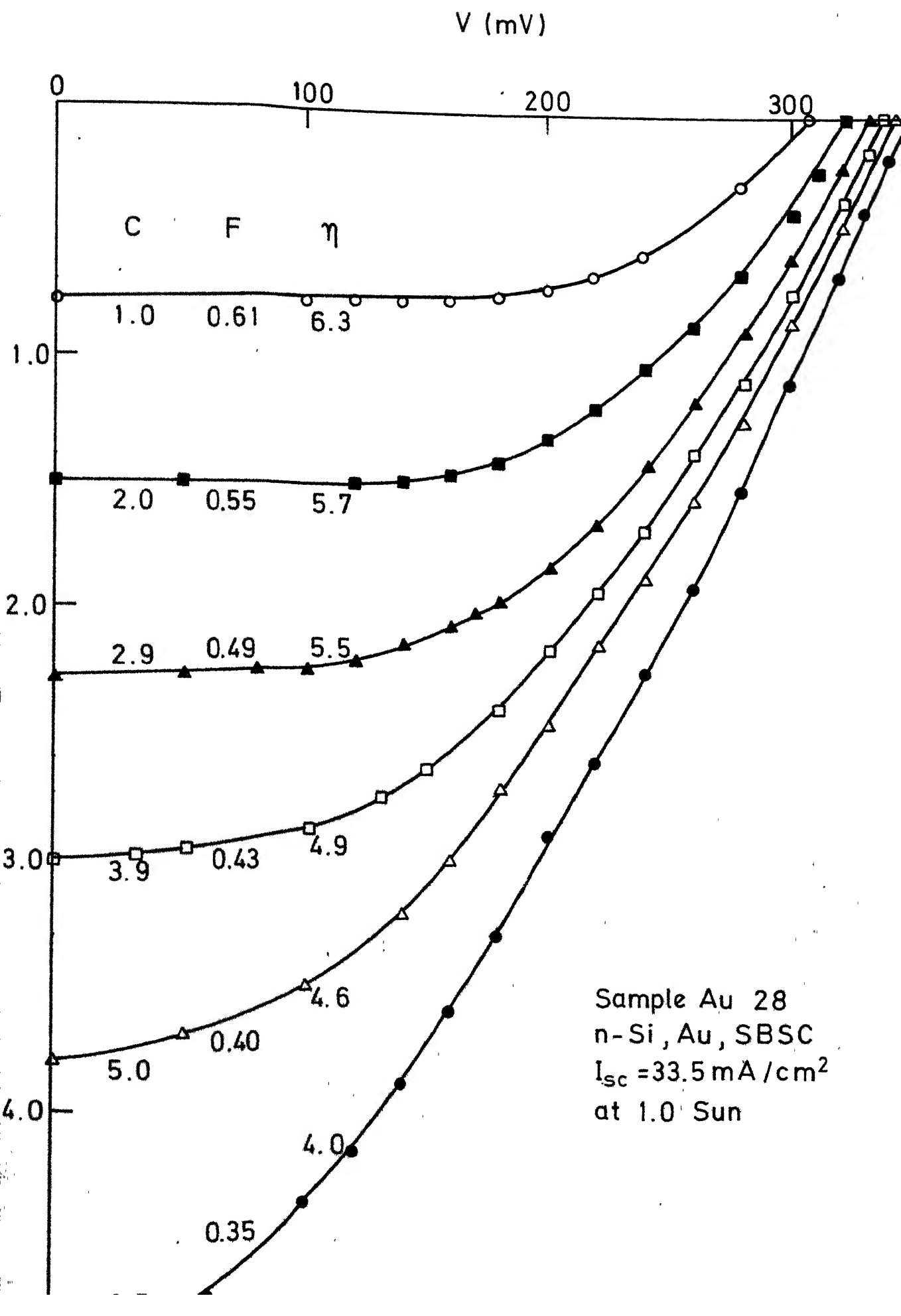
V (mV)
0
100
200
300
C F η
1.0 0.61 6.3
2.0 0.55 5.7
2.9 0.49 5.5
3.9 0.43 4.9
5.0 0.40 4.6
0.35 4.0
1.0
2.0
3.0
4.0
Sample Au 28
n-Si, Au, SBSC
I_{sc} = 33.5 mA/cm²
at 1.0 Sun

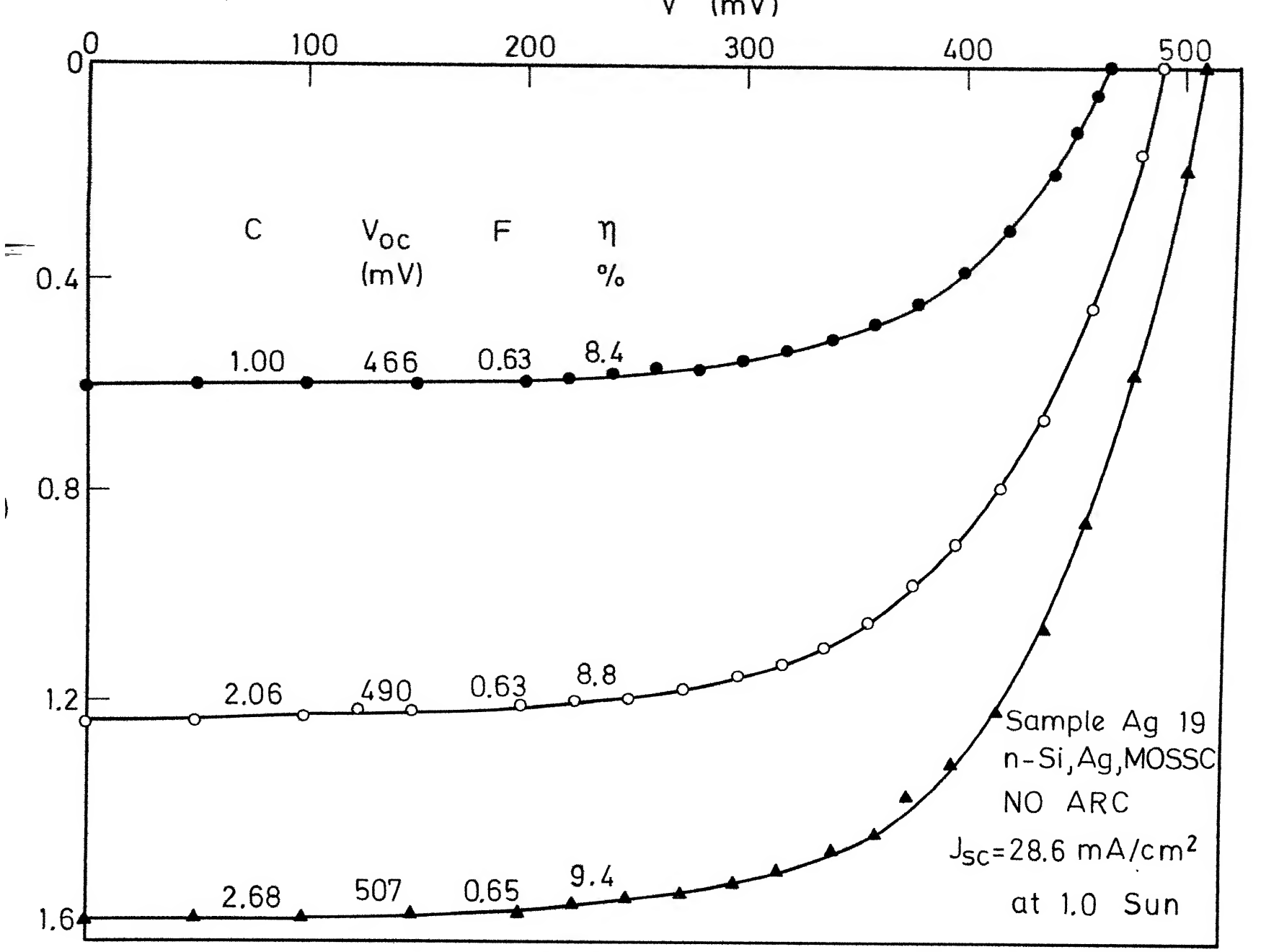
V (mV)
0
100
200
300
400
500
0
0.4
0.8
1.2
1.6
C
V_{oc} (mV)
F
η %
1.00 466 0.63 8.4
2.06 490 0.63 8.8
2.68 507 0.65 9.4
Sample Ag 19
n-Si, Ag, MOSSC
NO ARC
J_{sc}=28.6 mA/cm²
at 1.0 Sun

FIG 4.12

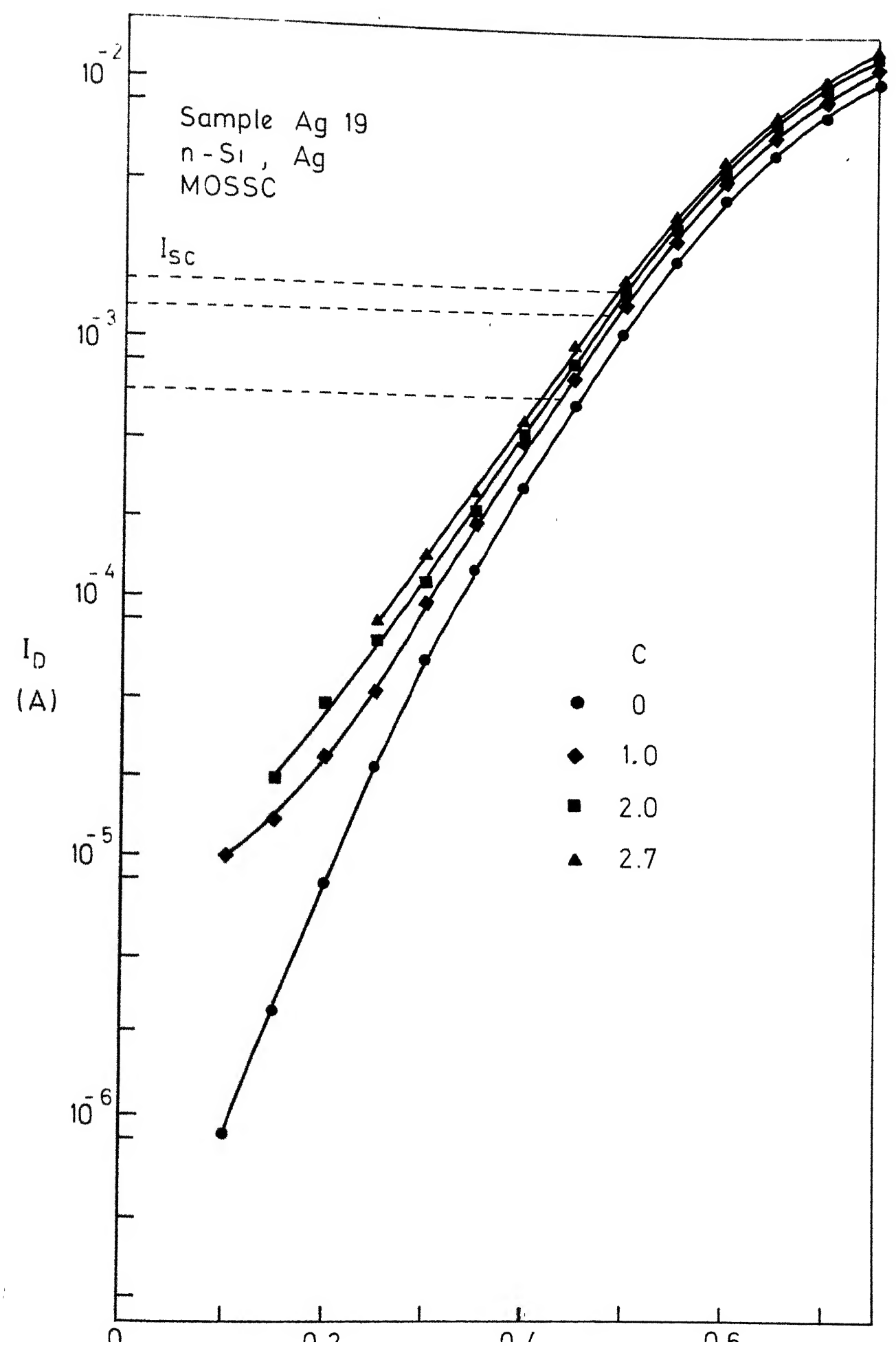
Sample Ag 19
n - Si , Ag
MOSSC
I_{SC}
10^{-2}
10^{-3}
10^{-4}
10^{-5}
10^{-6}
I_D
(A)
C
0
1.0
2.0
2.7
0
0.2
0.4
0.6

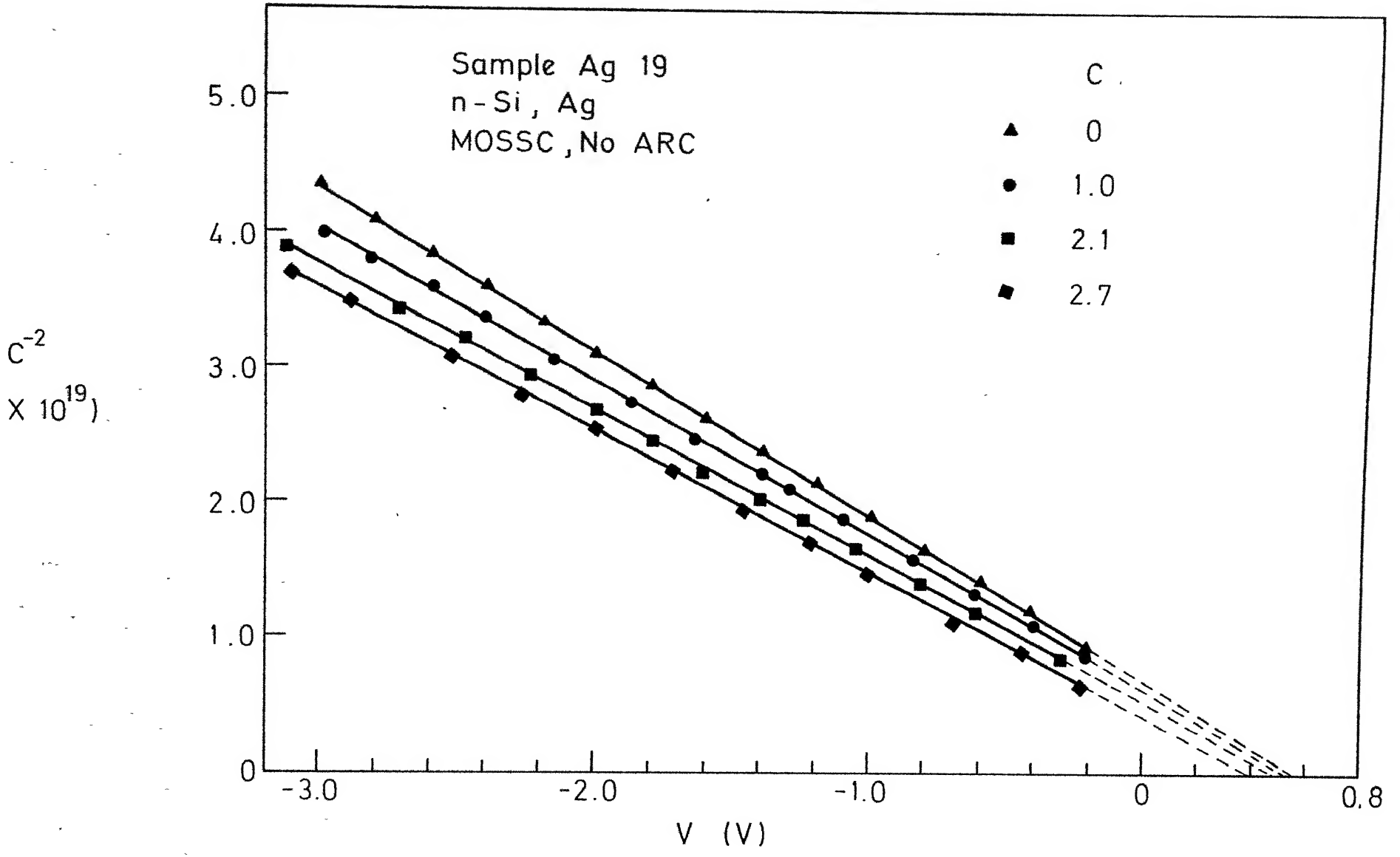
Sample Ag 19
n-Si, Ag
MOSSC, No ARC
C
0
1.0
2.1
2.7
5.0
4.0
3.0
2.0
1.0
0
-3.0
-2.0
-1.0
0
0.8
V (V)
C^{-2}
X 10^{19})

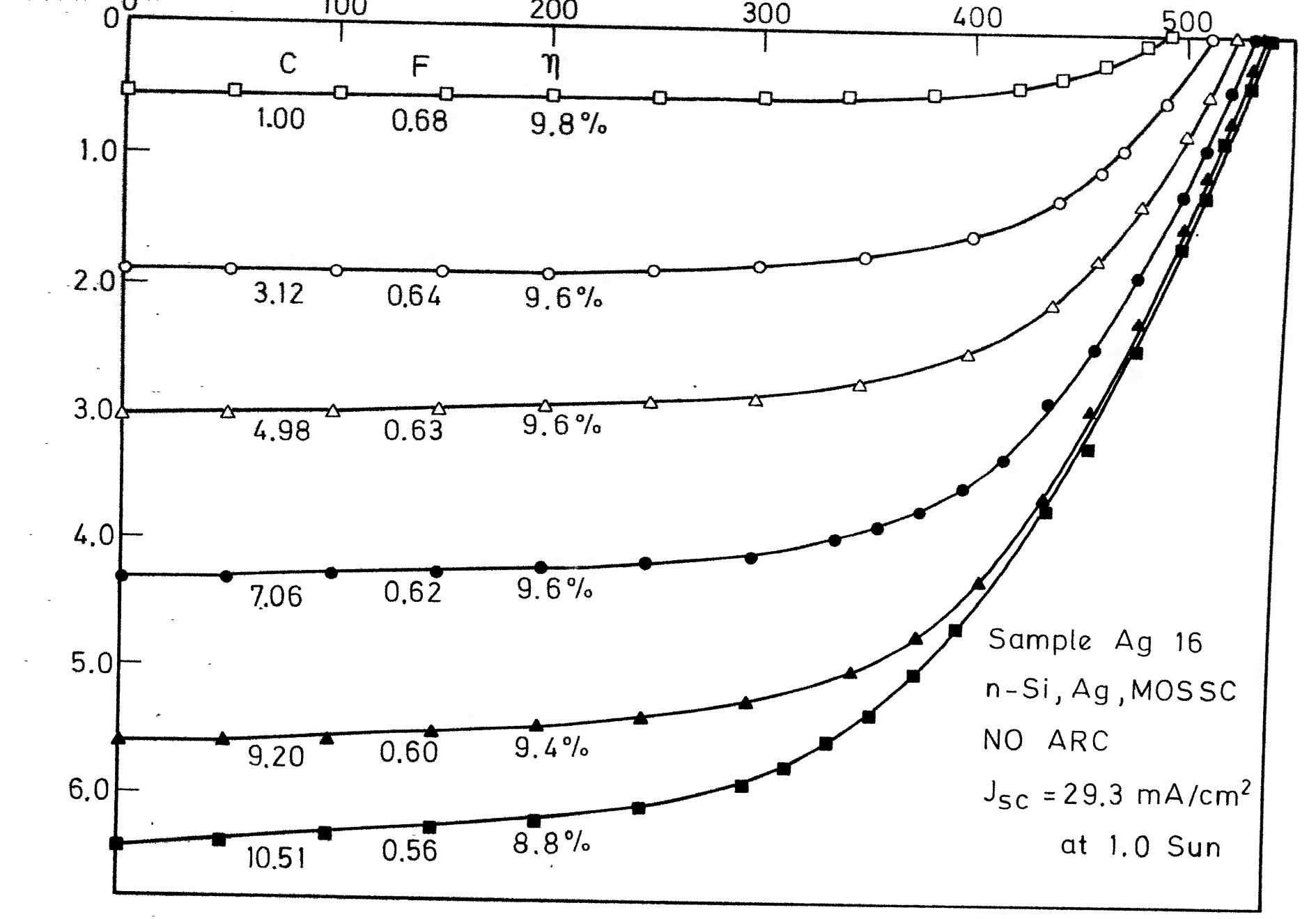
0
100
200
300
400
500
C
F
η
1.00
0.68
9.8%
1.0
2.0
3.12
0.64
9.6%
3.0
4.98
0.63
9.6%
4.0
7.06
0.62
9.6%
5.0
9.20
0.60
9.4%
6.0
10.51
0.56
8.8%
Sample Ag 16
n-Si, Ag, MOSSC
NO ARC
J_{SC} = 29.3 mA/cm²
at 1.0 Sun

FIG 4.20

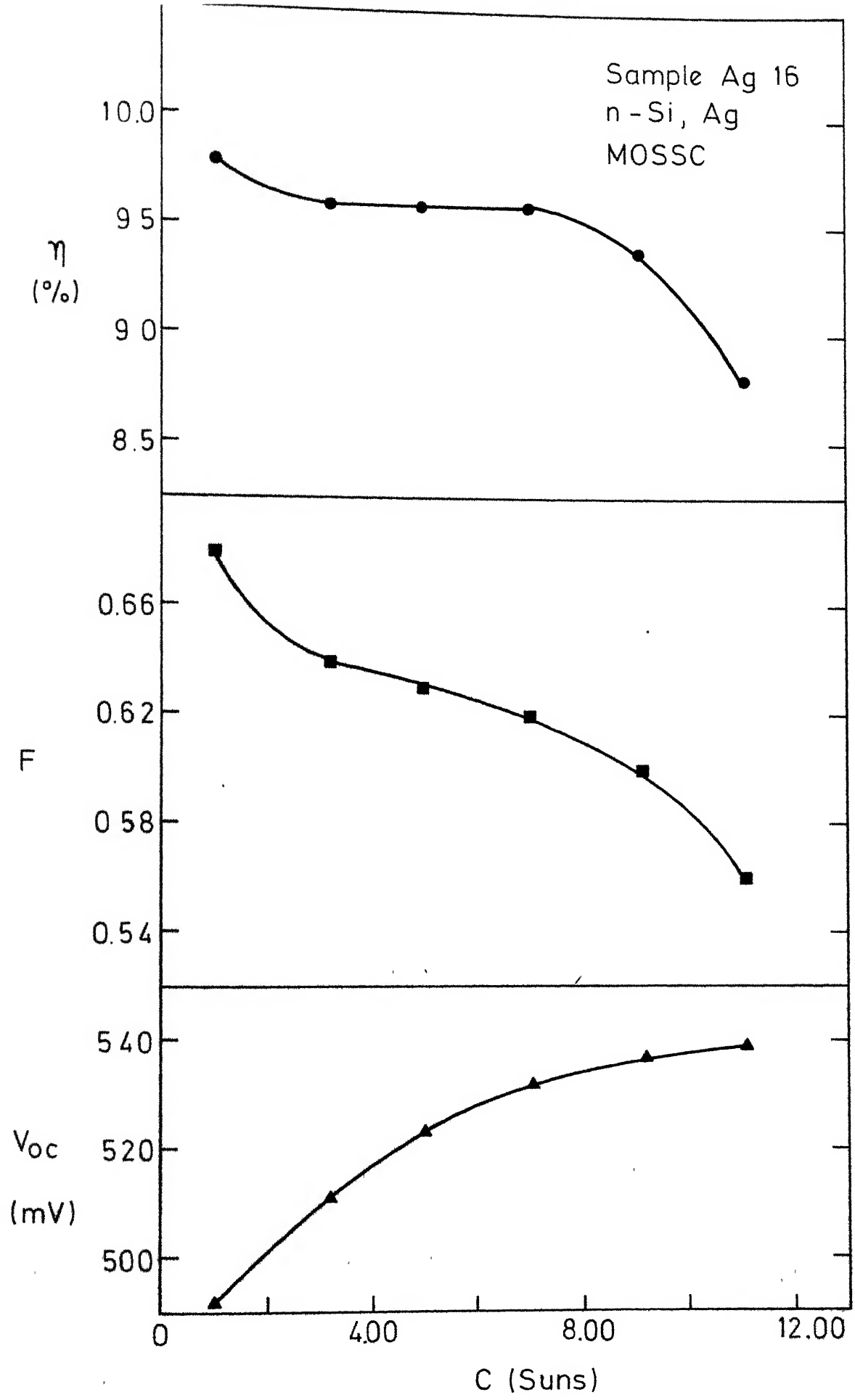
Sample Ag 16
n-Si, Ag
MOSSC
η
(%)
10.0
9 5
9 0
8.5
F
0.66
0.62
0 58
0.54
Voc
(mV)
540
520
500
0
4.00
8.00
12.00
C (Suns)

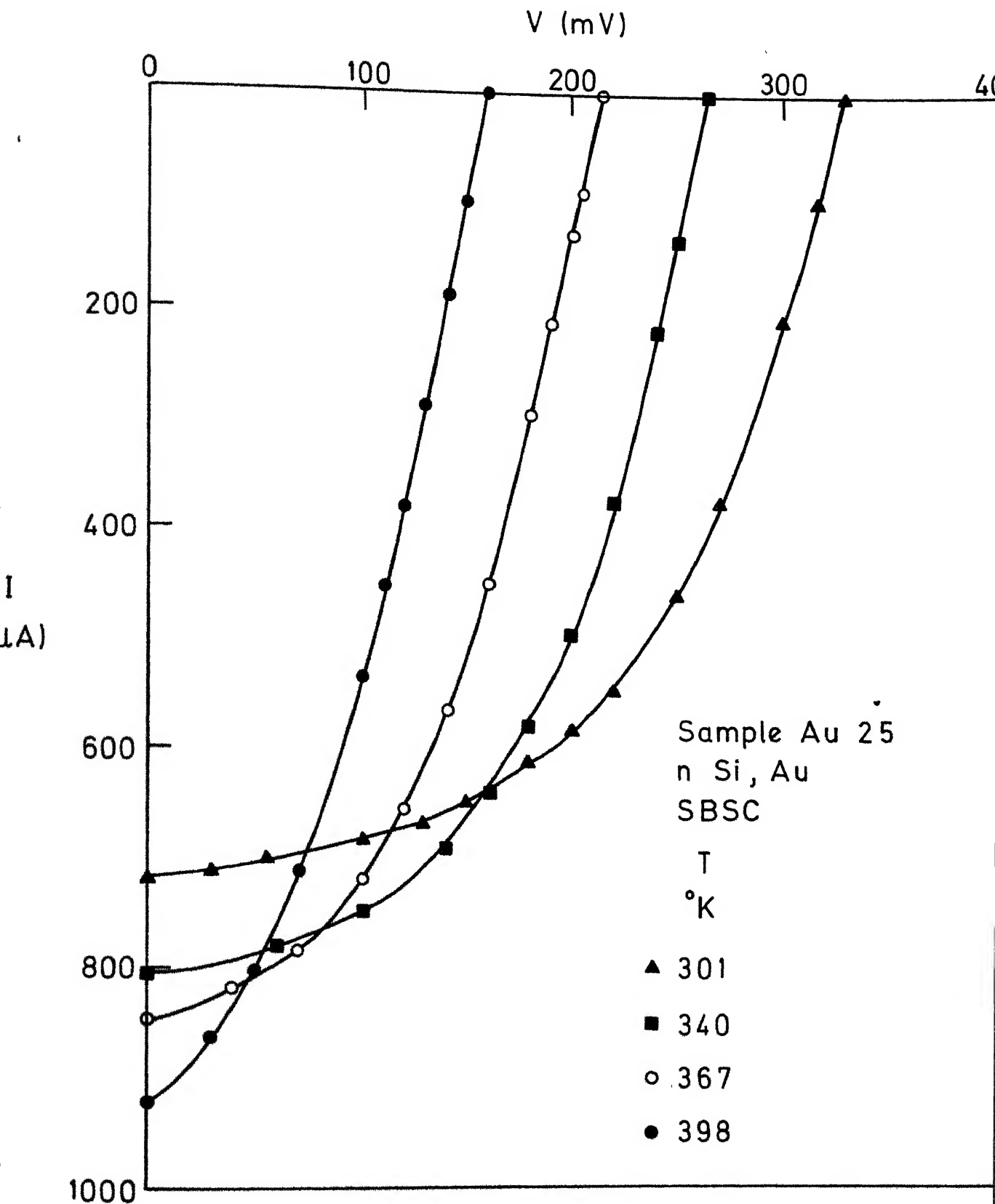
V (mV)
0
100
200
300
200
400
600
800
1000
Sample Au 25
n Si, Au
SBSC
T
°K
▲ 301
■ 340
○ 367
● 398

FIG. 4.24

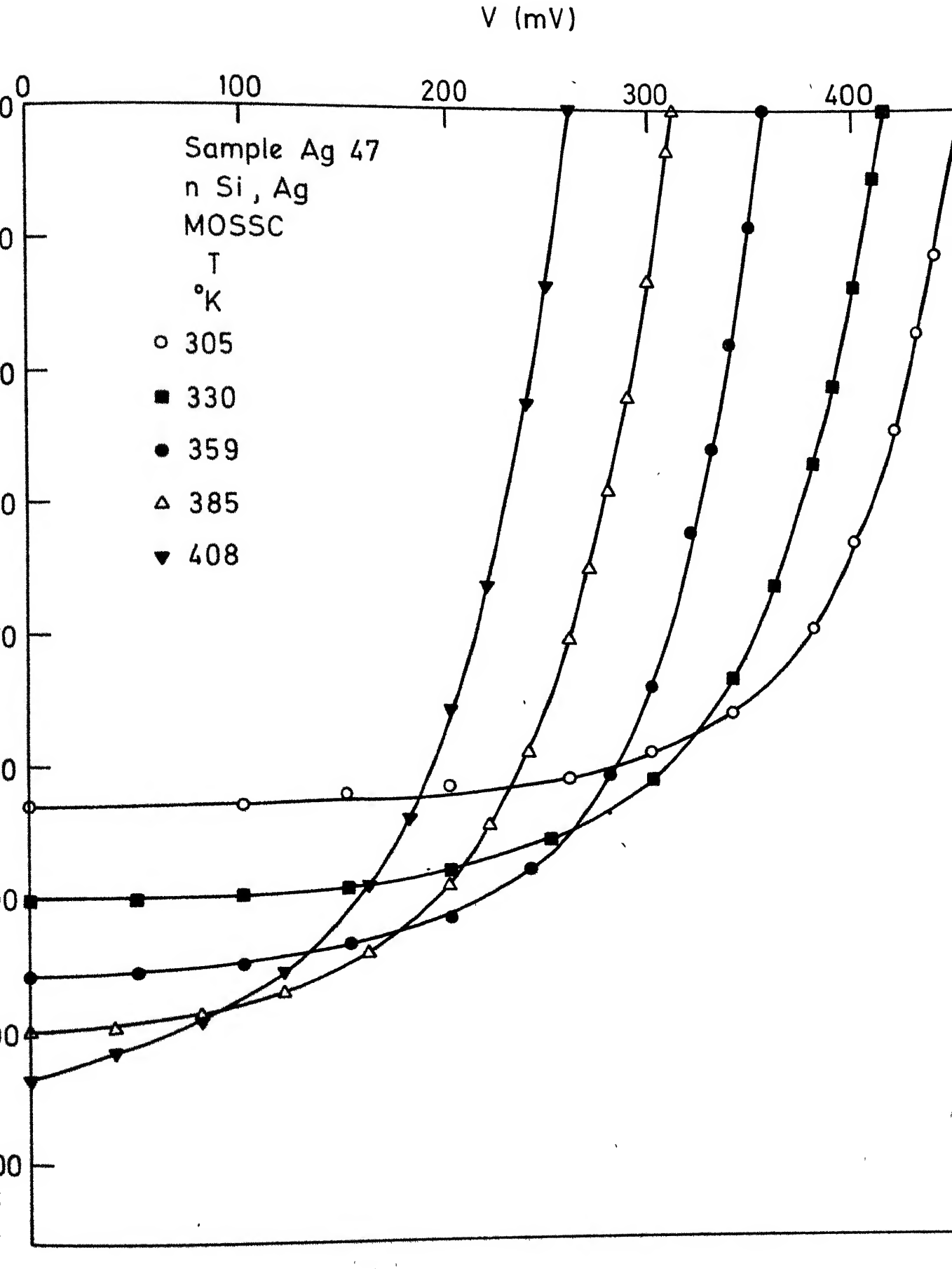
V (mV)
0
100
200
300
400
Sample Ag 47
n Si , Ag
MOSSC
T
°K
305
330
359
385
408

FIG 4.25

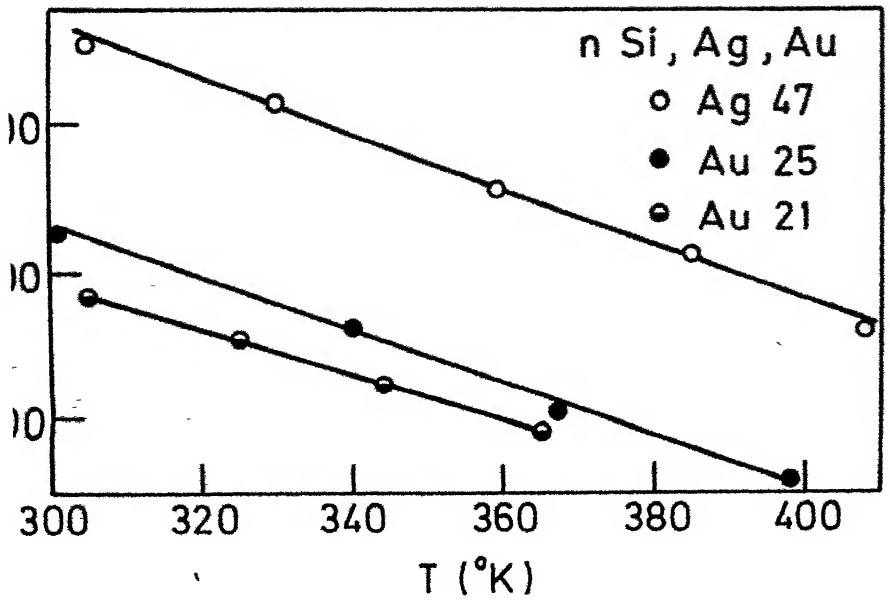

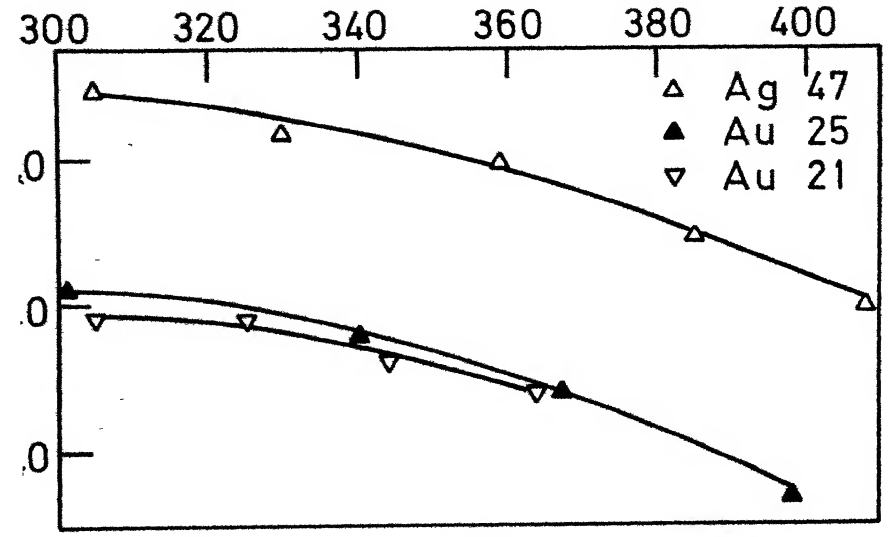

FIG.4.26(a)

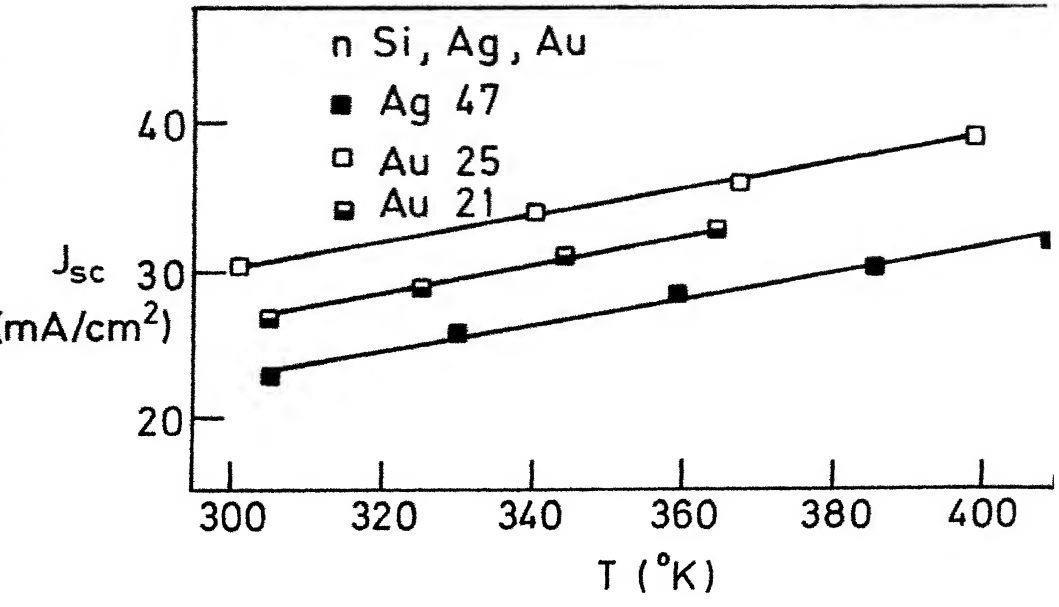

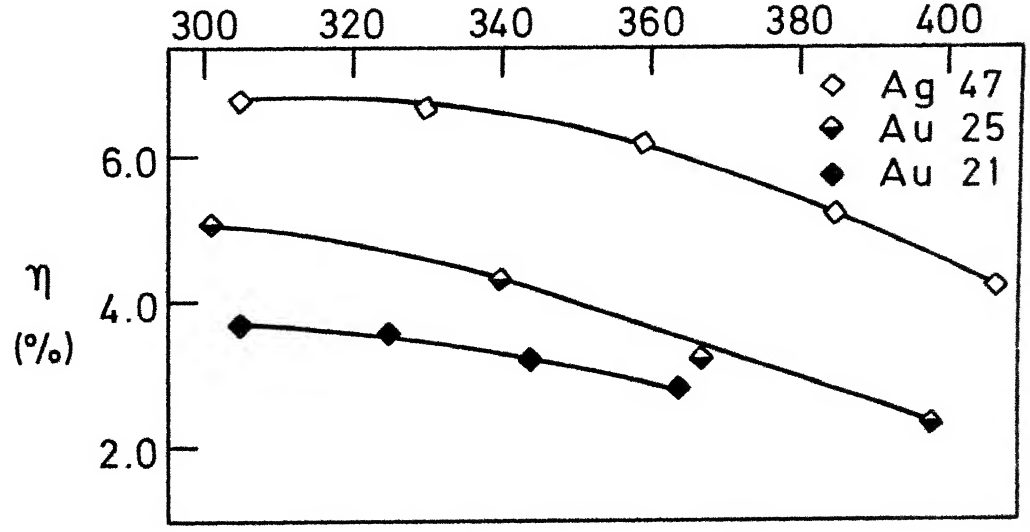

FIG.4.26(b)

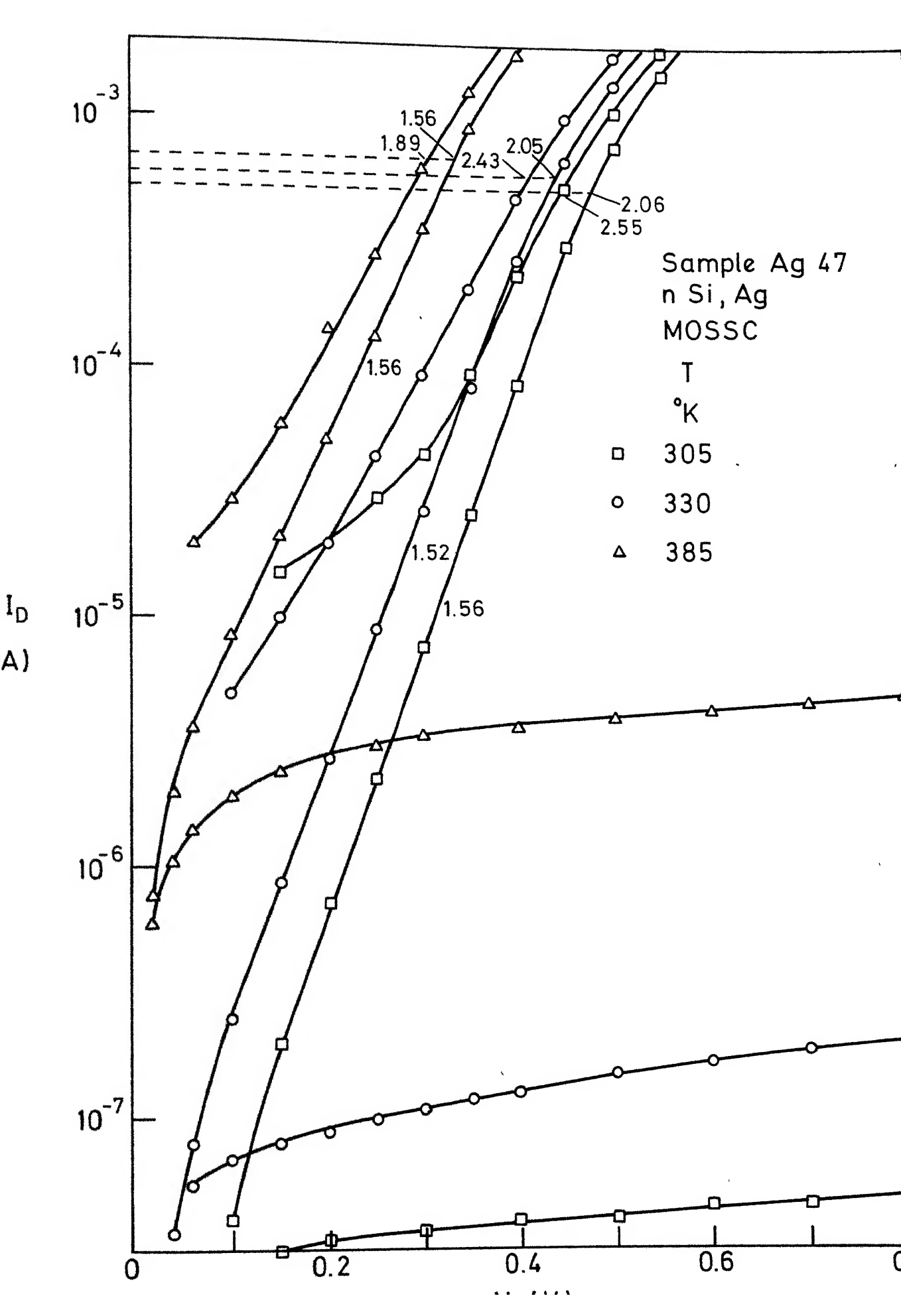
10^{-3}
10^{-4}
10^{-5}
10^{-6}
10^{-7}
I_D
A)
1.56
1.89
2.43
2.05
2.06
2.55
1.56
1.52
1.56
Sample Ag 47
n Si, Ag
MOSSC
T
°K
305
330
385
0
0.2
0.4
0.6

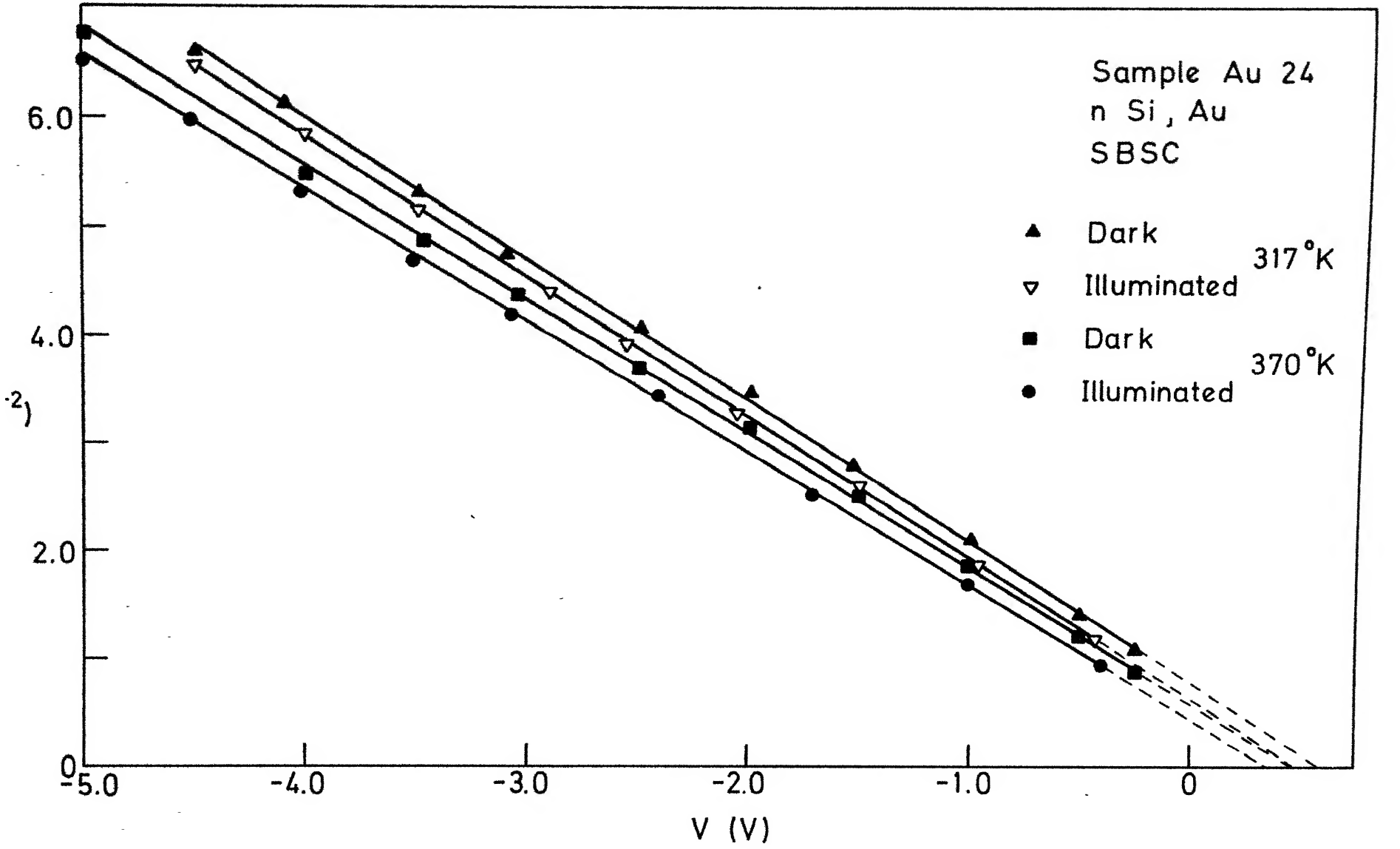
Sample Au 24
n Si , Au
SBSC
Dark
Illuminated
317 °K
Dark
Illuminated
370 °K
6.0
4.0
2.0
0
-5.0
-4.0
-3.0
-2.0
-1.0
0
V (V)

FIG. 4.28

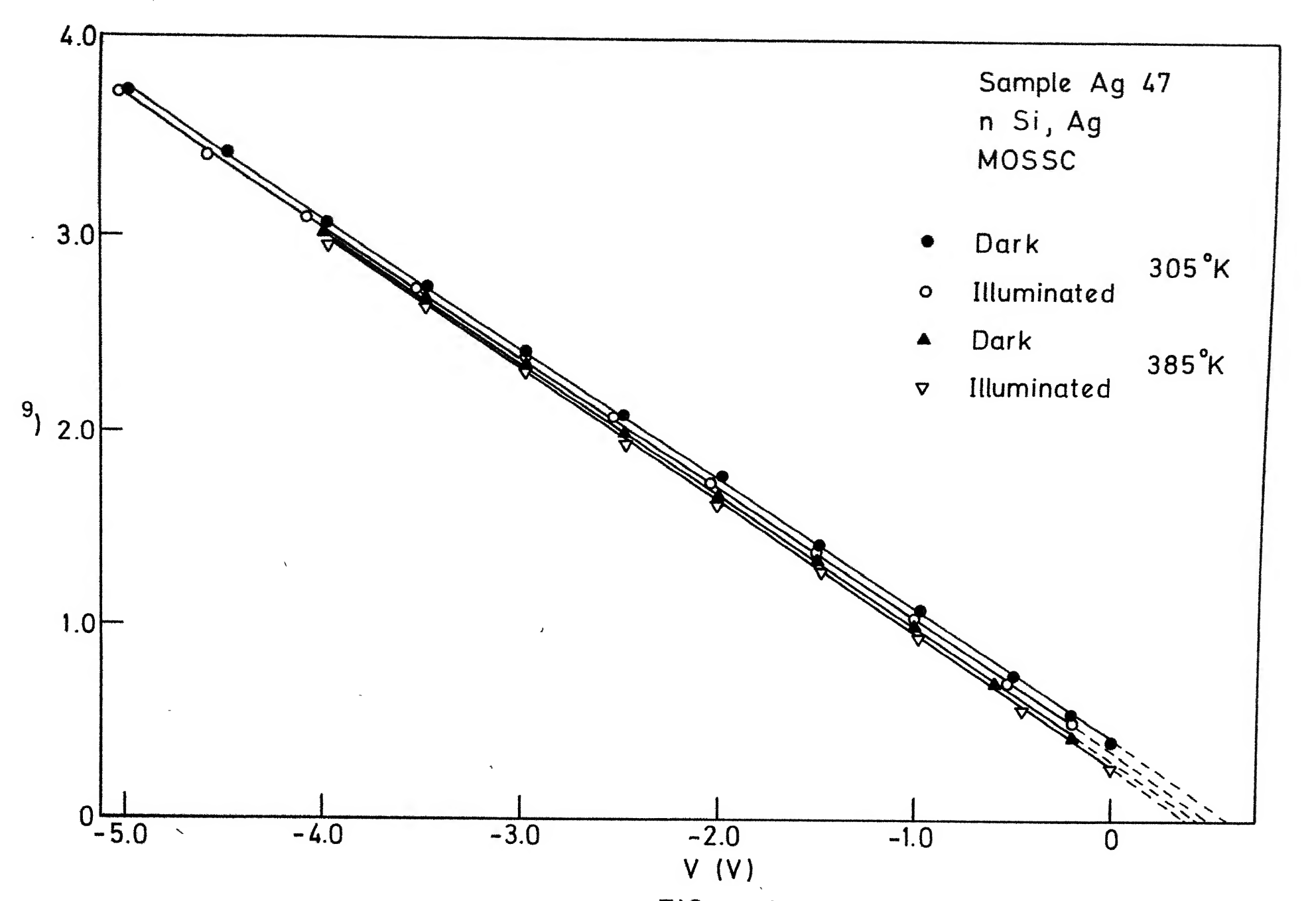
Sample Ag 47
n Si, Ag
MOSSC
Dark
Illuminated
305°K
Dark
Illuminated
385°K
4.0
3.0
2.0
1.0
0
-5.0
-4.0
-3.0
-2.0
-1.0
0
V (V)

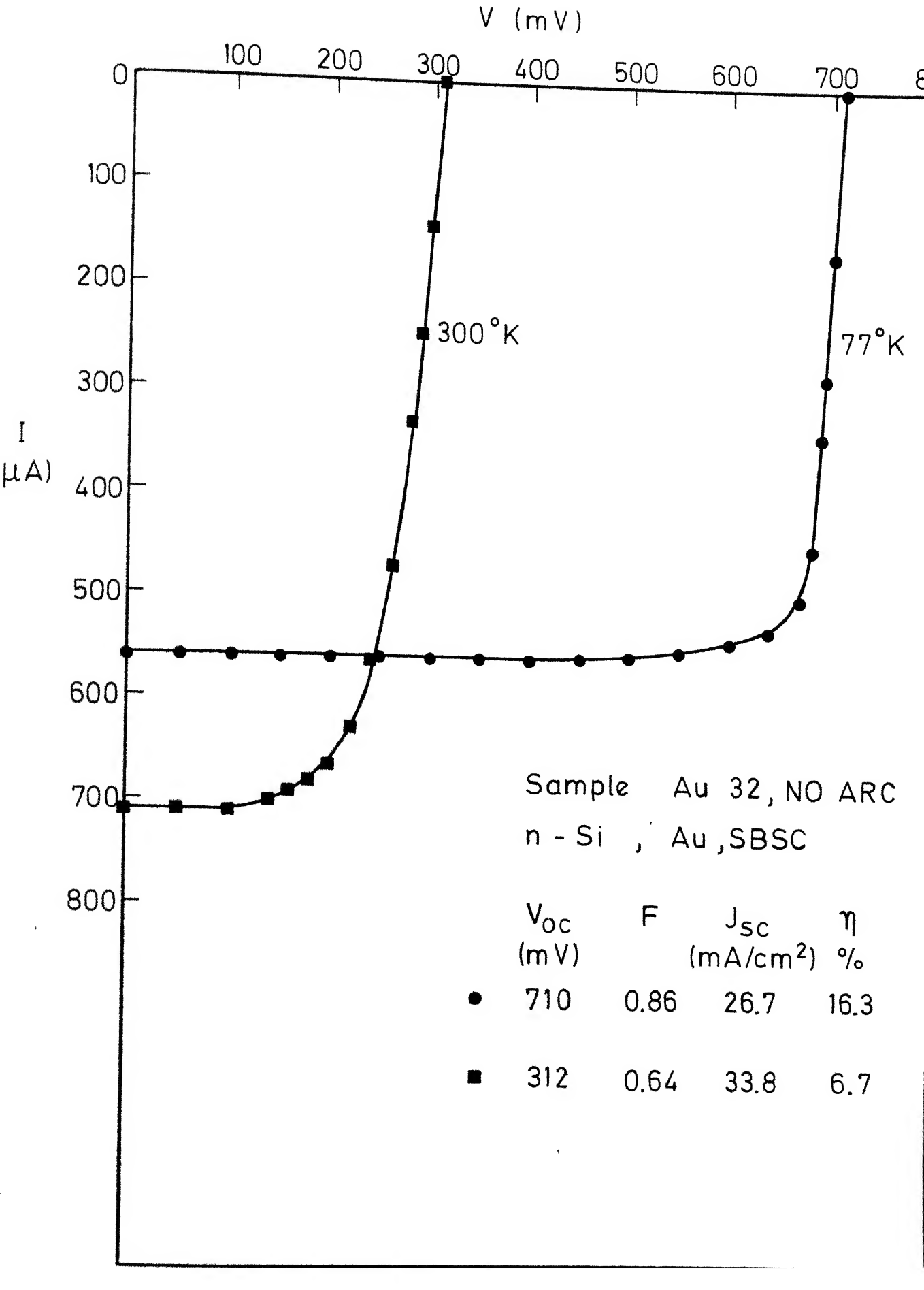
V (mV)
0
100
200
300
400
500
600
700
100
200
300
400
500
600
700
800
I
(μA)
300°K
77°K
Sample Au 32, NO ARC
n - Si , Au, SBSC
V_{oc} (mV)
F
J_{sc} (mA/cm²)
η %
● 710 0.86 26.7 16.3
■ 312 0.64 33.8 6.7

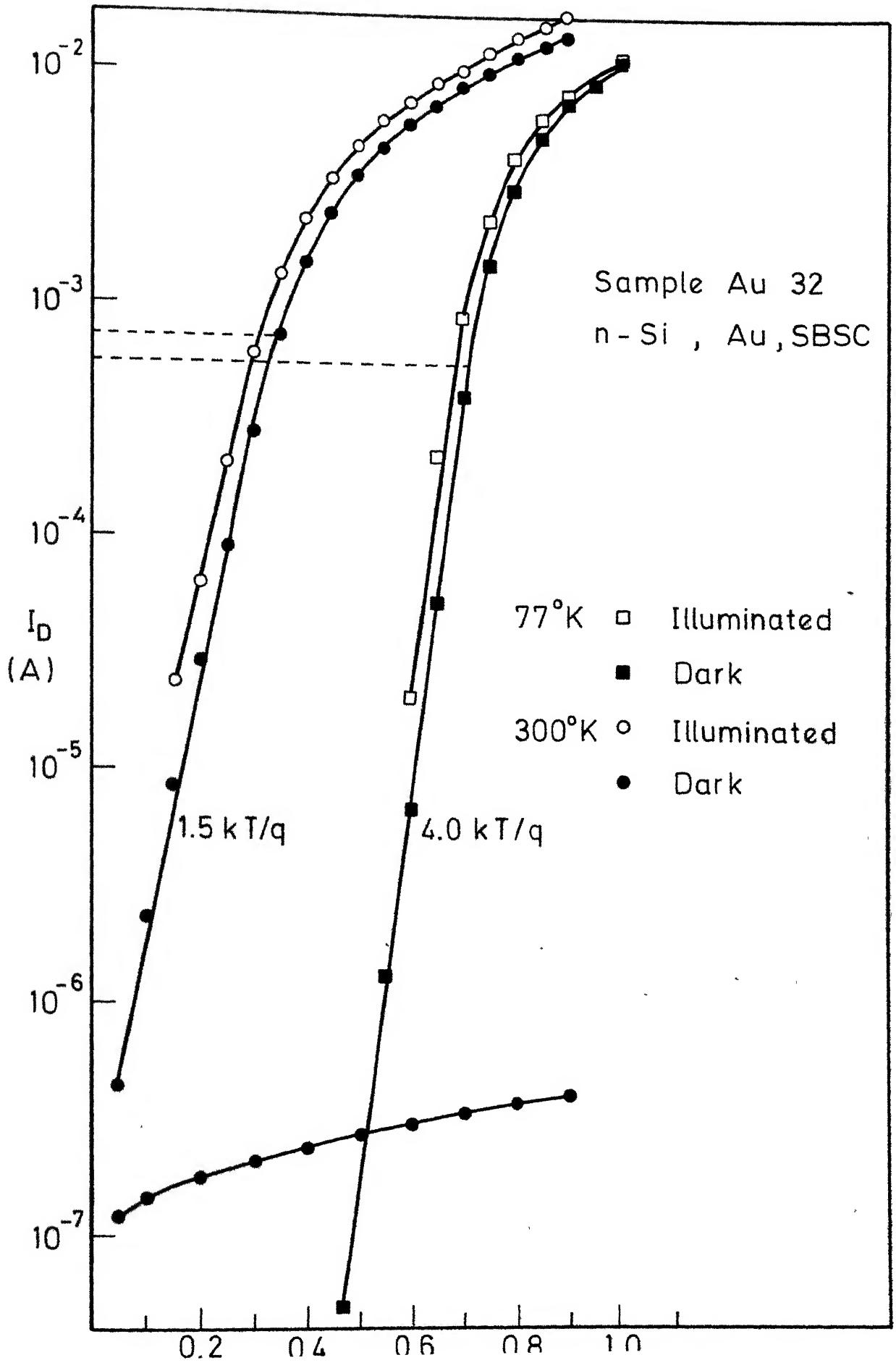
Sample Au 32
n-Si , Au, SBSC
77°K Illuminated
Dark
300°K Illuminated
Dark
1.5 kT/q
4.0 kT/q
I_D (A)
10^{-2}
10^{-3}
10^{-4}
10^{-5}
10^{-6}
10^{-7}
0.2
0.4
0.6
0.8
1.0

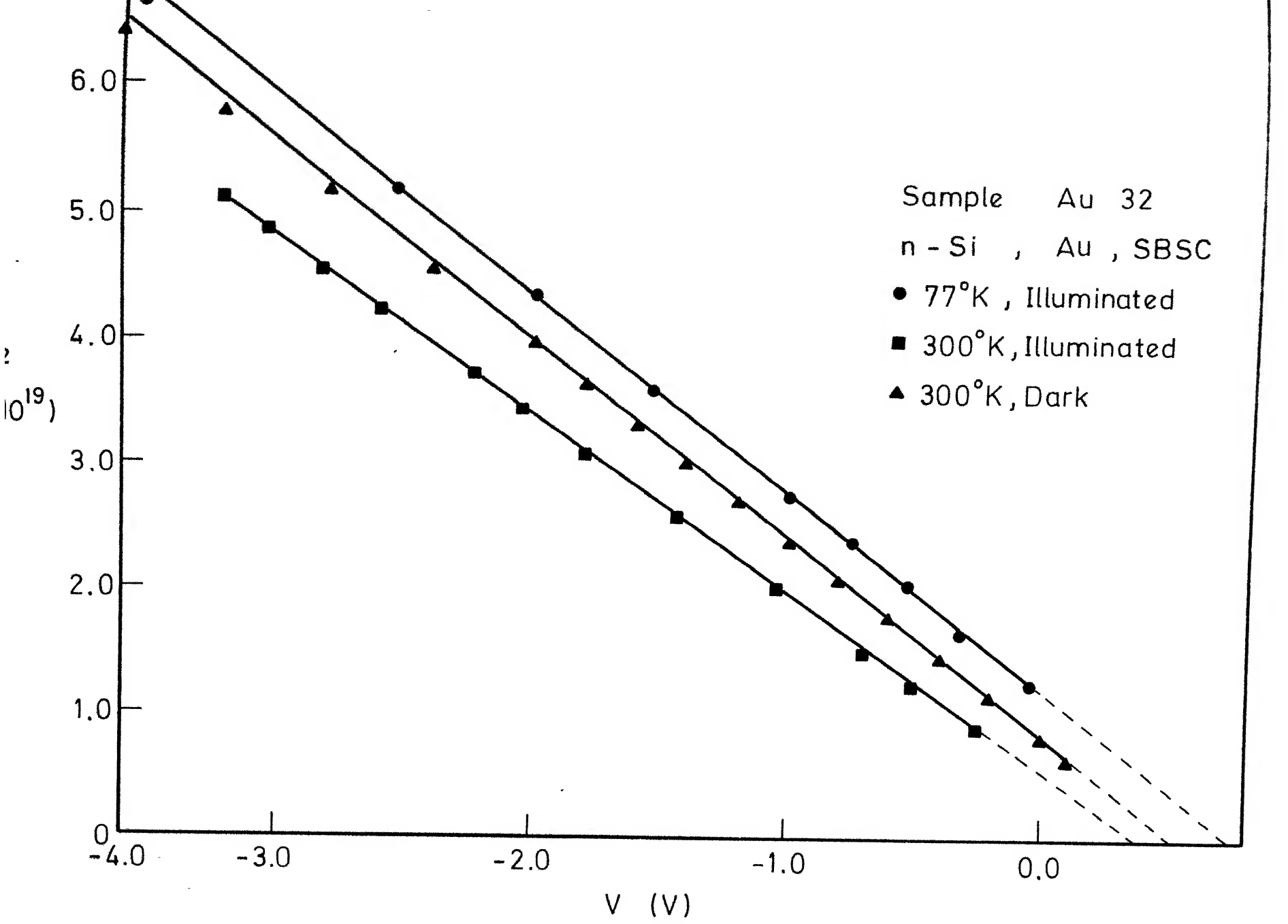
Sample Au 32
n - Si , Au , SBSC
● 77°K , Illuminated
■ 300°K, Illuminated
▲ 300°K, Dark
6.0
5.0
4.0
3.0
2.0
1.0
0
-4.0
-3.0
-2.0
-1.0
0.0
V (V)

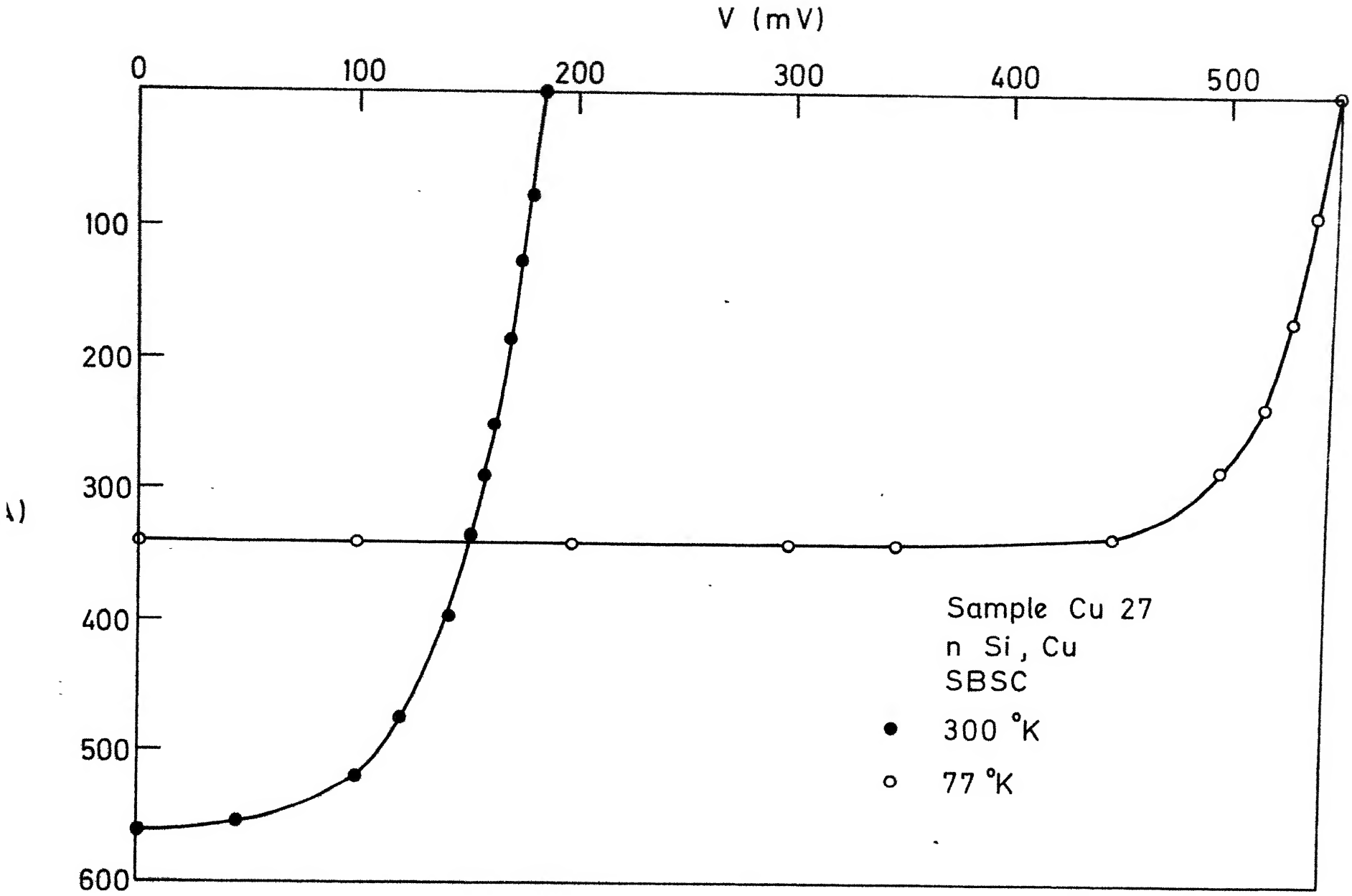
V (mV)
0
100
200
300
400
500
100
200
300
400
500
600
Sample Cu 27
n Si , Cu
SBSC
300 °K
77 °K

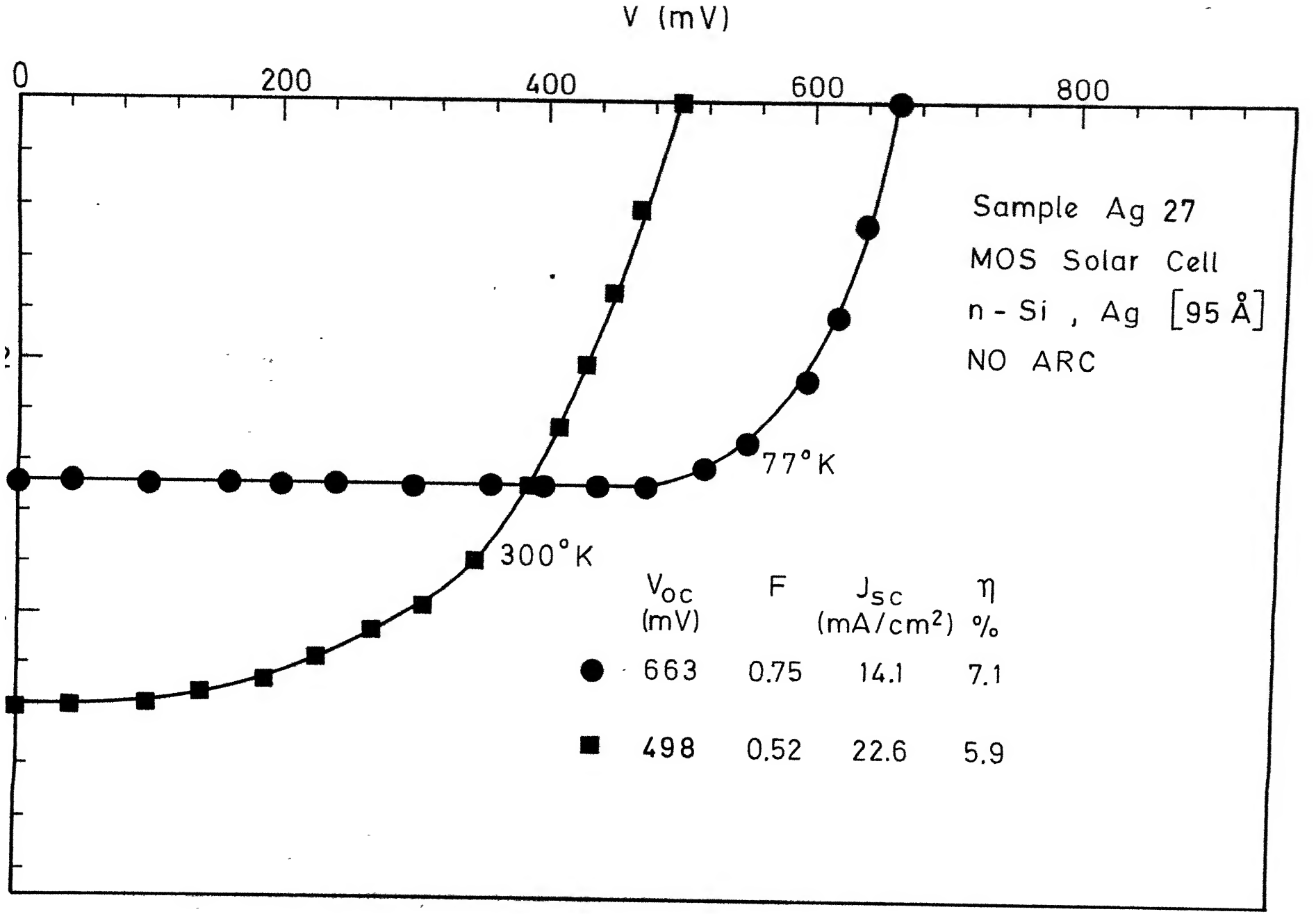
V (mV)
0
200
400
600
800
Sample Ag 27
MOS Solar Cell
n - Si , Ag [95 Å]
NO ARC
77°K
300°K
Voc (mV)
F
Jsc (mA/cm²)
η %
663
0.75
14.1
7.1
498
0.52
22.6
5.9

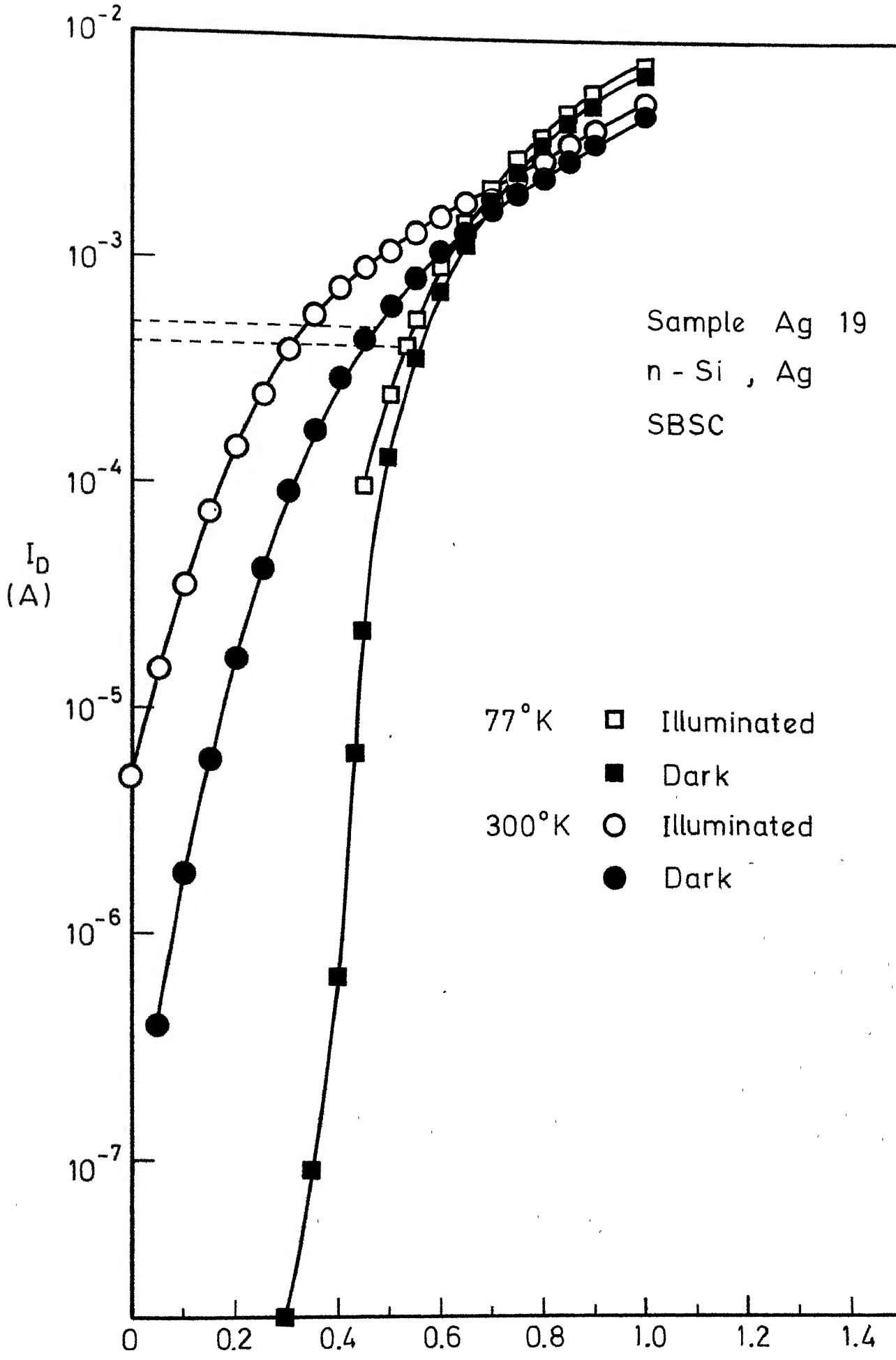
10^{-2}
10^{-3}
10^{-4}
10^{-5}
10^{-6}
10^{-7}
I_D (A)
0
0.2
0.4
0.6
0.8
1.0
1.2
1.4
Sample Ag 19
n - Si , Ag
SBSC
77°K
Illuminated
Dark
300°K
Illuminated
Dark

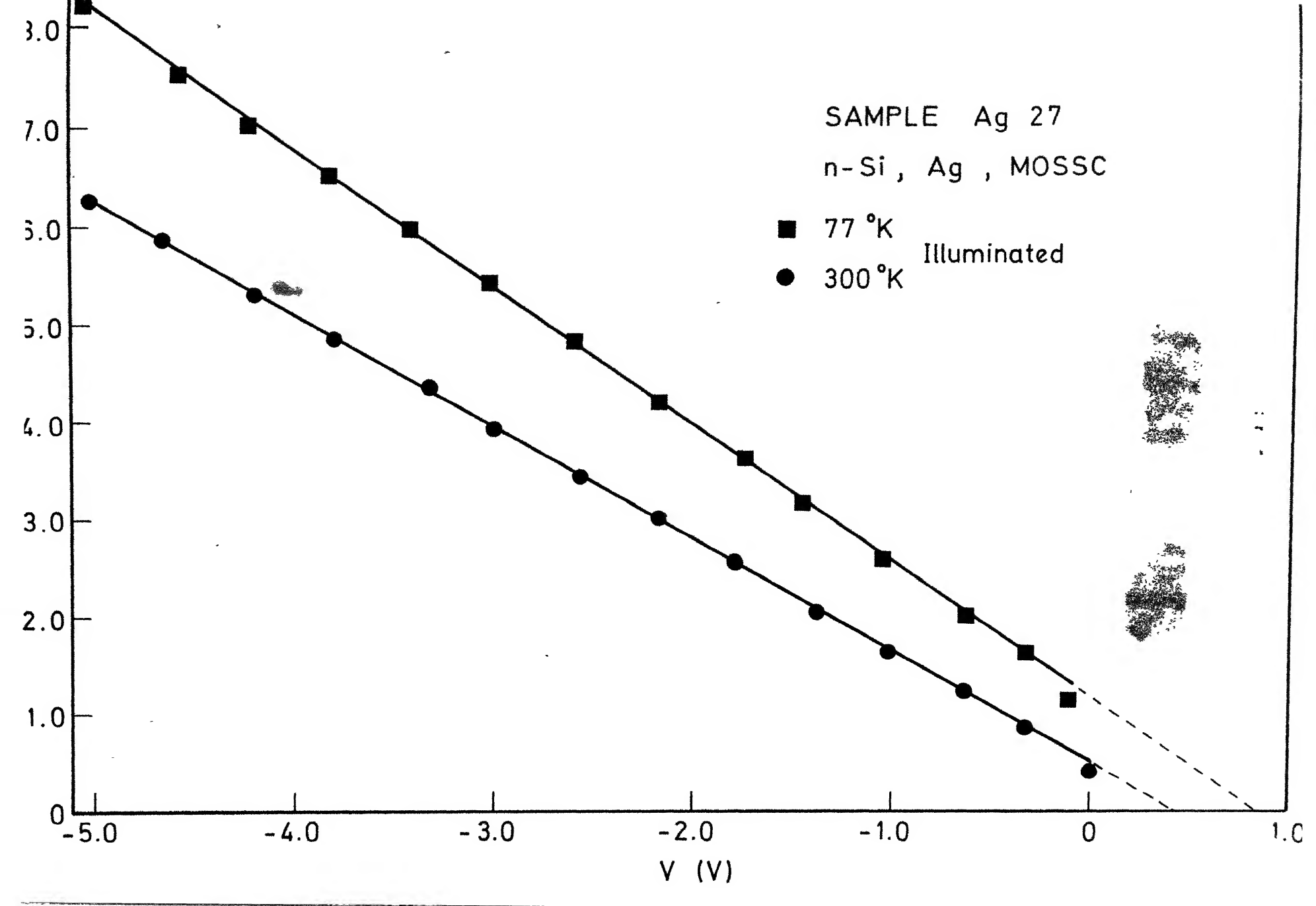
SAMPLE Ag 27
n-Si , Ag , MOSSC
77 °K
300 °K
Illuminated
3.0
7.0
5.0
5.0
4.0
3.0
2.0
1.0
0
-5.0
-4.0
-3.0
-2.0
-1.0
0
1.0
V (V)

MS-1978-M-BHA-INV